U.PORTO

FEUP FACULDADE DE ENGENHARIA
UNIVERSIDADE DO PORTO

Implementation of DoE (Design of Experiments) for optimization of 3D printing parameters for PEI

Rodrigo Marques Miranda de Souza Praça

Master's Thesis

Supervisor at FEUP: Prof. Pedro Sousa
Supervisor at INEGI: Eng. Tiago Domingues
Supervisor at INEGI: Dr. Gonçalo Cipriano

Master's in Mechanical Engineering

July 2023

“Everything ends, and it’s always sad, but everything begins again, too. And that’s always happy. Be happy.”

The Doctor

Abstract

Additive manufacturing (AM) processes such as Fusion Deposition Modelling (FDM) are becoming common in industry due to their capabilities of quickly obtaining cost-effective prototypes. The emergence of high-performance materials has now created the possibility of obtaining not only mock-ups but functional parts with properties that can even be compared to some metals. Still, to achieve peak performance, knowledge of the effect that printing parameters have on the final product is needed.

This work investigates the effect of temperature related printing parameters, namely the nozzle, bed, and chamber temperatures, on the final tensile strength of polyetherimide (PEI) samples. The influence of said factors on the final response is also analyzed and ranked, through the use of a design of experiments method, the central composite design.

Due to the lack of 3D-printed parts testing standards, some exploration of different standards and sample configurations had to be made before starting the experiment. It was discovered that a minimum bed temperature of 120ºC was needed in order to print acceptable samples and that the ASTM D638 V specimens printed with two perimeters were the most consistent when submitted to tensile strength testing.

The samples were all printed on the custom 3D printer that had previously been built at INEGI and was upgraded during this work. They were also prepared for digital image correlation analysis through air-brush painting in order to obtain a speckle pattern. After the testing, out of the 57 planned samples only 48 fractured in the critical zone, being the only ones considered for the statistical study.

The analysis of the results showed that an increase in the overall temperature of the process also increased the samples tensile strength and reduced their ultimate strain. It was also found that out of the three studied parameters, the bed temperature is the one with the highest influence on the final response followed by the nozzle and the chamber temperature. The interactions between the parameters revealed little to no impact on the final properties obtained.

Additionally, a regression model capable of predicting and optimizing the tensile strength given the 3 temperature parameters was generated and validated through experimental testing. In the end, it was found that the optimal parameters for printing PEI in INEGI's custom built printer are a bed temperature of 187.6ºC a nozzle temperature of 400ºC and a chamber temperature of 98.5 ºC.

Keywords: Additive Manufacturing, Fused Deposition Modelling, PEI, Design of Experiment, 3D printing, tensile strength.

Resumo

Processos de fabrico aditivo (AM), como a modelagem por deposição fundida (FDM), estão a tornar-se comuns na indústria devido às suas capacidades de obtenção rápida de protótipos e bom custo-benefício. O aparecimento de materiais de elevado desempenho criou agora a possibilidade de obter não só modelos experimentais, mas também peças funcionais com propriedades que podem até mesmo ser comparadas a de alguns metais. No entanto, para atingir o máximo desempenho, é necessário conhecer o efeito que os parâmetros de impressão têm no produto final.

Este trabalho investiga o efeito dos parâmetros de impressão relacionados com a temperatura, nomeadamente as temperaturas do bico, da cama e da câmara, na resistência máxima à tração de amostras de polieterimida (PEI). A influência dos referidos fatores na resposta final é também analisada e classificada, através da utilização de um método de planejamento de experimentos (DoE), mais especificamente o *central composite design* (CCD).

Devido à falta de normas de ensaio de peças impressas em 3D, foi necessário explorar diferentes normas e configurações de amostras antes de iniciar a experiência. Descobriu-se que era necessária uma temperatura de cama mínima de 120ºC para imprimir amostras aceitáveis e que os espécimes ASTM D638 V impressos com 2 perímetros eram os mais consistentes quando submetidos a testes de resistência à tração

As amostras foram todas impressas na máquina previamente construída no INEGI e que foi atualizada durante este trabalho. Foram também preparadas para a análise de correlação de imagem digital através de pintura a ar, de modo a obter um padrão de pequenos pontos. Após os ensaios, das 57 amostras previstas, apenas 48 partiram na secção crítica, pelo que foram as únicas consideradas para o estudo estatístico.

A análise dos resultados mostrou que um aumento da temperatura global do processo também aumentou a resistência à tração das amostras e reduziu a sua deformação. Verificou-se também que, dos 3 parâmetros estudados, a temperatura da cama é a que tem maior influência na resposta final, seguida da temperatura do bico e da câmara. As interações entre os parâmetros revelaram pouco ou nenhum impacto nas propriedades finais obtidas.

Adicionalmente, foi gerado e validado através de testes experimentais um modelo de regressão capaz de prever e otimizar a resistência à tração tendo em conta os 3 parâmetros de temperatura. No final, verificou-se que os parâmetros ótimos para imprimir PEI na impressora personalizada da empresa são: uma temperatura de cama de 187.6ºC, uma temperatura de bocal de 400ºC e uma temperatura de câmara de 98.5 ºC.

Palavras-chave: Fabrico Aditivo, Modelagem por Deposição Fundida, PEI, Planejamento de Experimentos, Impressão 3D, Resistência à Tração.

Acknowledgments

During the execution of this thesis much time and effort, whether in the laboratory or in research, were necessary to achieve the outlined objectives. However, some people were responsible for, directly or indirectly, relieving this pressure and I to whom would like to thank:

To Prof. Pedro Sousa, my supervisor at FEUP, for his support, availability and help during the work, especially in the preliminary stages where knowledge of 3D printer software and hardware was needed.

To Engineer Tiago Domingues, my supervisor at INEGI, for welcoming me into the company, helping in both the theoretical and practical work and giving his valuable opinion.

To Dr. Gonçalo Cipriano, my co-supervisor at INEGI, for sharing his useful knowledge on statistical methods.

To all INEGI collaborators, which I had the pleasure of meeting and were very helpful in various stages of the work, sharing their expertise on different processes and treating me with respect and sympathy.

To all the Professors at FEUP, who in the last 5 years have been responsible for my academic development and have provided me with a good foundation on the most diverse engineering topics.

To my parents, Simone and Moacyr, for being responsible for everything that I have and am today, making every effort to give me anything I needed and supporting me in all my decisions. To whom I am eternally grateful and can´t express in words the joy and privilege that is being their son.

To the rest of my family, the ones that are still here and the ones that have already passed away, for being a part of who I am today.

To my friends here in Portugal, who welcomed me on this overseas adventure and with whom I created the most amazing memories over the last 5 years. A special thanks to the friends made on the academic traditions and the ones made on the student's association, in particular the ones on the recreational department, with whom I spent many remarkable days and nights.

To my friends back home, who were part of my growth and with whom I learned many things about life. That despite the distance between us, never stopped supporting me and kept in touch. Even though the feeling of longing was always a constant, our friendship was enough to overcome it, and may it continue this way.

Contents

Abstract ..... **i**

Resumo ..... **iii**

Acknowledgments ..... **v**

Abbreviations ..... **ix**

1 Introduction **1**

1.1 Layout 1
1.2 Context 2
1.3 The project and INEGI 2
1.4 Objectives 3

2 State of the art **5**

2.1 Additive Manufacturing 5
2.2 FDM technology 7
2.2.1 FDM parameters and their influence 9
2.2.2 FDM materials 17
2.3 Design of Experiments 19
2.3.1 Main DoE methods 21
2.3.2 Data Analysis 25

3 Material and Methods **29**

3.1 Material 29
3.2 Methodology Analysis 30
3.2.1 The printer 30
3.2.2 Process Parametrization 33
3.2.3 Design of Experiments Implementation 39
3.2.4 Printing of the samples 40
3.2.5 Tensile Strength Test 43
3.2.6 Digital Image Correlation 44

4 Results and Discussion **47**

4.1 Maximum Tensile Strength Results 47
4.2 Design of Experiments Results 49
4.2.1 ANOVA 49
4.2.2 Regression Model 49
4.2.3 Plots and Charts 50
4.2.4 Contour and Surface Plots 52
4.2.5 Factorial Plots 55
4.2.6 Optimizer 56
4.3 Discussion 57
4.3.1 Nozzle Temperature 57

4.3.2 Chamber Temperature 58
4.3.3 Bed Temperature 59
4.3.4 Interactions 59
4.3.5 Model accuracy 59
5 Conclusions and Future Works 61
5.1 Conclusions 61
5.2 Future Works 62
References 63
ANNEX A - Stress-Strain graphs and maximum values 69

Abbreviations

ABS – Acrylonitrile Butadiene Styrene
AM – Additive Manufacturing
ANOVA – Analysis of Variance
ASA – Acrylonitrile Styrene Acrylate
BBD – Box-Behnken Design
CAD – Computer Aided Design
CCC – Central Composite Circumscribed
CCD – Central Composite Design
CCF – Central Composite Face Centered
CCI – Central Composite Inscribed
CNC – Computerized Numerical Control
DED – Direct Energy Deposition
DIC – Digital Image Correlation
DoE – Design of Experiment
DSD – Definitive Screening Design
FDM – Fused Deposition Modelling
FFD – Full Factorial Design
FFF – Fused Filament Fabrication
INEGI – Instituto de Ciência e Inovação em Engenharia Mecânica e Engenharia Industrial
LOM – Laminated Object Manufacturing
OFAT – One Factor at a Time
PBD – Plackett-Burman Design
PC – Polycarbonate
PEEK – Polyether Ether Ketone
PEI – Polyether Imide
PETG – Polyethylene Terephthalate Glycol
PLA – Polylactic Acid

PSU – Polysulfone

RSM – Response Surface Methodology

SEM – Scanning Electron Microscope

STL – Standard Tesselation Language

T_g – Glass Transition Temperature

TPEE – Thermoplastic Elastomer

TPU – Thermoplastic Polyurethane

UV – Ultraviolet

List of Figures

Figure 1 - Seven different additive manufacturing processes, adapted from [11]. 6
Figure 2 - First ever replicated machine next to its predecessor [16]. 7
Figure 3 - Schematic of the extruder head (adapted from [19]). 8
Figure 4 - Cartesian printers.; a) core XY; b) Y slider [21, 22]. 8
Figure 5 - a) Delta printer; b) polar printer [23, 24]. 9
Figure 6 - Samples with different perimeters (infill in red, outer perimeter in orange and inner perimeters in yellow). 10
Figure 7 - Sample with different printing orientations. 11
Figure 8 - Samples with different layer thickness. 12
Figure 9 - Samples with different infill patterns and densities (represented in red). 13
Figure 10 - SEM images of tensile fracture surface of samples with different bed temperatures [47]. 14
Figure 11 - Samples with different raster angles (infill in red). 15
Figure 12 - Schematic of some printing parameters [70]. 16
Figure 13 - Pyramid of materials according to their use. 18
Figure 14 - Example of a 23 a) design geometry and b) test matrix [86]. 22
Figure 15 - Design geometry of a) Box-Behnken and b) Central Composite Design [87]. 24
Figure 16 - Example of a contour plot. 27
Figure 17 - Example of a response surface plot [85]. 28
Figure 18 - Spool of PEI 1010 used in the experiments. 29
Figure 19 - a) Initial disassembled printer and b) enclosure. 31
Figure 20 - Resistance added to the enclosure. 31
Figure 21 - Final printer assembly; a) some components of the machine; b) printer on the lab table. 32
Figure 22 - Failed parts; a) severe warpage; b) part detached from bed. 34
Figure 23 - ASTM D638 V geometry. 36
Figure 24 - ISO 527-2 1BA geometry. 36
Figure 25 - ISO 527-2 5 geometry 36

Figure 26 - Rectangle geometry. 36
Figure 27 - Results of the second standards test. 38
Figure 28 - Results of the perimeters No experiment. 38
Figure 29 - Inscribed, face centered and circumscribed CCD methods. 39
Figure 30 - Samples printing process cycle. 41
Figure 31 - NanoPolymer adhesive by VisionMiner. 42
Figure 32 - Filament in the oven overnight. 42
Figure 33 - Final specimens 43
Figure 34 - Tensile tests setup. 43
Figure 35 - DIC setup; a) speckled sample; b) camera setup. 44
Figure 36 - DIC; a) definition of interest zone; b) positioning of a digital extensometer; c) maximum strain before failure. 45
Figure 37 - Samples after the tensile strength test. 46
Figure 38 - Samples removed from the analysis. 47
Figure 39 - Example of a) low temperatures behavior and b) high temperatures behavior. 48
Figure 40 - Average tensile stress of each combination of temperatures. 48
Figure 41 - ANOVA table. 49
Figure 42 - Regression Model Equation and Model Summary. 50
Figure 43 - Normal Probability Plot of the Residuals. 50
Figure 44 - Fits and Diagnostics for Unusual Observations. 51
Figure 45 - Normal Plot of the Standardized Effects. 51
Figure 46 - Half Normal Plot of the Standardized Effects. 51
Figure 47 - Pareto Chart of the Standardized Effects. 52
Figure 48 - Contour Plot of Tensile Strength for Chamber temp. vs. Nozzle temp. 53
Figure 49 - Contour Plot of Tensile Strength for Nozzle temp. vs. Bed temp. 53
Figure 50 - Contour Plot of Tensile Strength for Chamber temp. vs. Bed temp. 53
Figure 51 – Surface Plot of Tensile Strength for Chamber temp. vs. Nozzle temp. 54
Figure 52 – Surface Plot of Tensile Strength for Nozzle temp. vs. Bed temp. 54
Figure 53 – Surface Plot of Tensile Strength for Chamber temp. vs. Bed temp. 55
Figure 54 - Factorial Plots of the Main Effects for Tensile Strength. 55
Figure 55 - Interaction Plots for the Different Factors Combinations. 56
Figure 56 - Optimized parameter values for maximum tensile strength. 56
Figure 57 - Tested samples with optimized parameters. 57
Figure 58 - Stress-Strain curve of samples with parameters combination 1 69
Figure 59 - Stress-Strain curve of samples with parameters combination 2 69
Figure 60 - Stress-Strain curve of samples with parameters combination 3 70
Figure 61 - Stress-Strain curve of samples with parameters combination 4 70

Figure 62 - Stress-Strain curve of samples with parameters combination 5 70
Figure 63 - Stress-Strain curve of samples with parameters combination 6 71
Figure 64 - Stress-Strain curve of samples with parameters combination 7 71
Figure 65 - Stress-Strain curve of samples with parameters combination 8 72
Figure 66 - Stress-Strain curve of samples with parameters combination 9 72
Figure 67 - Stress-Strain curve of samples with parameters combination 10 73
Figure 68 - Stress-Strain curve of samples with parameters combination 11 73
Figure 69 - Stress-Strain curve of samples with parameters combination 12 73
Figure 70 - Stress-Strain curve of samples with parameters combination 13 74
Figure 71 - Stress-Strain curve of samples with parameters combination 14 74
Figure 72 - Stress-Strain curve of samples with parameters combination 15 74

List of Tables

Table 1 – Average printing speed of different FDM filaments [37-46]. 12
Table 2 - General purpose materials characteristics [75]. 18
Table 3 - Engineering grade materials characteristics [75]. 18
Table 4 - Ultra-performance materials characteristics [38-45]. 19
Table 5 - PEI filament physical properties [45]. 30
Table 6 - PEI filament recommended printing settings [45]. 30
Table 7 - Baseline working temperatures based on manufacturer's data [42-45]. 33
Table 8 - First set of temperatures levels. 33
Table 9 - Analysis of the effect of bed temperature. 34
Table 10 - Final parameters levels for the experiment. 35
Table 11 - Printing parameters for the first standards test. 37
Table 12 - Results of the first standards test. 37
Table 13 - Parameters levels combinations. 40
Table 14 - Printing parameters of the samples (PrusaSlicer). 41
Table 15 - Max stress of the optimized samples and its average. 57
Table 16 - Maximum Stress and Strain 75

1 Introduction

1.1 Layout

This master thesis is structured into five comprehensive chapters focusing on distinct aspects of the research. The following sections outline the organization and content covered in each chapter:

1. **Introduction** – In this chapter, a context for the addressed topic of this work is presented as well as a brief description of INEGI and the framework of this investigation on its operations.

2. **State of the Art** – A review of the FDM process and previous research done on the effect of printing parameters as well as assessment of the DoE methods and their different variations is performed in this section.

3. **Materials and Methods** – In this portion the material, machines and experimental techniques used are presented. Additionally, the pre-experimental investigation where the minimum bed temperature, standard and temperatures range used in the final experiment were defined is explained.

4. **Results and Discussion** – In this segment, the results of the experiments are displayed with a brief description followed by a discussion of the findings.

5. **Conclusion and Future Works** – In this final chapter, a series of conclusions derived from the study are drawn and future works and investigations are proposed based on the results obtained.

1.2 Context

In the last decades, manufacturing technologies have taken a leap into the additive manufacturing processes. This new branch opened new horizons for the way products are prototyped and produced. With capabilities such as faster manufacturing rates, reduction in wasted material, highly customizable process parameters and many other, AM techniques are expected to revolutionize the industry as it is and enable advancements in other areas of technology like the automotive, aerospace, and medical.

The FDM process distinguishes itself as the most popular AM process due to its ease to use and low cost. In this extrusion-based method the raw material, a thermoplastic in filament form, is melted and extruded through a nozzle in a layer-by-layer fashion until the final part is obtained. On its early stages, one of the main limitations of this technique was the lack of variety in the raw material, as just a few thermoplastics were able to be manufactured into filament shape and their mechanical capabilities weren't great. With time, more and more materials were made available in the market to a point where today, high-performance materials with mechanical properties compared to with some metals can be easily purchased by anyone.

Despite being considered easy to use, the FDM process is hard to master as the possibility of choosing the inputs of the printing parameters allows for the creation of the same part with different mechanical characteristics. Because of that, knowledge on the effect of each parameter on the final behavior of the manufactured component is fundamental in order to obtain the desired attributes.

With this in mind, the objective of this work is to investigate the printing parameters, namely the nozzle, bed, and chamber temperatures, on the final properties of PEI printed samples and determine their optimum values. To achieve this goal, a Design of Experiments methodology was implemented through the use of Minitab statistical software. The material, printer, and testing machines necessary for the completion of the work were supplied by INEGI and the investigation was carried out in their facilities.

1.3 The project and INEGI

INEGI - *Instituto de Ciência e Inovação em Engenharia Mecânica e Engenharia Industrial* -, is a Technological Interface Centre, created in 1986 and dedicated to carrying out technology-based research and innovation activities, technology transfer, consultancy, and technological services oriented towards the development of industry and the economy in general.

As 3D printing is becoming an increasingly important production process in the current context and, in order to remain at the forefront of knowledge about this technology, INEGI has developed a specialized additive production equipment for high performance plastics, such as PEI or PEEK. In this sense, the goal of this work was the planning and execution of a Design of Experiments (DoE) to optimize the printing parameters of this machine for the production of PEI parts.

UMAI - *Unidade de Monitorização Avançada e Integridade Estrutural* - the company unit that proposed this subject, had as the ultimate goal the exploration of the capabilities and *modus operandi* of their previously developed 3D printer, along with optimizing the printing parameters used in high-end materials. The final objective was to enhance the printer's performance, enabling it to produce functional parts and prototypes effortlessly whenever required while also defining the best parameters when dealing with PEI. By leveraging these advancements, the unit can streamline its operations and achieve greater efficiency.

1.4 Objectives

As mentioned earlier, the core purpose of this dissertation revolves around the planning and execution of a Design of Experiments (DoE) with the objective of optimizing the printing parameters of the 3D printer for efficient production of PEI parts. To achieve this goal a series of steps had to be sequentially taken. Among those, the more significant were:

1. Review of the state of the art, in order to gain knowledge and understanding of the fusion deposition modelling process and the influence of different printing parameters on different materials, already researched in previous works, as well as a literature review of the DoE methods and capabilities that could be used for the analysis.

2. Upgrade and reassemble of the previously built 3D printer present at INEGI facilities allowing the unit to produce parts using high-end materials.

3. Implementation of a DoE model with the final goal of obtaining a regression model capable of predicting the mechanical properties of parts and determining the optimal working parameters.

4. Process parametrization to define the best conditions for the success of the experiments namely the temperatures range and the most appropriate standard and base parameters.

5. Printing of the PEI samples using the custom-built 3D printer following the pre-defined order of parameters combinations gaining knowledge and practical experience in the additive manufacturing field.

6. Testing of the samples through the use of a tensile strength testing machine and digital image correlation software.

7. Evaluation of the results obtained from the registered load and strain and processed using Minitab statistical software.

2 State of the art

2.1 Additive Manufacturing

As it happens with many other breakthrough technologies, additive manufacturing wasn´t invented by a single man but conceived by many independent inventors from around the world at approximately the same period in history. In 1981, Hideo Kodama from the Nagoya Municipal Industrial Research Institute came up with two 3D manufacturing technologies. Three years later in 1984 a similar version of the technology was patented by Alain Le Méhauté, Olivier de Witte, and Jean Claude André of the French General Electric and CILAS companies. Only three weeks after, Chuck Hull, an inventor from the United States filled his own patent for a 3D printing technology called stereolithography. Despite all the contributors, Chuck Hull became widely known as the inventor of 3D printing once French General Electric and CILAS abandoned the patent [1].

In 1987 the STL file format was developed by 3D Systems Inc. and quickly became the standard for every additive manufacturing process. The method of creating an STL file mostly involves converting the continuous geometry included in a CAD file into a header, a set of small triangles, or a triplet list of coordinates for x, y, and z together with the normal vector for the triangles. This method is imprecise since triangles are never able to fully represent curved surfaces and edges but, by elevating their number, they get closer to reality. Vertices cannot share a point with a line, and the right-hand rule is used to distinguish between inner and exterior surfaces. Such simple and fast way to transform 3D objects into data lead to a huge leap in AM technologies [2].

Traditional manufacturing techniques such as CNC machining and lathes are based on subtractive principles, starting with a block of material from where material is removed until the final part is obtained. Although still used for most of the parts in industry, some of its drawbacks such as waste of material, somewhat slow processing times and the difficulty of obtaining more complex parts allowed the rise of additive manufacturing that has become more and more popular due to its capability of solving those problems.

Despite the different additive methods used to obtain the final part, almost all of them are based on a layer-by-layer process. First, a 3D model of the object must be made using computer aided design or 3D scanning, then, using specific software this model is sliced into individual layers and a code (usually called g-code) responsible for the toolpath is generated. Finally, depending on the used technology, the machine employs a certain method to duplicate the model in the real world starting from the base slice and continuing until the object is finished.

From the 1980s until today AM technologies have evolved a lot and are now divided into several different methods of producing parts using a variety of materials such as fluids, waxes, powders, filaments, etc. Still, most of them remain based on the addition and bonding of material in a layered fashion way. Since then, the additive manufacturing technologies have been known for their breakthroughs in manufacturing for various reasons such as the capacity

to automate production, quickly validate a prototype and produce complicated geometries that are impractical to manufacture with conventional techniques.

According to the ISO/ASTM52900-15 [3] standard of AM process categorization there are seven different types of additive manufacturing process (Figure 1): Sheet Lamination, Direct Energy Deposition, Powder Bed Fusion, VAT Polymerization, Binder Jetting, Material Jetting and Material Extrusion. For contextualization purposes, a short summary of each of these methods is given in the following paragraphs.

In the sheet lamination process, also known as LOM, a cutting tool, pressure or heat and an adhesive is used to layer and connect sheets of material, usually paper or plastic but also composite materials and even metals. Each layer is bonded together and cut into shape until the desired part is achieved. Models, prototypes, and patterns required for casting are frequently produced using this method [4, 5].

Direct Energy Deposition is a process where a thin powder is melted and fused all at once and deposited onto a substrate using a laser or electron beam. The technique is used in the automotive and aerospace industries as several materials such as metal, ceramics or polymers can be used to create parts. DED can also and is often used for maintenance of bigger parts and is able to achieve high quality mechanical properties [4, 6, 7].

In powder bed fusion, a thin coat of metallic or plastic powder is spread onto the build platform for each layer and a laser or electron beam is responsible for melting and fusing that powder in a specific pattern. The process is then repeated until the final part is obtained. Although a costly alternative, the obtained parts have almost the same properties as the cast ones but with the possibility of greater complexity [4, 8, 9].

In the additive manufacturing technique known as Vat polymerization, a liquid photopolymer resin is cured by a light source, usually a UV laser or projector, to produce a solid part. The building platform is submerged in liquid resin and the light source is responsible for selectively curing the designated regions to obtain the final part, the platform then moves up one layer and the process goes on. After finished, the part must undergo some post-processing operations like cleaning and support removal but is able to achieve high geometric precision [4, 10].

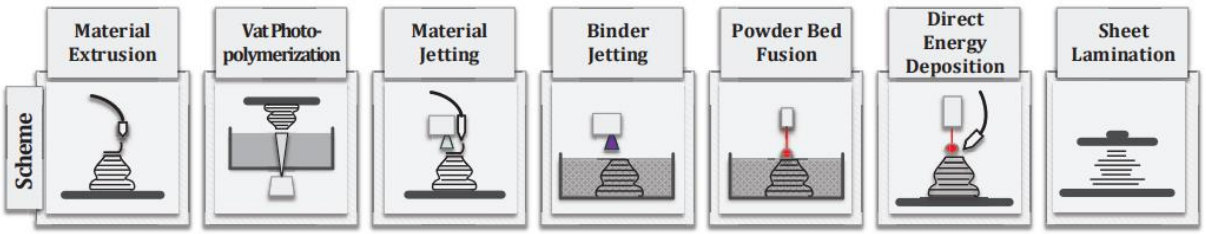


Figure 1 - Seven different additive manufacturing processes, adapted from [11].

Binder jetting is one of the non-fusion-based technologies in which materials are printed without using a power source to heat them up. In this method a layer of powder is deposited onto the printing bed and then a binder is applied (typically a liquid polymer) along the path laid out in the CAD file, to consolidating the powder and joining the newly printed layer to the ones that came before. Finally, the part undergoes post-processing after extraction to attain the necessary qualities. Binder jetting 3D printing have great advantages such as allowing flexible modifications on microstructure, material composition, and dose in the printed products and has applications in various industries, including construction, pharmaceuticals, and medical modeling [4, 12, 13].

Material jetting is a process where the small droplets of the material, a liquid photopolymer or wax, are deposited layer by layer to obtain the final part. The printer head(s) move back and

forth over the build platform depositing the material that is then cured by a UV light. The process is known for its high accuracy and for producing multiple objects on a single print, but the mechanical properties are not great, and some post processing is often needed [4, 14] .

Finally, we have material extrusion, an additive manufacturing process based on the use of thermoplastics that are heated up, extruded through a nozzle, and deposited layer by layer. The machines used in the process can come in many forms, but they all share some core components, a bed, where the first layer of material is deposited, and the extruder head, where the material is melted and extruded in a pre-determined tool path in order to build the object from the bottom up. The used thermoplastics usually come in filament format, but pellets are also common. This method is known for its speed, ease to use and availability in the market but also for the anisotropy of the produced parts and limitations in terms of materials and surface finish [4, 15].

2.2 FDM technology

One of the most know and used material extrusion process, Fusion Deposition Modelling (FDM), also known as Fused Filament Fabrication (FFF), as the first one is a trademark name used by the company Stratasys, is nowadays the most popular additive manufacturing process due to its ease of use and open-source movement that made it available to everyone. Back in 2004 Professor Adrian Bowyer started the project RepRap, short for replicating rapid prototyper, with the goal of making 3D printing accessible for everyone by sharing all the information online under an open-source license. Professor Bowyer based himself on the phenomenon of symbiosis where the people would help to spread the machines and would receive printed parts as reward [16, 17].

3D printers were not a new process at the time, but a commercial one sold for around 20 000 euros and could not replicate itself. In 2007 they were able to produce the first machine, the Darwin, with full capability of printing around 50% of its own parts, making it possible to build a new machine with only a 500 euros investment (Figure 2). The project continues on, with machines capable of producing 70% of their own parts [16, 17]. Due to that, commercial machines also had to adapt and reduce their costs to a point where a brand-new hobbyist machine can be found for around 100 to 250 euros.

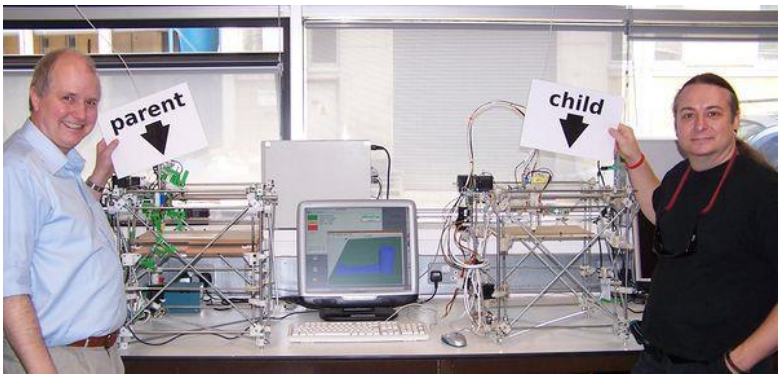


Figure 2 - First ever replicated machine next to its predecessor [16].

The first step in the FDM process is to create the called g-code, a series of commands that control the movements of the machine. Through a software, commonly known as slicer (because it slices the part in layers), the g-code can be created based on a geometry file (STL, 3MF, etc.), and some of the parameters such as speeds and temperatures as well as infill patterns and more advanced aspects of the process can be controlled.

In the printing phase, the used material, usually a thermoplastic in filament form, is pulled by a stepper motor into the extruder head. This pull system can be a Bowden tube setup, where the

motor is fixed and the filament must pass through a plastic tube in order to reach the extruder head, or a direct drive setup, where the motor moves along the extruder head and feeds the filament directly.

The extruder head is composed of an extrusion mechanism responsible for feeding the filament to the head. After that it enters a channel, usually known as heat-sink, that acts as a barrier between the hot and cold parts of the extruder to maintain the filament in the correct state. Following the filament´s path we have the heating block, responsible for melting the filament and finally the nozzle with a calibrated diameter [18]. A schematic of the extruder head can be found in Figure 3.

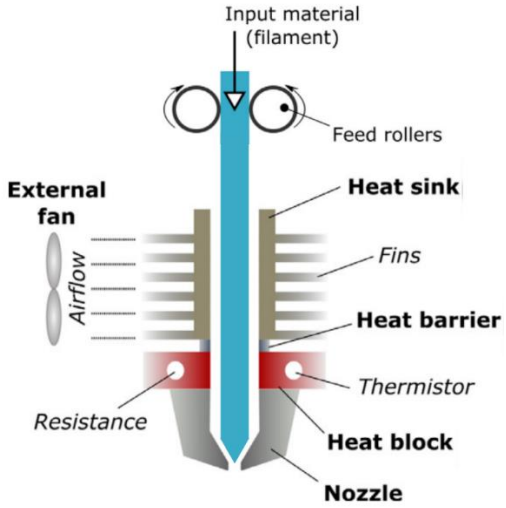


Figure 3 - Schematic of the extruder head (adapted from [19]).

As the filament enters the heated chamber it is also responsible for pushing the semi-molten material in front of it, generating pressure and extruding the polymer through the nozzle at a constant rate. The nozzle diameter can also be changed, the most common being 0.4mm. Smaller nozzles allow for fine details at the cost of longer printing time while larger ones print faster but with more evident layer lines and less details [18].

The extruder head movement, in order to deposit the material on the XY plane, is done differently depending on the machine hardware. Cartesian 3D printers are the most common ones and use the cartesian coordinate system to define the toolpath (Figure 4). They can be divided in core XY printers where the head moves in the XY plane and the bed only moves in the Z axis, and Y sliders (bed slingers) printers where the head moves in the XZ plane and the bed slides on the Y axis [20].

a)

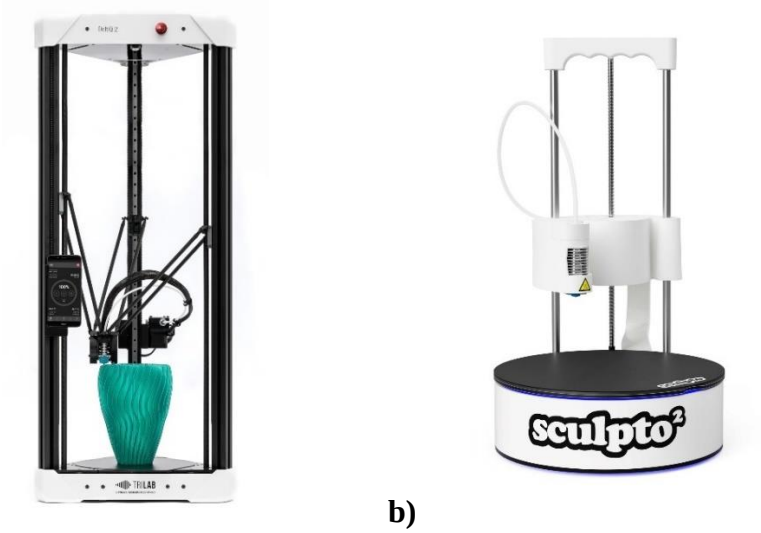


b)



Figure 4 - Cartesian printers.; a) core XY; b) Y slider [21, 22].

Delta printers also use the cartesian coordinate system but have their bed fixed at the bottom and an extruder head fixed at 3 triangular points that can move in all directions making the extruder head the only moving part (Figure 5 a). Lastly, we have the less common polar printers that are based on the polar coordinate system with a bed that spins around the Z axis, and combined with the head movement follow a polar coordinate g-code to obtain the parts (Figure 5 b) [20].



a) **b)**

Figure 5 - a) Delta printer; b) polar printer [23, 24].

There are also some novelty prototypes of machines that make use of robotic arms to move the extruder head in all directions and multi-axis machines capable of creating parts without the need of support structures, but those are not widespread and available on the market.

Even with different hardware two other components are present in most of the commercially available 3D printers. The bed, which can be heated or not, facilitates first layer adhesion, and can be made of different materials such as glass or PEI sheets. The other component, the cooling fans, are used to quickly cool the material extruded through the nozzle. Pointed at the exit of the nozzle, their purpose is to maintain geometric accuracy, apart from some high-end materials where cooling fans are not used as they would induce too much warpage due to thermal contractions.

After the first layer is deposited on the bed, the printer moves on to the next layer, following the pre-determined path given by the g-code, and the process continues on until the part is completed.

2.2.1 FDM parameters and their influence

Besides hardware variations, what really makes the FDM process stand out is the ability to control the properties of the manufactured part locally and quickly change those properties without changing the part itself [25]. This is due to the different combinations of printing parameters that are pre-defined during the slicing phase in the software.

The values chosen for the different parameters in FDM can in many cases be more significant than the properties of the material itself, which is contrary to the vast majority of manufacturing processes. The same part, made from the same material and in the same machine can have completely different properties [25].

The effects of each property and even more important the effect of how different properties interact with each other has been extensively studied by many in the last two decades. Thus,

this chapter intends to introduce the parameters and summarize some of the findings on the effect of these different inputs.

Perimeters

In the FDM technology the term perimeters refer to the outer boundaries or walls that outline a printed object, as can be seen in Figure 6. In the slicer it is possible to define the number of perimeters from 0 up to a layer composed only by them. Perimeters are widely known for increasing the strength of the part since they are aligned with the direction of the loading, but they also are more time-consuming and can lead to stress concentration problems.

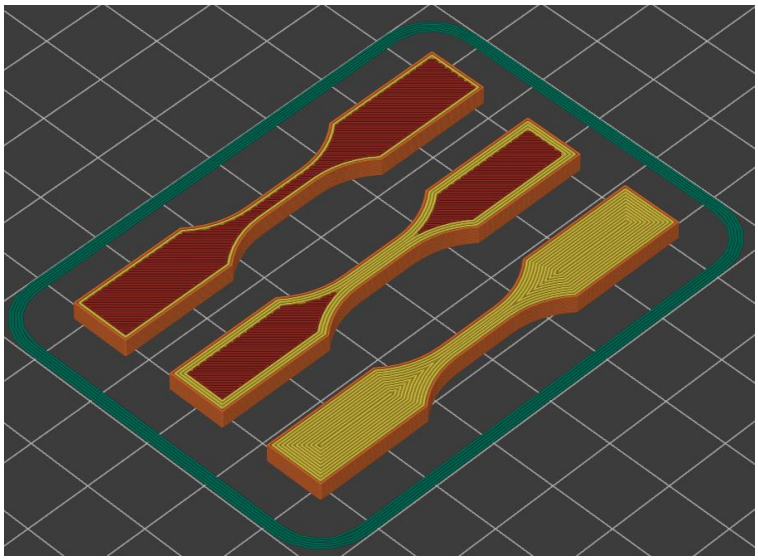


Figure 6 - Samples with different perimeters (infill in red, outer perimeter in orange and inner perimeters in yellow).

Ahn *et al.* [26] mentioned that they have a positive effect on the tensile strength and are important because they limit stress concentration at notches. The same authors also mentioned that they improve the surface finish as the part outer shape becomes well defined. Later on, Croccolo *et al.* [27] performed a study on the effect of the number of perimeters on ABS and concluded that with its increase there was also an increase in tensile strength and stiffness. For PEI, Gebisa *et al.* [28] also stated that the increase in the number of perimeters is beneficial to the flexural properties of the printed parts since those loads are mainly supported by those contours.

Printing Orientation (Build orientation)

Printing orientation is the definition of how the part is positioned on the print bed while it is being manufactured. This orientation is usually based on the X, Y and Z axes and must be considered since they heavily influence the properties of the parts as well as the printing time and the necessity of support structures. An example of some different printing orientations for the same sample can be seen in Figure 7.

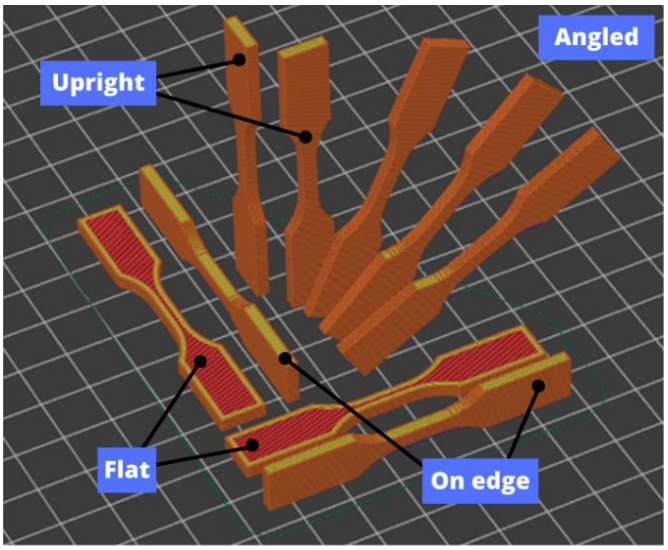


Figure 7 - Sample with different printing orientations.

Onwubolu *et al.* [29] mentions that parts printed in PLA parallel (flat) to the build plate have higher tensile strength. In a deeper analysis with ABS, Chacón *et al.* [30] found out that flat (XY) and on edge (XZ or XY) printing orientations have the highest tensile and bending strength since the layer lines were parallel to the loading direction causing a trans-layer failure instead of an inter-layer failures, that were observed in specimens printed in upright orientation. The same results were also found by Sood *et al.* [31] through the use of response surface methodology and Hernandez *et al.* [32] although the last one also concluded that depending on the application, building orientation may not make a huge difference on the strength, stiffness, and toughness of the part.

Górski *et al.* [33] defined a range of orientations where ABS parts change their failure behavior from "brittle" to "yield point" which was again explained by a thread fracture mechanism or a layer disjoint mechanism. For PEI, Forés-Garriga *et al.* [34] and Zaldivar *et al.* [35] reached a similar conclusion about the failure but the on edge orientation, such as the one on Figure 7, presented the highest mechanical properties. Byberg *et al.* [36] reached a similar conclusion that edge built have a higher tensile strength, but the highest flexural and compressive strength were, like the previous materials, higher for the flat built. That fact, as explained by the author, was caused by a greater number of contours when the specimen was printed on the edge orientation since its width is longer than its thickness.

Printing Speed

Printing speed is the general term referring to the speed in the XY plane during the print. This speed is usually particular for the different sections and instructions during the print, for example, the speed while the head is traveling i.e., not extruding any material is usually much higher than when it is doing perimeters or infills. Furthermore, the speed must also be adjusted according to the material (Table 1). For instance, ABS, PLA and PETG can all be printed in the range of 30 to 90 mm/s [37] while PEEK and PEI can only go up to 50 mm/s [38-45].

Table 1 – Average printing speed of different FDM filaments [37-46].

Filament	Speed (mm/s)
PLA	30-90
ABS	40-80
PETG	40-90
PC	30-70
TPU	10-30
PEEK	15-30
PEI	15-50

Printing speed is also known for affecting the print quality of parts. High speeds tend to produce parts with poor surfaces but have the advantage of taking less time and low speeds have the opposite effect. Too low or too high speeds can affect not only the surface but also the structure of parts as this parameter is also related to the inter layer bonding of filaments. If the head moves too quickly the extrusion volume of melting material is reduced and the printed part loses stability as the extruded material doesn´t have enough time to weld with surrounding printed components. If it moves too slowly over extrusions may occur which can lead to imperfections and layer issues [47].

For PLA, Li *et al.* [48] verified that an increase in printing speed leads to a decrease in tensile strength and bonding between the deposited filaments. On an extensive study of the influence of 13 different parameters on the tensile strength of ABS specimens, Qureshi *et al.* [49] ranked printing speed in 5th place only behind component scale, number of perimeters, raster angle and build plate temperature. Peng *et al.* [47] while studying the effect of 4 parameters on PEEK, CF/PEEK and GF/PEEK (a combination of PEEK and carbon fibers and glass fibers) concluded that with the increase in speed from 5mm/s to 25mm/s the tensile, flexural and impact strength of all 3 materials decreased and massive voids were observed through microscopy of the fractured surfaces.

Layer Thickness

Layer thickness is the parameter that defines the heigh increase in the Z axis between each layer. Smaller values of layer thickness can produce parts with better surface finish since the layer lines are less noticeable but in exchange greatly increase the printing time. In Figure 8 it is possible to see that the same sample can be produced using different layers. The usual value for this parameter is 0.2mm but depending on the application it can usually go from 0.08mm to 1mm. It is also highly dependable on the used nozzle diameter, as values above 80% of the diameter are not recommended [50, 51].

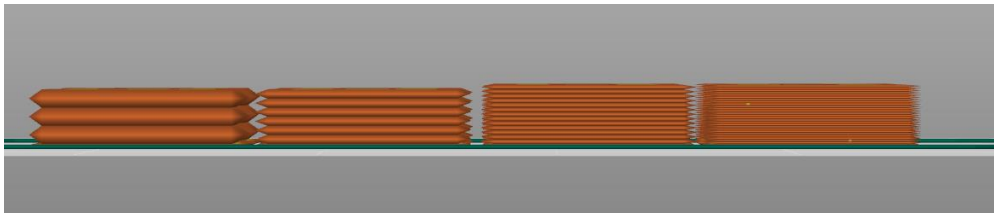


Figure 8 - Samples with different layer thickness.

The literature review of the effect of this parameter on the mechanical properties of the parts is very similar for all the most common materials. For PLA Li *et al.* [48] verified that the layer thickness has a predominant role in the bonding of the deposited material and studying the temperature profile of the specimens during the print concluded that smaller layer thickness enhance the bonding degree and thus the tensile strength of the part. For the same material, Chacón *et al.* [30] also came to the same conclusion, except for parts printed in the upright orientation that were stronger with bigger layer thickness since it proportionated less layers and hence less places for inter layer failures.

For ABS, a number of researchers [29, 52-54] all reached the same conclusion, that reducing the thickness increases the mechanical properties due to better diffusion between layers. Weinmann *et al.* [52] also suggested that a combination of high temperatures and small layer thickness is even more beneficial. Rankouhi *et al.* [53] even uses a functional part, an A-frame, and obtained similar results. On the other hand, Sood *et al.* [54] stated that with smaller thickness there are more heating and cooling cycles which generate residual stresses in the part.

In the engineering materials category Pandelidi *et al.* [55] verified that a combinations of small layer thickness and negative air-gar yield the best results for PEI. Similar results were also achieved by Peng *et al.* [47] using PEEK and GF/CF PEEK. Wu *et al.* [56] differed from the previous and concluded that the best layer thickness for PEEK is 0.3mm verifying a decrease in tensile strength for 0.2mm and 0.4mm.

Infill

The infill parameters are related to how the interior of the part is filled. In FDM each layer starts with the perimeters and then the interior part. How this interior is filled can be determined in terms of pattern and density. The variation of these two parameters affects the printing time, material consumption, structure of the part and hence its mechanical properties. It has been widely discussed by many authors that infill patterns that align with the loading direction are able to give the parts more strength. The density can go from 0% which corresponds to a hollow part, up to 100% which corresponds to a solid part. Some of the infill patterns present in PrusaSlicer (the software used in this work) and the difference in density can be seen in Figure 9.

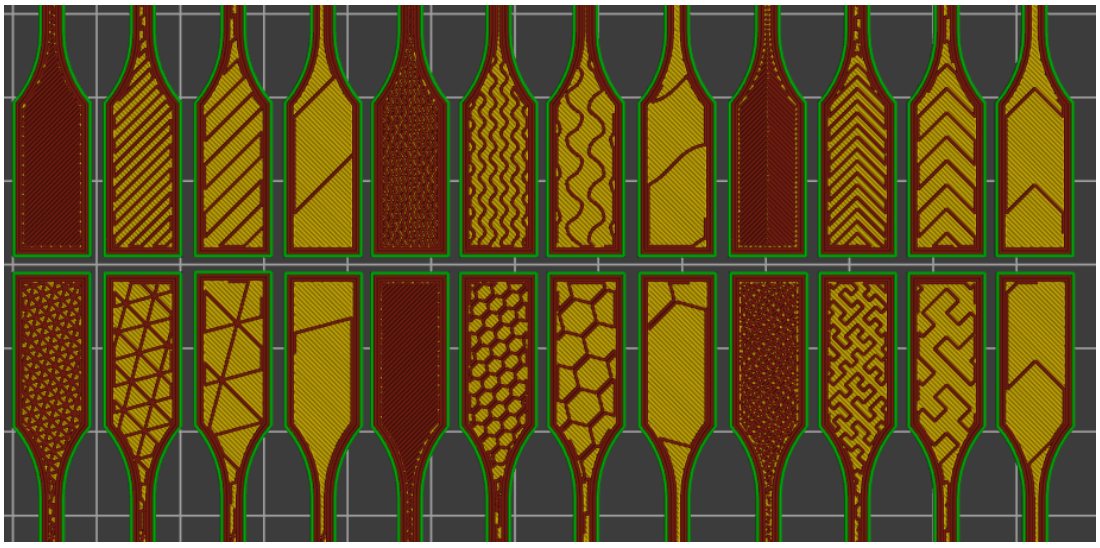


Figure 9 - Samples with different infill patterns and densities (represented in red).

In their results, Baich *et al.* [57] showed that low density settings produced cost saving parts with comparable strength performance to high density for tensile loading of ABS parts. Low density had considerable cost reductions for bending applications with no strength loss.

Additionally, it was discovered that although having a similar cost of production, the completely solid infill design had a better strength than the high-density infill design. A linear link between material volume and cost-strength performance was found during compression testing.

Also studying the effects of infill density and patterns on ABS, Qureshi *et al.* [49] concluded that those were almost the least relevant parameters out of the 13 studied. Nevertheless, Mahmood *et al.* [58] stated that an increase in density is justified since it produces more rigid and stronger parts. Chadha *et al.* [25] Compared the influence of three different infill patterns for PLA, grid, triangular and honeycomb and concluded that triangular and honeycomb exhibit better tensile strength and better flexural strength.

Bed Temperature

After being extruded, the plastic that has come out of the nozzle quickly cools, contracting, causing internal stresses, and losing its ability to adhere to other surfaces. To prevent these problems, heated beds were added to most of the available 3D printers nowadays. The heated bed guarantees a better adhesion of the first layer giving more stability to the whole print. It also tries to prevent warping of the parts that usually occur due to big temperature gradients [50].

The temperature of the bed must be adjusted for the different materials, as they have different melting and glass transition temperatures. Although very important for the whole process, the effects of the bed temperature on mechanical properties of the parts have yet to be extensively studied, being mentioned by just a few authors.

Spoerk *et al.* [59] studied the adhesion forces of ABS and PLA with a custom setup and concluded that for both materials increasing the bed temperature also increases the adhesion force. A great increase was observed by the authors when nearing the materials glass transition temperature (T_g) and a decrease in force right after. A very similar result was obtained by Chadha *et al.* [25]. Also for ABS, Qureshi *et al.* [49] considered bed temperature the 4th most important parameter for tensile strength out of the 13 studied. For PEEK, Xiaoyong *et al.* [60] achieved the highest tensile strength and fracture rate combining the maximum bed temperature and ambient temperature. Similar results were also observed for CF/PEEK and GF/PEEK studied by [47] that through SEM images (Figure 10) verified a better inter layer bonding when using higher bed temperatures.

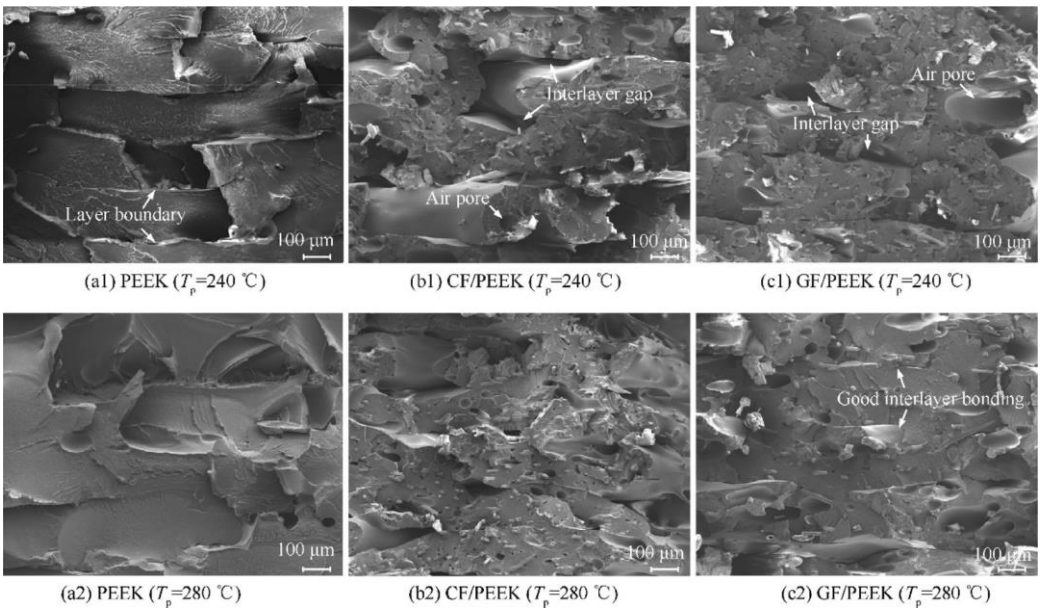


Figure 10 - SEM images of tensile fracture surface of samples with different bed temperatures [47].

Nozzle Temperature

Thermoplastic materials have the ability to melt and be reshaped many times due to their unique chemical structure and physical properties. 3D printing takes advantage of those properties by submitting them to controlled temperatures in order to shape them in the desired form.

Those temperatures are often called nozzle temperatures and refers to the temperatures of the heated zone of the extruder head responsible for partially melting the thermoplastic to a point where it is soft enough to be extruded through the nozzle and quickly solidify right after.

Those temperatures can greatly influence the geometric dimensions of the part as well as its mechanical properties. With higher temperatures, the plastic becomes more viscous and can more easily bond to the previous layer. On the other hand, excessively high temperatures are not recommended since they can induce temperature related problems and even burn the material. Temperatures lower than the recommended are also not good for the part as the material deposited is not able to bond with the previous layer, generating a weak part prone to delamination problems [50].

With regard to nozzle temperatures, Peng *et al.* [47] discovered that increasing the temperature of PEEK components from 400ºC to 440ºC improved their tensile and flexural strength due to stronger interlayer bonding that resist tensile and bending loads as a result of better material formability and melting fluidity at higher nozzle temperatures.

For PEI, Jiang *et al.* [61] concluded that as it plays a significant role in determining the bonding quality and directly influences the mechanical properties of the finished part. A nozzle temperature that is moderately high promotes the improvement of the mechanical properties of fabricated FDM. On the other hand, if the nozzle temperature during printing is too high, it may melt and destroy an adjacent layer.

Using more common materials such as ABS and with small temperature variations of 10 to 20 degrees, Weinmann *et al.* [52] stated that the nozzle temperature only has influence when combined with layer thickness and other investigators concluded that its effect is insignificant to the final result [26, 49, 62].

Raster Angle

Raster angle refers to the angle at which the filament is deposited with respect to the X or Y axis and sometimes is also defined in relation to the loading direction. Although important in all types, it usually has more impact on parts that have a linear or zigzag infill pattern. The raster angle has a great impact on the mechanical properties of the parts and has substantial influence on their mechanical anisotropy. Some examples of different raster angles can be seen in Figure 11.

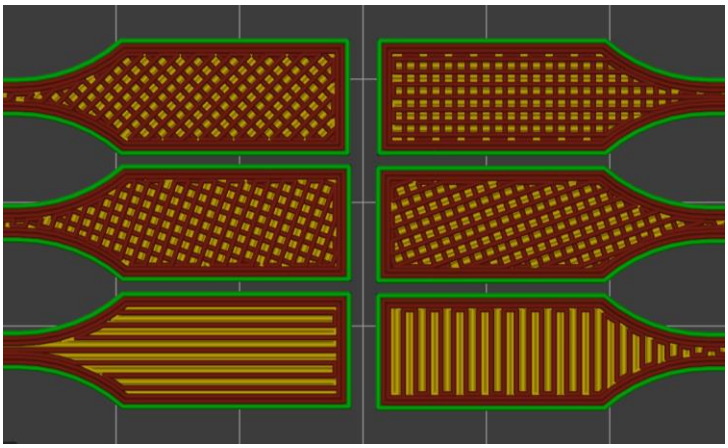


Figure 11 - Samples with different raster angles (infill in red).

Many software programs feature a zigzag pattern with a default raster angle of 45º/-45º as their default, although alternative configurations offer different benefits and drawbacks. This parameter has been vastly studied by many researchers in many different materials since it affects how the part behaves in different load conditions. For instance, for PLA, Tymrak *et al.* [63] used different printers and slicers and concluded that a 0º orientation (aligned with the loading direction) is far superior in terms of mechanical properties than a zigzag one. Liu *et al.*, [64] through statistical analysis stated that the raster orientation has the greatest influence on the final properties and again that the 0º raster achieved the best results.

For ABS, all the research reached the conclusion that filaments deposited parallel to the load directions are able to achieve greater tensile, flexural and impact strengths as well as fatigue life, when compared to any other orientation [26, 53, 54, 63, 65-68]. Sood *et al.* [54] also observed that although parallel lines yield the best result they are also responsible for creating stress accumulations and distortions since they are longer. Durgun *et al.* [67] explained this phenomenon based on the bonding of the deposited material, that is much stronger in the intra-layer region, i.e., in the deposited bead, that in the inter-layer region.

For the high-end materials, the same results were also obtained. Wu *et al.* [56] obtained better properties for 0º/90º orientation but recognized that it was due to the parallel aligned filaments. Different blends of PEI all reached the same results with higher loads supported by using angles parallel to the loading direction [28, 34, 55, 61, 69].

Air Gap

Air gap is another important parameter as it influences the bonding between the previous layer and the new one. It refers to the spacing between the deposited filament lines within each layer. Usually, this value is defined as 0 in the default setting of the machines, so that the deposited material only touches the previously deposited material but, in reality, a small air gap is always formed. If set to negative values, it will assure that the new filament overlaps with the old one and strongly bonds but this can lead to overfills. Adjusting this parameter can greatly influence the overall performance of the part and although it can be a very machine and software related parameter it is important to study its influence.

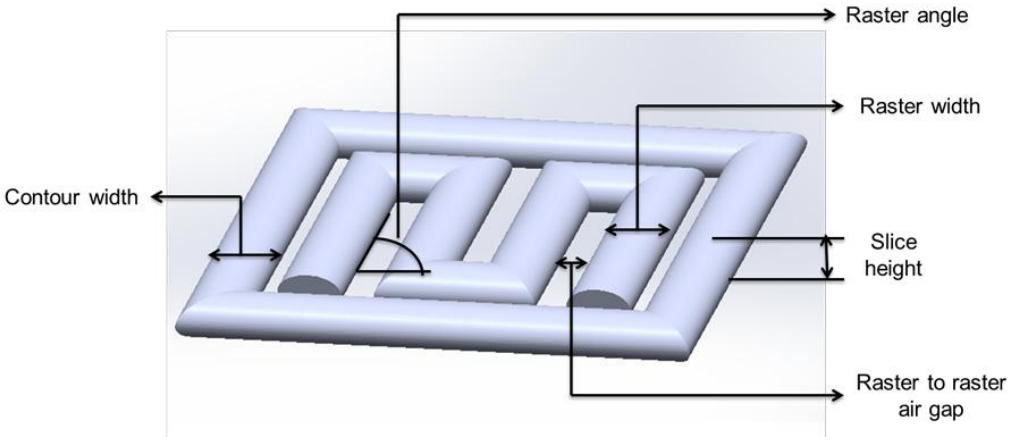


Figure 12 - Schematic of some printing parameters [70].

For ABS Li *et al.* [48] stated that a 0mm air gap improves the diffusion between adjacent raster but decreases heat dissipation and total bonding area while Weinmann *et al.* [52] maximized the mechanical properties of the parts using a negative air gap . Rankouhi *et al.* [53] through microscopic inspection of the fracture zone revealed that smaller air gap to material ratio can be the main factor contributing to higher strength and Ahn *et al.* [26] consider the air gap one

of the most relevant factor when it comes to tensile strength obtaining, better results using negative values.

Using PC, Shojib *et al.* [70] was able to greatly improve the mechanical properties of parts by removing the air gap, and very similar results were observed by Schöppner *et al.* [69] and Gebisa *et al.* [28] using PEI where this last one concluded that it is one of the parameters with greatest influence on the flexural properties of the part. Pandelidi *et al.* [55] also verified that for different layer thickness, negative air gaps always yield greater tensile strengths, and suspected that the use of filament overlap with 0.0254 mm air gap results in the increased presence of material at the cross-section of the fabricated specimens, which could explain the results.

Chamber Temperature

One of the least studied parameters, as it is not present in many desktop printers, the chamber temperature refers to the controlled ambient temperature around the printed parts when the printer possesses an enclosure. For common use materials like ABS and ASA this control usually allows for better print quality but for some materials it is a must due to warping caused by temperature gradients within the parts.

Sun *et al.* [62] concluded that for ABS, increasing the envelope temperature has an important effect on raising the lower limit in the temperature profile of the deposited filament, what have strong effects on the mesostructure and the overall quality of the bond strength between filaments. Alvarez *et al.* [71] observed that with an increase of only 5 degrees, from 70 to 75ºC the empty zone volume decreases, which assures that a better bond between filaments was achieved.

Same results were also obtained for PEI, where Zaldivar *et al.* [35] noted that the chamber temperature have an influence on inter-layer adhesion thus influencing the overall strength and Forés-Garriga *et al.* [34] stated that the use of the thermal chamber reduces the temperature gradient between the deposited filament and the last layer built what strengthens the unions, improves mechanical performance, and decreases the degree of orthotropy. For PEEK, Xiaoyong *et al.* [60] achieved higher binding forces between layers and better mechanical properties by increasing the chamber temperature.

2.2.2 FDM materials

Besides process parameters, the selected material also has a role on the final properties of printed parts. In FDM, most used filaments are thermoplastics or thermoplastics infused with some other material, due to the ability of being melted and reshaped over and over.

Lack of variety in the materials that could be converted into filament was one of the early issues with FDM but, with the evolution of 3D printing technologies a wide range of different filaments and variants have emerged (Figure 13). Despite that, the materials that are most used by the general public are Polylactic Acid (PLA), Polyethylene Glycol Terephthalate (PETG) and Acrylonitrile Butadiene Styrene (ABS) (Table 2) [72] .

PLA is one of the simplest materials to print with. It is affordable and appropriate for beginners. It is commonly used to print precise models, figures, and rapid prototypes that do not require strong mechanical, chemical, or thermal resistance. It can be printed quickly and at low temperatures, and it does not warp significantly. PETG is also another easy to print affordable material but, with a relatively high tenacity and temperature resistance, it is suitable for printing technical parts. It does require a heated bed and unlike PLA is suitable for exterior use [73].

ABS, due to its high tenacity and temperature tolerance, is a technical material appropriate for printing mechanically stressed components. It is commonly used to create affordable, strong mechanical components for engineer applications, although due to significant warping during

printing, it does need a heated bed and an enclosure with controlled temperature is recommended [74].

Table 2 - General purpose materials characteristics [75].

Material	Nozzle Temp.	Bed Temp.	Enclosure	Tensile Strength	Price ($/Kg)
PLA	185-235 ºC	50-60 ºC	No	38-65 MPa	20-60
ABS	230-255 ºC	95-110 ºC	Recommended	30-47 MPa	20-47
PETG	215-270 ºC	70-90 ºC	Not required	33-53 MPa	23-115

Beyond the general-purpose materials, we can find engineering grade materials that offer better properties in exchange for being more expensive and more difficult to use. Those materials are suitable for engineering applications and highly customized functional parts. In this category, the most outstanding are PC (Polycarbonate) and Flexible (TPU) (Table 3) [76].

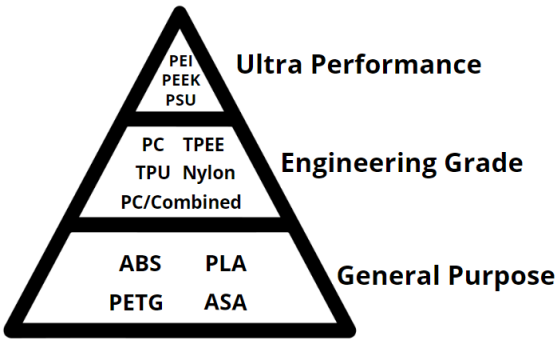


Figure 13 - Pyramid of materials according to their use.

PC is a high-tenacity, tensile-strength, and heat-resistant polymer. However, it is extremely difficult to print, requiring both a heated bed and an enclosure. Pure polycarbonate is not appropriate for 3D printing due to poor surface adherence and high thermal expansion with prints tending to distort and fracture. As a result, several additives are typically used to increase printability. This engineering grade material is typically used to print fully working items such as pulleys and hinges [77].

Flexible materials (TPU being the most known) are distinguished by their high degree of flexibility, tenacity, and chemical resistance. These materials are relatively uncommon and pricey, being only recommended for use with the correct parameters. They are often exceptionally resistant to wear (scratching), remain flexible even in cold conditions, and exhibit excellent resistance to various solvents with little to no shrinking or warping. Usually used to print spacing washers and other high-stress items, it is also capable of printing other functional parts that require some degree of elasticity [78].

Table 3 - Engineering grade materials characteristics [75].

Material	Nozzle Temp.	Bed Temp.	Enclosure	Tensile Strength	Price ($/Kg)
PC	270-275 ºC	110-115 ºC	Rquired	50-63 MPa	35-73
Flexible	220-260 ºC	40-85 ºC	No	8-25 MPa	34-84

Even beyond that we find ultra-performance materials, thermoplastics that have properties compared to aluminum. PEEK and PEI are two examples of materials of this category (Table 4). They have better thermal, mechanical, and chemical characteristics, being employed in high-end engineering applications that are subject to dynamic mechanical and thermal stresses. Nevertheless, they need special conditions to be printed correctly and achieve peak performance [76].

Polyether ether ketone, commonly called PEEK, was developed in 1978 by Imperial Chemical Industries and is often regarded as the best thermoplastic for high temperatures. It has a high glass transition temperature (T_g), a high melting temperature, and great flame resistance in addition to its semi-crystalline characteristic that yields significant mechanical resistance. Among its most valuable properties, it has a melting point temperature of 340ºC and a glass transition temperature of 144ºC. Despite being a difficult material to print, its mechanical qualities make it ideal for biomedical and aerospace engineering, as well as other demanding applications, which explains why it has been studied as a replacement for aluminum in certain aircraft parts [60, 79].

Table 4 - Ultra-performance materials characteristics [38-45].

Material	Nozzle Temp.	Bed Temp.	Enclosure	Tensile Strength	Price ($/Kg)
PEI	360-390 ºC	90 ºC+	Required	56-105 MPa	170-340
PEEK	370-440 ºC	100 ºC+	Required	100-105 MPa	320-740

Polyether imide, also known as PEI or by its brand name, ULTEM, is the second most used and researched high performance 3D printing material. It is an amorphous thermoplastic with a melt process comparable to PEEK but with significantly higher service temperatures. With a glass transition temperature of around 215 ºC, it can be employed in many structural applications requiring mechanical strength and thermal resistance. Among its main properties this material also displays excellent flame retardancy and low smoke generation which is why it is applied in biomedical, aerospace, and automotive industries. Nevertheless, its strengths are also its weakness as the high temperatures needed for its printing usually lead to difficulties and require the use of specific machinery and parameter selection [55, 61, 79].

As this material is known for its excellent high temperature resistance characteristics, it was viewed as the best choice for this work where the influence of different processing temperatures in the final tensile strength of the samples were investigated.

2.3 Design of Experiments

Nowadays, manufacturing companies conduct experiments to improve their understanding of various production processes. These studies generally consist of a series of trials or tests with measurable outcomes. Understanding process behavior, estimating the scope of variability, and analyzing its impact on the processes are essential for achieving continuous improvement in product or process quality. Experiments are used in engineering to estimate, verify or explore. Exploration requires examining process data, estimating entails figuring out how process variables or factors affect output performance, and verification involves approving the expected experiment outcomes [80].

It is of great interest to comprehend the effects that some key input variables may have on the final response performance. One of the classic methods for quantifying those effects is the one factor at a time approach (OFAT) where one input values is modified while all the others are

kept constant [80]. Although this method seems intuitive at first it possesses many disadvantages. Due to its reliance on the starting point, this approach rarely reveals the optimal conditions, and the results can be significantly influenced by it. It is challenging to differentiate between the actual enhancement and the "noise" resulting from the inherent variability of a system without repeating multiple reactions under identical conditions. Additionally, this method demands significant resources to acquire a limited amount of process-related data as it does not consider the interactions between parameters and solely their separate effects. One variable at a time experiments often prove unreliable, inefficient, and time-consuming, leading to false conclusions about the response and its respective optimal parameters [81].

In 1920 Sir Ronald Fisher at the Rothamsted Agricultural Field Research Station in London developed the Design of Experiments (DoE) method capable of overcoming the previous drawbacks. The first experience using the method was used to determine the effect of different fertilizers on different plots of land while still taking into account other factors such as soil condition, moisture on the soil, etc [80]. Since then, the method has been widely applied not only in the agricultural context but on every other field of science and industry, especially in chemical and mechanical investigations.

In contrast to the OFAT strategy and other earlier approaches, the DoE may assess how changes in one or more independent variables impact the result of the experiment while considering interactions between various variables. It is sometimes referred to be a very powerful statistical technique that makes it easier for researchers to plan, conduct, and evaluate studies methodically. Researchers can investigate the relationship between the variables impacting a process' output and the process's structure and organization using this technique, which provides a more thorough examination of the variables' effects [82].

Apart from being able to quickly detect the variation of parameters and their different interactions affecting the response yield and quality in an efficient manner, DoE methods also present other advantages such as the ability to eliminate researcher bias leading to the discovery of reaction conditions that were not previously considered [81], the greater control over extraneous variables, the possibility of replication of the experiments giving greater levels of confidence to the results and the capability of maximizing the amount of information that can be obtained for a given amount of experiments [82].

The DoE method can be used for three different objectives, first as a screening for the most influential parameters when they are not obvious, second when verifying the robustness of a design space, what can be seen as a more refined screening and finally when optimizing the final response where the experiment is already reduced to very few factors.

Although the DoE may seem tiresome and time-consuming at first glance, since the number of experiments is defined beforehand, it is important to know that the quality of the obtained results justify it. Still, in order to obtain those results, it is important to thoroughly follow a prescribed workflow of 7 steps [83] :

1. **Recognition of the problem/Definition of the objectives** – In this first step the main objective of the analysis must be defined: Frequently the goal is the optimization of a given process by maximizing or minimizing the response, but the robustness of a process can also be investigated to see the impact of small changes in a continuous factor.

2. **Selection of the process variables and their ranges –** The selection of the factors and their levels is of great importance to the overall analysis. The number of factors must be chosen carefully since it can greatly increase the number of runs and the resource usage.

Their range must also be chosen wisely. A good practice is to use existing process knowledge and pick low and high values that are meaningful and achievable.

3. **Selection of the response variables –** The responses are the outcomes of the experiment and are closely related to the defined objective. Multiple responses can be obtained from the same DoE without the need for extra runs. Their accuracy and reproducibility must be assured.

4. **Choice of the experimental design –** Choosing the experimental design is perhaps the most critical step in a DoE and depends on all the previously made decisions and influences all the next steps. This decision also affects the number of runs and the use of resources, thus an achievable design must be chosen while also considering their analysis method in order to obtain the desired results.

5. **Performing the experiments/Executing the design** – Also another crucial step, it must assure that every run is performed under identical conditions. The experiments must be done in the specified randomized order and in a systematic way. If maintaining the same conditions is not possible, statistical methods can be implemented afterwards to account for that variation.

6. **Analyze and interpret the data obtained –** Once the runs are over the obtained data can be used in statistical software capable of analyzing each response individually and, by selecting a mathematical model, it can fit the data into an equation capable of predicting the outcome of a theoretical set of conditions. The output of the analysis can also be obtained in a graphical manner with plots that facilitate the understanding of the process**.**

7. **Confirmation of the results –** The final step of the DoE is to confirm the projected responses obtained after the analysis since it is only a model prediction and must be verified experimentally to validate the results.

2.3.1 Main DoE methods

Most of the DoE method designs consist of a factorial combination of variables, still there are many designs that yield different results. The choice of an experimental design depends on the objectives of the experiments and the number of factors to be investigated, choosing the "correct" design entails figuring out the most effective method for sampling the range of alternatives. Based on their resolution and feasibility, the vast variety of methods can be divided into four main types: screening, factorial, Taguchi, and response surface each with their advantages and disadvantages.

Screening

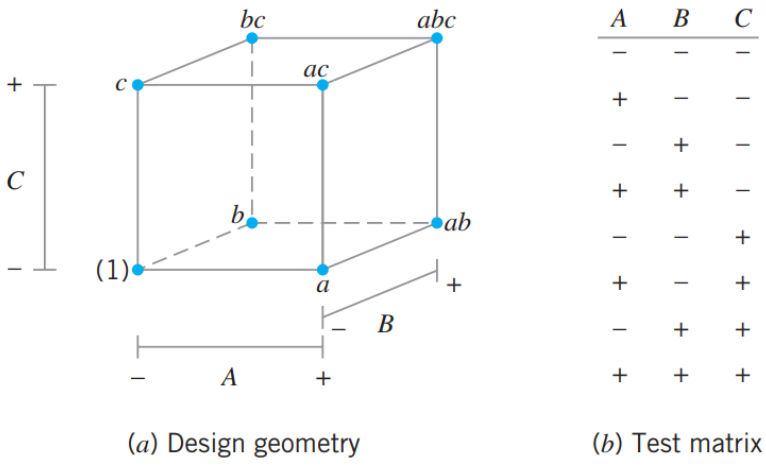
Screening methods are experimental approaches that are used when a large number of potential causal factors need to be investigated in order to pinpoint the most significant ones that might have an impact on one or more responses. The main objective of this type of design is to narrow down the field of investigation, defining right at the start what are the most relevant parameters. After that, other methods can be used to achieve more refined analysis [84]. The two main screening DoE methods are the definitive screening and the Placket-Burman.

Definitive Screening Design is the name used for the statistical technique used in experimental design to optimize processes using the fewest possible experiments. It is a form of design of experiments methodology that enables identifying from a vast number of parameters those that are crucial for improving a process response. In contrast to other screening approaches, it introduces a third (middle) level for continuous factors. The number of runs depends on the number of factors (k) being equal to 2k +1 and even though it is a relatively small number, the method is still capable of estimating two-factor interactions. All things considered, DSD is a good option for screening and even characterization of complicated processes that are influenced by a variety of factors and interactions [81].

The other most recognized and applied screening design, the Placket-Burman design (PBD) was developed in 1946 by R.L. Plackett and J.P. Burman [81]. In order to enable wise decision-making, it was created to enhance the quality control process that could be utilized to research how design parameters affect system status. The orthogonal arrays that Plackett and Burman developed are helpful for screening since they produce accurate estimates of the primary effects in the smallest design [84]. The minimum number of factors is seven which results in a design with 8 runs and can go up to 27 factors in a 28-run design, always following the k+1 rule. It is based on a pre-defined matrix of factor level combinations and with a run number multiple of 4. Although it is able to greatly reduce the number of runs when dealing with a large number of variables, PBD is only capable of considering their main effects on the response. Even so, assuming all interactions are insignificant in comparison to the few significant main effects, it is still thought to be very helpful for economically detecting large main effects [85]

Factorial

Factorial methods are the base for most DoE methods since they aim to investigate the effect of various system factors on the final response and consider how their interaction affects that response. As the name suggests, factorial experiments are based on the factorial operation that defines the number of runs on the experiment based on the number factors and levels being investigated, for example a 2^k experiment is composed by a k number of factors with 2 levels each. Figure 14 shows examples of a 2^3 design geometry and test matrix. This way, it can systematically design the investigation by pairing different factors in an orderly manner.



A	B	C
−	−	−
+	−	−
−	+	−
+	+	−
−	−	+
+	−	+
−	+	+
+	+	+

(*a*) Design geometry (*b*) Test matrix

Figure 14 - Example of a 2^3 a) design geometry and b) test matrix [86].

The first and most basic factorial method is known as the full factorial design (FFD) and is an experiment whose design includes every possible arrangement of the levels and factors that could be used. This design is powerful and, in comparison to other experimental designs, offers the most thorough insight into the behavior of the system as it takes into account the effects of all factors (main effects) and interactions among them [81] . On the other hand, with a slight

increase in the number of factors or the level of the factors being study the number of runs grow drastically and, in many cases, become impossible to perform making this method only advantageous when investigating a reduced number of variables.

When budgetary, time, or scientific restrictions prevent the execution of full factorial studies, fractional factorial experiments are crucial alternatives. Furthermore, fractional factorial experiments are frequently used in trials with a large number of factors since it is not essential to test all potential factor-level combinations in order to estimate the significant factor effects, which are typically the main effects and low-order interactions [87]. The secret of this method is confounding some of the effects with one another thus allowing for a reduced number of experiments. Although very practical, it is important to notice that fractional factorial experiments don´t always yield the most accurate results.

Taguchi

Developed by Dr. Genichi Taguchi and with a divided reception in the scientific community, the Taguchi methods are a series of different DoE methods that can be used by engineers and scientists without the need for prior advanced statistical knowledge. The methods are based on the use of orthogonal arrays making them simple and of easy adaptability to more complex analysis with large number of factors and levels and even a different number of levels for each factor. Due to its simplicity, it became the most commonly applied experimental design, both in industry and science. The orthogonal arrays distribute the factor levels in a balanced way reducing the number of experimental runs. Even so, it is capable of providing the desired results with the least amount of runs and with adequate precision [81, 88].

Taguchi orthogonal arrays are a set of design matrices that provide a systematic way of varying factors and levels in an experiment. There are a large number of orthogonal arrays available within Taguchi methods, each suited for different experimental scenarios. The specific number of Taguchi orthogonal array methods is not fixed as new designs can be developed or modified based on specific requirements. Most orthogonal arrays simply consider the primary effects, however other designs enable the estimation of particular interactions. Some of the designs can be used for screening, whilst others are better suited for thorough characterization and optimization.[81]

Response Surface

Response Surface designs were first developed by Box and Wilson in 1951 in order to take into account higher order interactions that couldn´t be analyzed through the previous methods presented. Although they offer a general understanding of the system behavior they are primarily oriented toward optimizing the system [81].

This method can characterize the relationship between response and a set of quantitative factors of interest by constructing a model of the response over the applicable range. The name response surface comes from the fact that it is able to generate a one- or two-dimension plot of the response as a function of one or more quantitative factors. After being plotted it can be analyzed to determine important characteristics of the runs and relevant tradeoffs [87].

Response surface methods are one of the most refined methods of statistical analysis since they can also determine the sensitivity of the response to the various factors. Also, different from factorial experiments, that are extremely useful in exploring the factor space, only RSM is capable of detecting curvatures i.e., higher order interactions between the factors [87]. The two main RSM methods are the Central Composite design method and the Box-Behnken designs (Figure 15), and they differ mainly in number of runs and the level of detail each one provides.

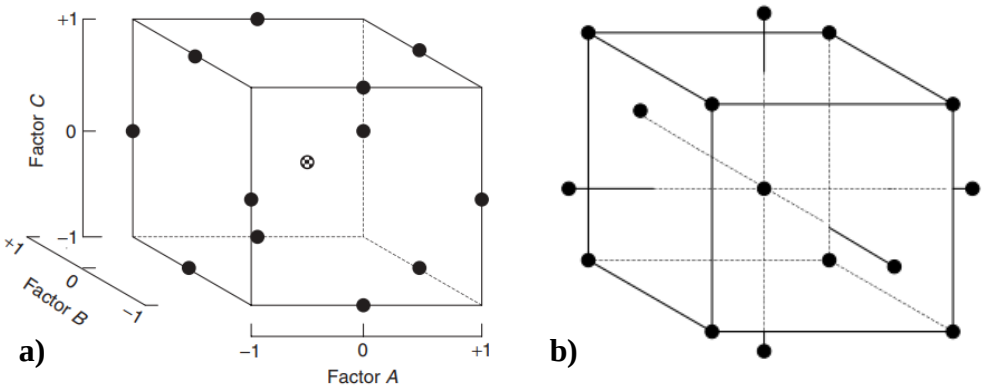


Figure 15 - Design geometry of a) Box-Behnken and b) Central Composite Design [87].

Box-Behnken response surface design was developed by Box and Behnken in 1960 and consists of a particular subset of the factorial combinations from the 3^k factorial design being an alternative for this kind of design. BBD requires fewer experiments than other similar response surface methods since it does not contain points at the extremes of the cubic region. All the points are either on a sphere or at the center of the cubic region. The lack of those extreme points brought popularity to this design method since they are usually prohibitively expensive or impossible to test due to physical constraints on the experimentation [81, 87-89].

The construction of the design is made by combining two-level factorial designs with balanced or partially balanced incomplete block designs resulting in a design that makes efficient use of the experimental units and is also rotatable or nearly so. Box and Behnken [90] list a number of design arrangements for k = 3, 4, 5, 6, 7, 9, 10, 11, 12, and 16 factors. Although very popular and used in industry BBD contains regions of lower prediction quality.

The second most known response surface methods, the Central Composite Designs, were first proposed by Box and Wilson back in 1951 [91] and quickly became one of the most popular designs among the second-order designs [89]. It consists of three sets of points that when combined are capable of providing good insight into curvature of response and estimation of higher-order effects. The three sets of points are:

a) The factorial portion, composed of a complete (or fractional) 2^k factorial design. In this set, the points are coded with the values +1 and -1 and correspond to the vertices of the cube space.

b) The axial portion, composed of 2k axial points located at the axis of each control variable and at a distance α from the center of the cube region known as (0,0,0). Those 2k points are also known as star points and the value of α can vary depending on the CCD method chosen, but 1.68 or $\sqrt{2}$ is usually used.

c) The center points, located at the center of the cube (0,0,0). The number of center points can be chosen since they are used to obtain the error in the analysis, but a number between 3 and 5 is recommended.

CCD is usually only used after important factors were already filtered through a screening method since it still has a high number of runs caused by the five levels in each factor. The great advantages of the CCD designs, besides being able to compute higher order designs and obtain response surfaces that consider curvature, is that it allows a factorial first-order study to

be extended to a second-order by only adding the star points and some center points [91] . The CCD also exhibit outstanding design qualities across a broad range of design criteria and by choosing the appropriate values of α and center points some desirable properties can be achieved such as rotability and orthogonality [89].

Since a small number of factors were studied in this work, the CCD was chosen in order to obtain a thorough analysis of their influence. More on the CCD method and parameter chosen will be talked about in the next chapters.

2.3.2 Data Analysis

Data analysis is essential to the Design of Experiments because it enables researchers to comprehend the connections between variables and the responses. It facilitates the optimization of processes by identifying important components and their connections, facilitating the decision-making by giving findings a scientific foundation. The reliability of experimental results is guaranteed by data analysis through validation and replication. Overall, DoE relies on data analysis to obtain relevant insights, measure the effects of factors, optimize processes, and support informed decision-making.

After performing the experiments, regardless of the chosen design, the gathered data must be processed to obtain the desired results. Such processing is usually made with the help of computer software capable of applying the respective mathematical models and generating results of easy understanding like plots and tables. Many outputs can be obtained depending on the DoE design, parameters and on the analysis technique chosen. The most employed techniques are the Normal probability plots, the creation of regression models, contour plots, ANOVA tables and response surface graphs and a brief description of each one is provided below.

Normal and Half-Normal probability plots

The normal probability plot is a graphical method for determining whether or not a data set is roughly normally distributed. It was first proposed by John Chambers in 1983. In this method, the obtained data in plotted against a theoretical normal and the obtained points form an approximate straight line. Any point that deviates from that straight line also deviate from normality and are considered outliers [85].

In DoE, normal probability plots are used to find outliers but also to judge the significance of effects. By arranging the data in ascending order and calculating their cumulative frequency we can plot those values and obtain a series of points that, in most cases, can be fitted into a straight line. When using residual values from tests we obtain the normal probability where points that fall away from the straight line are considered residuals and shouldn´t be considered in the final analysis. If values of factor effects are used, it is possible to identify the most significant effects, again by the points that are furthest from the straight line [88].

A variation of the Normal Probability Plot is the Half-normal Probability Plot. Usually used for plotting the factor effects when there are only few effects. It follows a similar process as the normal probability plot but instead of using the actual factor effects, the absolute values of those effects are used. This way, all of the significant estimated effects are away from the line and displayed in the right corner [88].

Regression models

Regression models are the base for many plotting methods after performing a DoE. It involves fitting the obtained results into an equation able to relate the input parameters, their influence and the process final response. When the factors are quantitative, this strategy is quite beneficial as the model may be used to forecast behavior of factor combinations not yet tested [88].

The simplest regression model is known as first order regression model and takes the form of:

$$y = \beta_0 + \beta_1 x_1 + \beta_2 x_2 + \beta_{12} x_1 x_2 + \varepsilon \quad (2.1)$$

Where β_0 is the grand average, β_s is a regression coefficient relative to each factor influence on the final response and x_i is a coded variable. The relationship between natural and coded variables is:

$$x_i = \frac{A - \frac{(A_H + A_{L)}}{2}}{\frac{(A_H - A_{L)}}{2}} \quad (2.2)$$

Where A if the factor and the subscripts H and L define if it is a high or low value of that factor. The grand average can be calculated by dividing the grand total by the number of runs (2.3) and the regression coefficients are estimated as one-half of their respective effects (2.4).

$$\beta_0 = \frac{Grand\ Total}{N} \quad (2.3)$$

$$\beta_s = \frac{\text{Effect of A}}{2} \quad (2.4)$$

It takes into account the individual effects of each factor and also the effect of their interaction. Despite being very useful in predicting values, a potential concern in this regression model is the assumption of linearity in the factor effects, i.e., we assume that the interactions will have little to no impact and thus are usually ignored. When the effect of the interaction is significant, the plotted contour and surface shows some curvature but it is often not adequately modelled which requires the use of higher order models to correctly represent them [88].

Second order regression models (2.5) take a similar form as the first order ones but due to β_{11}e β_{22} it is able to measure pure quadratic effects.

$$y = \beta_0 + \beta_1 x_1 + \beta_2 x_2 + \beta_{12} x_1 x_2 + \beta_{11} x_1^2 + \beta_{22} x_2^2 + \varepsilon \quad (2.5)$$

This model can produce more accurate response surface predictions but to work it also needs some extra points, the center points located between the +1 and -1 (high and low) pre-defined values. This points, and its replication provide protection against curvature from second-order models and also facilitate independent estimate of error [88].

Third order or higher models can also be applied but are usually rare since it is unusual to have significance between many factors.

Contour plots

Contour plots are defined as "A topographical map drawn from a mathematical model, usually in conjunction with response surface methods (RSM) for experimental design. Each contour

represents a continuous response fixed at some value." [92] and are an alternative to plotting a two-factor interaction response surface. In this graphical method, a 3-dimensional surface is expressed through contours on a 2-dimensional format by constructing lines that link (x, y) locations where specific values of z (the response) occurs (Figure 16) [85].

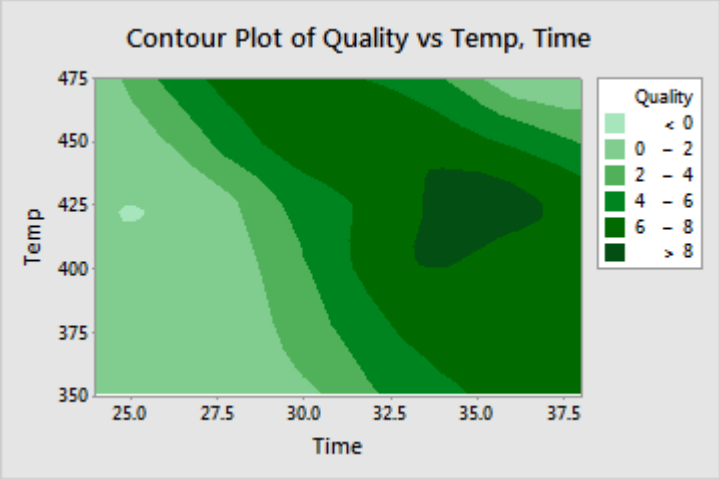


Figure 16 - Example of a contour plot.

Contour Plot are fundamental in the analysis of a DoE since they facilitate the visualization of the best response and can also determine the sensitivity of the response to various factors. The method can be used for low and high order effects displaying straight or curved lines. Although very useful they have two drawbacks, only being able to relate two factors at a time and display one response to that interaction so when analyzing more than two factors, the others must be fixed at a value. A workaround to the multi-response problem can be achieved by overlaying the different response contours in order to obtain an optimal region for all responses or visualize the tradeoffs.

ANOVA

The analysis of variance, also called ANOVA, is one of the first and most fundamental statistical analysis methods. ANOVA is a technique that divides the overall variance in an experiment into responsible sources of variation. It is a statistical strategy for interpreting experimental data and making conclusions regarding the parameters under consideration [88]. It also evaluates the influence of factors, their interactions on response variables and estimates the proportion of variance that cannot be explained or assigned to factors and their interactions [81].

Usually, the ANOVA is displayed in a final table, called the ANOVA table, which can display a series of statistical information. The most common properties are the sum of square, the adjusted mean square, the degree of freedom, the F-Value, and the P-Value. The sum square column can be obtained by performing a sum of squares following (2.6) for both the effects, the interaction effects and the error [92].

$$SS = \frac{N}{4}(\text{Effect}^2) \tag{2.6}$$

The degrees of freedom column is associated with the sum of squares and is based on the number of levels a factor has, i.e., factors with high and low levels contributes 1 degree of freedom for the sum of squares. The mean square column is obtained by dividing the value of

the sum of squares of each factor by the degrees of freedom. The next column, denominated F-value, is obtained by dividing the mean square of each factor by the mean square of the residuals (error) and its value must be compared with an appropriate F-distribution table based on the degrees of freedom to verify the significance of the factors in the model [92].

Finally, in the last column we can find the P-Value, a value calculated based on the F-Value, which can go from 0 to 1. It corresponds to the area to the right of the observed F-Value in an F distribution plot. Usually, P-Values below 0.05 indicate that the factor is significant for the final response since it corresponds to a 95% probability that the factor influences the final output [92].

Response surfaces

Response surfaces are another way of looking at the response outcome based on the interaction of two factors. They work very similar to contour plots but instead of being represented on a 2-dimensional plane they appear as 3-dimensional surfaces in a given space what may provide a clearer picture of the response. An example of a response surface plot can be observed on Figure 17. With the surfaces, investigators can better perceive the behavior of the response and even predict its value for different factor combinations.

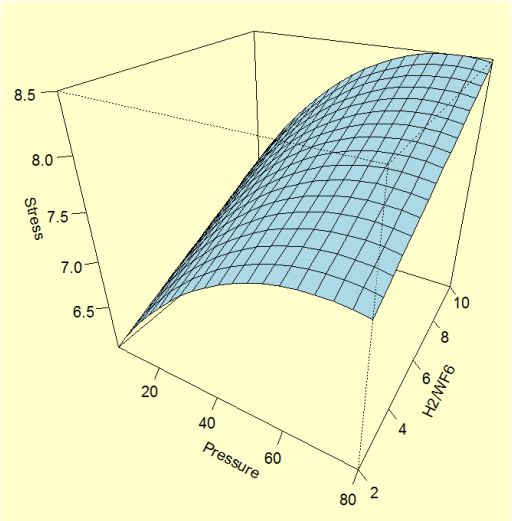


Figure 17 - Example of a response surface plot [85].

The fitted response surface will be a plane if the regression model comprises just the main factors and no interaction effect and will be curved rather than straight if the model considers interactions between the factors. All in all, this plotting method aid researchers in understanding the nature of the interaction between the factors and the outcome an also are often used to find a direction of potential improvement for a process [93].

3 Material and Methods

3.1 Material

Polyetherimide, also known as PEI, is an amorphous thermoplastic that can be employed in a variety of structural applications that call for thermal resistance and mechanical strength. The PEI chain's aromatic imide units offer greater thermal stability, while the flexible ether linkages offer improved processability. This results in a Young modulus of approximately 3 GPa and a glass transition temperature of 215ºC. Those extraordinary thermal and mechanical qualities can be achieved by additive manufactured parts by using PEI filaments [79].

ULTEM 9085, ULTEM 1000, and ULTEM 1010 are the three main varieties of PEI utilized in the AM industry at the moment. ULTEM 9085 is an aerospace-grade material blend that is frequently utilized in the low-volume fabrication of highly customized jigs and fixtures. The general-purpose grade unfilled material called ULTEM 1000 is ideal for interior automotive and aerospace vehicle construction where chemical resistance is required. Finally we have UTEM 1010 that due to its outstanding performance in high temperatures has a variety of uses in various industries, from the automotive and aerospace to the medical and railway [55].

In this work the used material was a 1.75mm filament of PEI 1010 made by the company 3d4makers (Figure 18). This blend of PEI is an amorphous, amber to translucent thermoplastic with a glass transition temperature (T_g) of 217 °C that can function continuously up to 170 °C, according to the manufacturer's description. It also has UL94 V0 and 5VA ratings as it is naturally flame resistant [45].

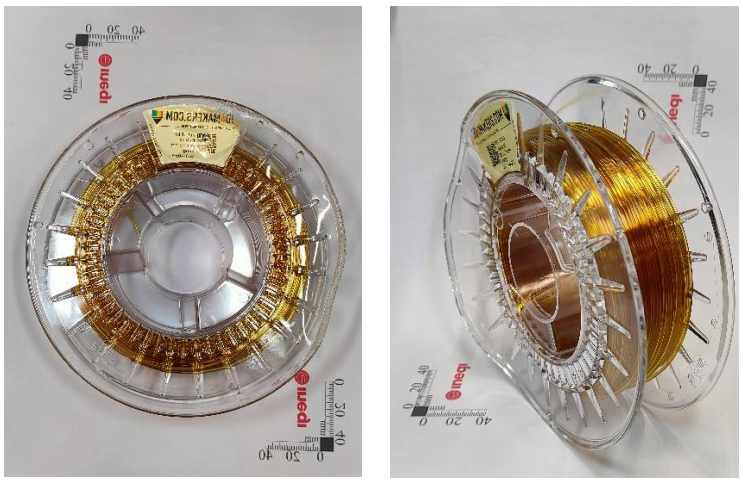


Figure 18 - Spool of PEI 1010 used in the experiments.

The filament dimeter had a tolerance of ± 0.05mm and a roundness of 95%. Its physical properties (Table 5) and recommended printing settings (Table 6) can be found below.

Table 5 - PEI filament physical properties [45].

Description	Value	Test Method
Density	1.27 g/cm3	ISO 1183
Tensile Modulus	3.2 GPa	ISO 527
Tensile Strength	105 MPa	ISO 527
Impact Strength Notched Izod	5.0 Kj/m2	ISO 180

Table 6 - PEI filament recommended printing settings [45].

Description	Value
Nozzle Temperature	360-400
Bed Temperature	120-160
Adhesion	Use of an adhesive
Drying reccomendations	120ºC, minimal 4h

3.2 Methodology Analysis

After the definition of the material involved, this subchapter describes the experimental part of this work. The characteristics of the custom printer utilized to produce the samples are addressed, as well as the investigation of the best range of parameters for the tests.

Some insight on the design of experiment implementation and the steps taken during the printing process are also given. Finally the tensile strength tests and the final data treatment using direct image correlation and the interpolation of values are also mentioned.

3.2.1 The printer

The first step in the experimental phase of this work was to assemble the custom printer available at INEGI´s facilities that had previously been developed by Domingues *et al.* [94] and was disassembled due to facility changes (Figure 19). The printer was based on the structure of a 3D Systems CubeX printer where the metal frame, rollers and stepper motors were kept, and the other components modified to meet the requirements needed to print high-performance polymers. Firstly the machine control unit had been replaced by a Duet 2 Wi-Fi card since the original proprietary solution didn´t allow for much configurability [94].

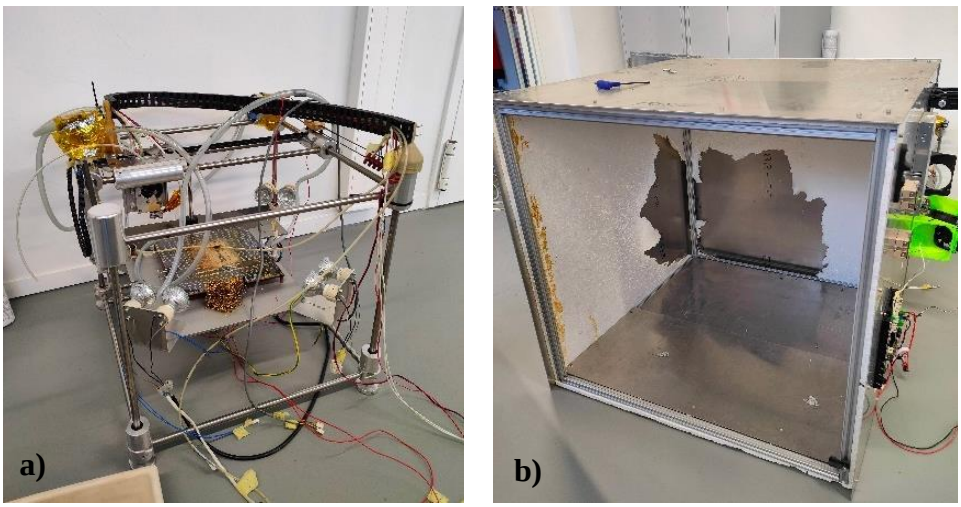


Figure 19 - a) Initial disassembled printer and b) enclosure.

The original extruder had been swapped for the commercially available Titan Aqua by the company E3D with the capability of reaching 500ºC and being able to support water cooling, much needed in the high temperature environment. A heated bed had also been added since it wasn´t present in the original printer. An E3D – High Temperature Heated Bed was chosen as it can reach surface temperatures of 200ºC. A water cooling system using heat exchanger blocks attached to each stepper motor and circulating ethylene glycol through radiators and fans had also been implemented in order to maintain the stepper motors functional on environmental temperatures of up to 120ºC [94].

To achieve those environmental temperatures quicker some changes were made from the original setup of Domingues *et al.* [94]. First, the material of the enclosure that provides the thermal insulation was changed from 15mm polystyrene foam plates to 20mm calcium silicate plates as the previous plates weren´t able to support the high temperatures in the chamber as can be seen in Figure 19 b). The new plates not only support temperatures of up to 1100ºC but also provide better thermal insulation making the environmental heating process a lot faster. The heating element previously composed of only a heat gun was replaced by a system composed of a heat gun (Black and Decker KX2200) and a resistance (Figure 20) both with 2000 Watts each and both controlled by a bang-bang system to maintain a constant temperature in the chamber.



Figure 20 - Resistance added to the enclosure.

Finally, the radiant heating system composed of 6 halogen bulbs LUXTEK 220-240V-50W in 3 pairs was upgraded to 8 bulbs in 4 pairs placed on all corners of the build plate to illuminate and heat the all the printed part surfaces during print. This radiant system was first proposed by Gardner *et al.* [95], in order to increase and maintain the part temperature, and was found to increase the part surface temperature during the print by 30ºC and enhance the overall surface finish of the parts [94]. Other small changes such as sensors and cable replacements as well as some cable managements were also performed. Some final images of the final assembly can be found in Figure 21 below.

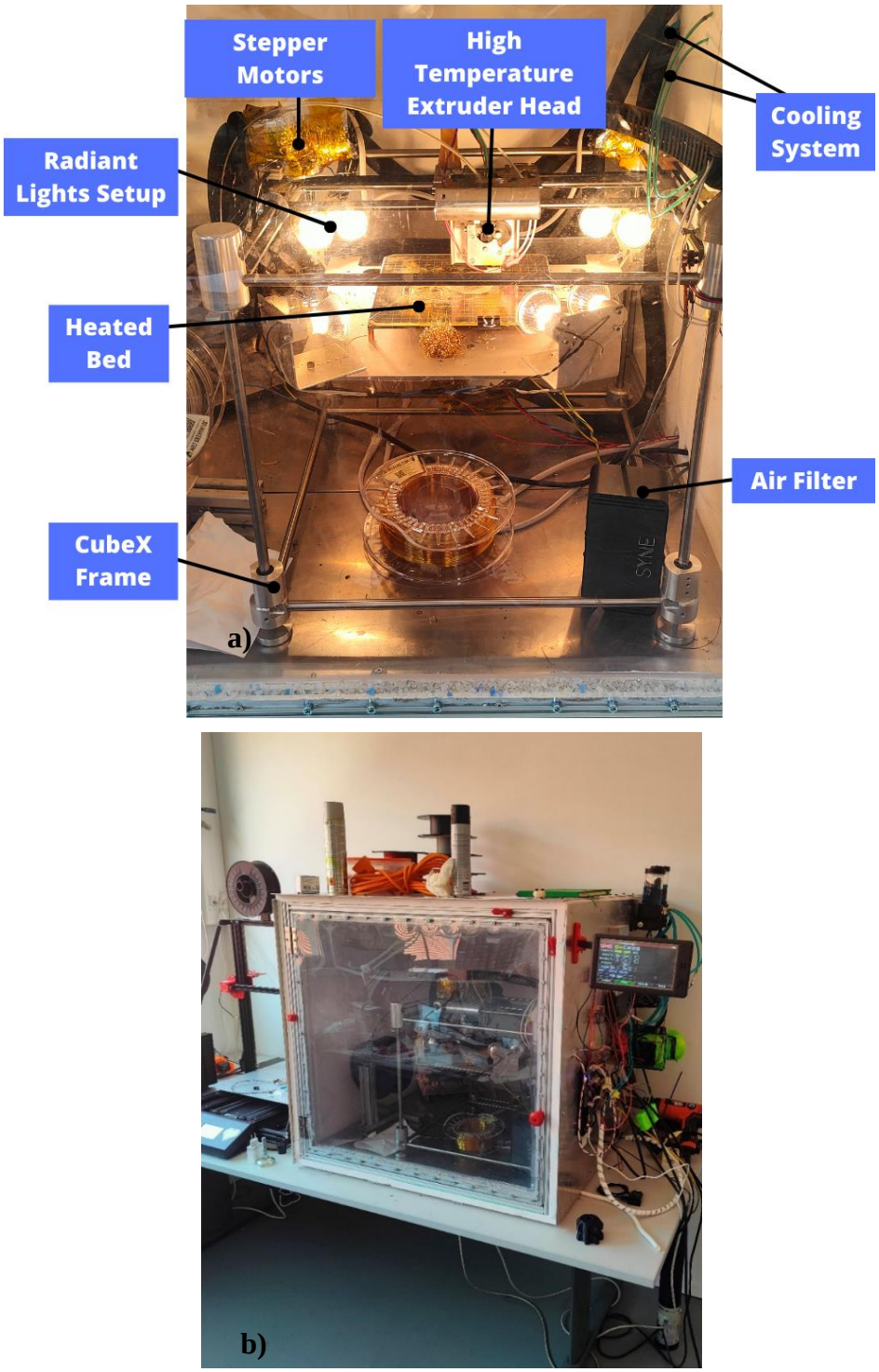


Figure 21 - Final printer assembly; a) some components of the machine; b) printer on the lab table.

3.2.2 Process Parametrization

Some conditions had to be set before beginning with the sample printing in order to produce an optimal experiment. In this chapter the investigation of these conditions is presented.

First, the variables to be modified had to be determined. After some discussion, the DoE method was defined as a CCD with 3 replicas thus the number of factors could not exceed 3 as it would result in a number of tests not viable in the determined timeframe of this work. Since one of the properties of great interest in PEI is its high working temperature, 3 factors related to temperature were selected, chamber temperature, nozzle temperature and bed temperature. After being selected, their high and low limits needed to be defined. Following the indication of several manufacturers [42-45] the baseline working temperatures were as indicated in Table 7.

Table 7 - Baseline working temperatures based on manufacturer's data [42-45].

Parameter	Low (ºC)	High (ºC)
Nozzle Temperature	355	390
Bed Temperature	120	160
Chamber Temperature	90	-

It is also important to remember that due to the CCD method the high and low values are actually not the highest and lowest temperatures used since the star points fall out that range. Following the manufacturer's recommendations, the first temperatures defined for the tests were as follows.

Table 8 - First set of temperatures levels.

Parameter	Star Low (ºC)	Low(ºC)	0 (ºC)	High (ºC)	Star High (ºC)
Nozzle Temperature	350	360	375	390	400
Bed Temperature	100	120	150	180	195
Chamber Temperature	83	90	100	110	117

After some testing with this set of levels it was found that the only parameter that caused the printing of unacceptable parts was the bed temperature as parts printed with temperatures below 120 ºC presented severe warping and even completely detached from the printing bed during the process (Figure 22).

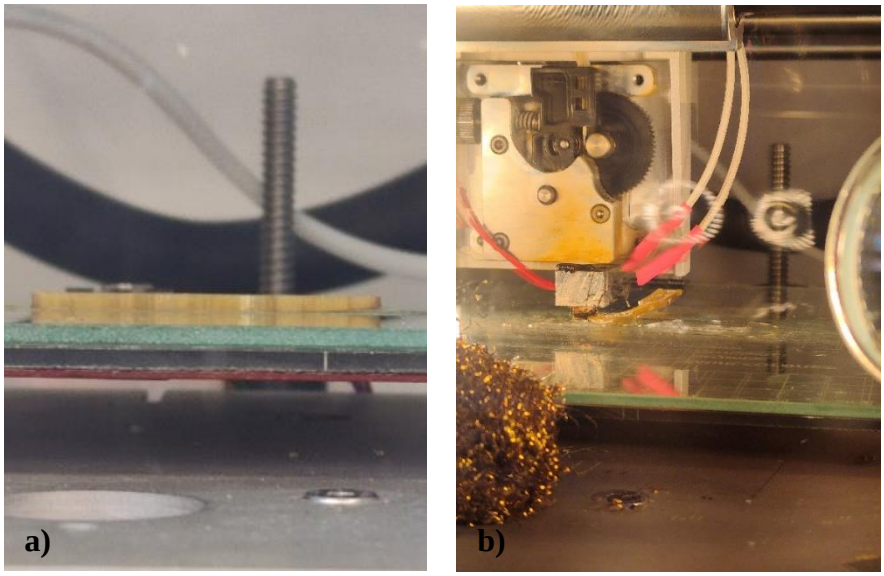
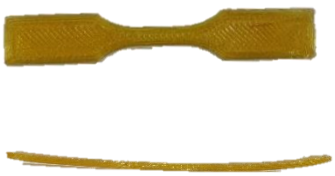
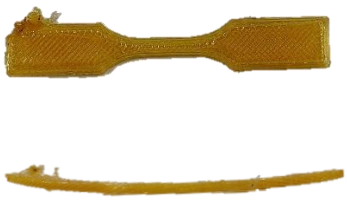


Figure 22 - Failed parts; a) severe warpage; b) part detached from bed.

With this discovery, a throughout analysis of different bed temperatures with and without the radiant lights was performed (Table 9). The nozzle and chamber temperatures were fixed at 380ºC and 83ºC and the bed temperature was varied. Although adequate parts were achieved with 100ºC it was very unreliable and a minimum temperature of 120ºC was set for the star low point. The final parameter levels were as in Table 10.

Table 9 - Analysis of the effect of bed temperature.

Without lights	With lights	Bed Temp.
		100ºC
		100ºC
		120ºC

Continuation of Table 9.

Without lights	With lights	Bed Temp.
		120ºC
		120ºC
		130ºC

Table 10 - Final parameters levels for the experiment.

Parameter	Star Low (ºC)	Low(ºC)	0 (ºC)	High (ºC)	Star High (ºC)
Nozzle Temperature	350	360	375	390	400
Bed Temperature	120	135	157	180	195
Chamber Temperature	83	90	100	110	117

Another parameter that was researched before starting the experiment was the specimen shape. Due to the lack of standards for mechanical testing of 3D printed plastics, standards for general plastics are often used. Although not considering many particularities of additive manufactured parts such as intra and inter layer behavior, the stress concentration on specific zones, the air gaps and many others, those standards are the best approximation available.

In this work 3 different standards were analyzed as well as a simple rectangular geometry with PLA printed tabs. The objective os this analysis was to see which of the standards would produce specimens able to fracture at the desired location since it is usual for 3D printed specimens to fissure at stress concentration regions during tensile strength tests. The standards chosen were the ASTM D638 V [96], ISO 527-2 1BA and ISO 527-2 5A [97]. All the geometries were modeled in SolidWorks software, exported as a STL file, and imported to the 3D printing software PrusaSlicer. The samples 3D design and dimensions can be found below.

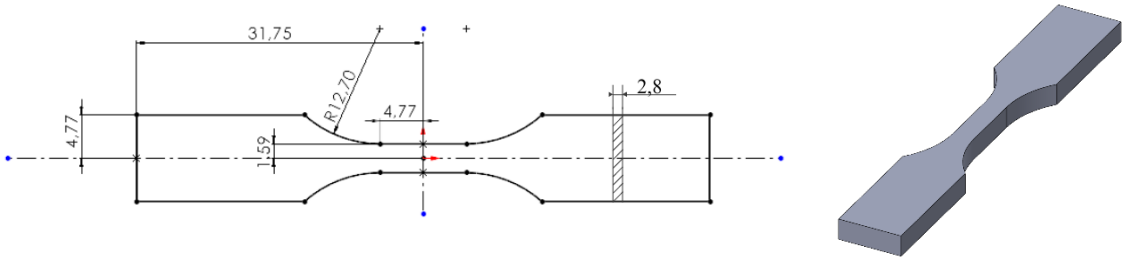


Figure 23 - ASTM D638 V geometry.

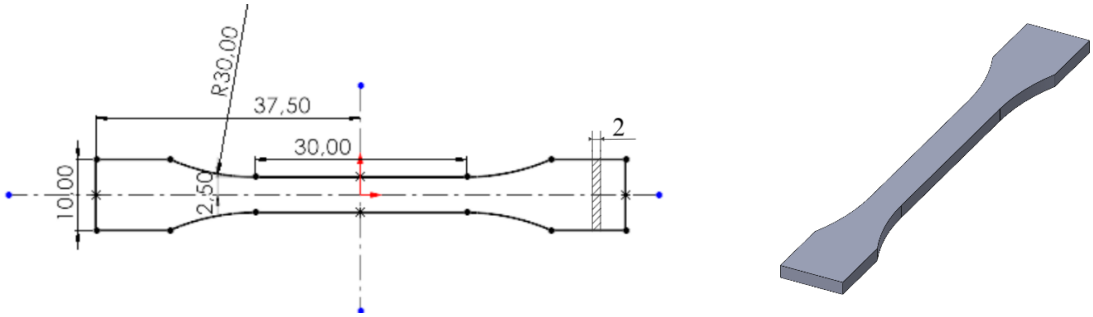


Figure 24 - ISO 527-2 1BA geometry.

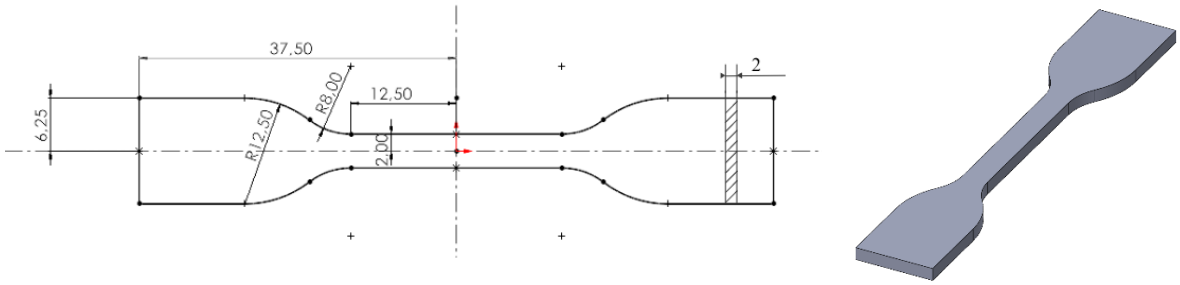


Figure 25 - ISO 527-2 5 geometry.

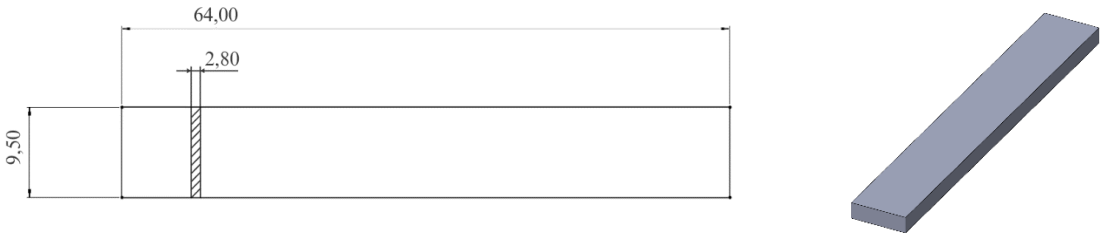


Figure 26 - Rectangle geometry.

The first test was performed before the final temperature levels were defined and considered only the ASTM D638 V, ISO 527-2 5A and the rectangular geometry following the parameters in Table 11. With the results (Table 12) it was possible to verify that the rectangular geometry fractured in the region of the tabs revealing itself to be a bad choice for the final work. Both the standards had two fractures in the correct zone and one outside the range.

Table 11 - Printing parameters for the first standards test.

Parameter	Value
Printing speed	30mm/s
Perimeters	3
Bed temp.	150ºC
Nozzle temp.	375ºC
Chamber temp.	100ºC
Layer Thickness	0.2mm

Table 12 - Results of the first standards test.

ASTM D638 V	Failure
	Inside the range
	Outside the range
	Inside the range
Rectangle	**Failure**
	Outside the range
	Outside the range
ISO 527-2 5A	**Failure**
	Outside the range
	Inside the range
	Inside the range

After the final temperatures were defined the analysis was redone now considering 3 standards and using a thickness of 2.8mm for the ASTM sample. The final results can be seen in Figure 27. It became evident that despite the standard, all the specimens are prone to fracture right on

top of the acceptable zone limit, a tendency that was expected since that zone possess stress concentrations and is prone to break first. After some consideration the ASTM D638 V was chosen as it had the fastest printing time, less material usage and was also one of the most used standards in the reviewed literature on tensile strength tests of printed components [34, 35, 69].

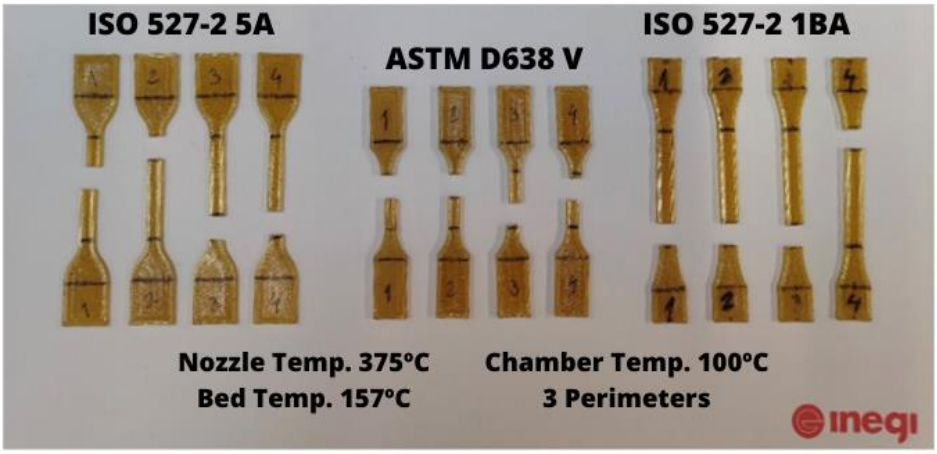


Figure 27 - Results of the second standards test.

The final factor that was considered in this pre-experiment analysis was the number of perimeters for the specimens. As previously reviewed in the literature, perimeters are known for limiting stress concentrations and increasing the tensile strength and overall, the mechanical properties of printed parts. Nevertheless, their effect was again studied in order to verify the number of perimeters where the parts would fracture on the correct location. The values were then varied from 0 perimeters where the part was composed only by its infill up to 4 perimeters where the critical section was composed only by perimeters (Figure 28).

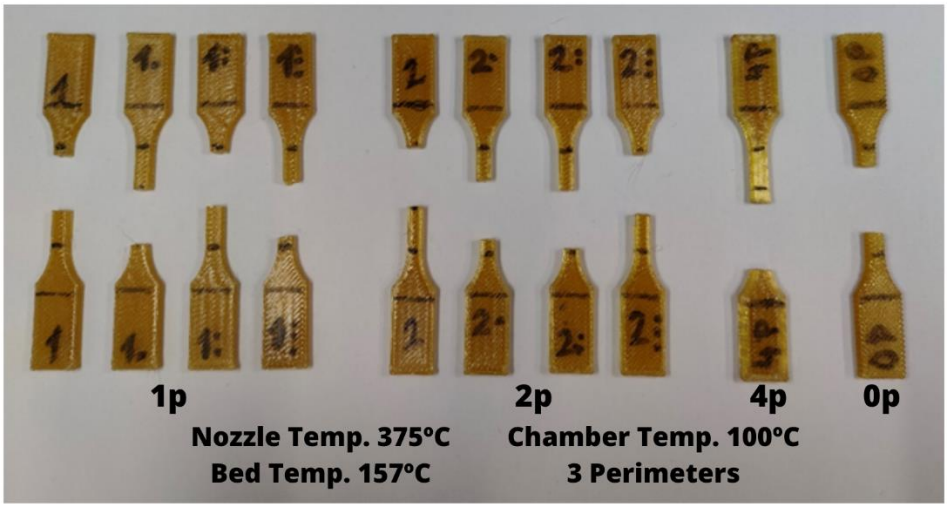


Figure 28 - Results of the perimeters No experiment.

As expected, the sample printed with 4 perimeters fractured way out of the desired zone. Because its critical section was composed only of filaments deposited aligned with the loading direction, the zone that was supposed to be the easiest to break was actually the hardest to do so and the failure occurred out of the desired range. The 0 perimeter part fractured right in the middle but since printing with 0 perimeters is something that is not really practical the

hypothesis was discarded. The most consistent results were achieved with parts printed with 2 perimeters thus this was the value chosen for the final experiment.

3.2.3 Design of Experiments Implementation

The design of experiments implementation was done at the same time as the process parametrization in order to define the range of temperatures and their levels and also after all the testing phase was finished to produce the desired results. Even so, all the steps followed prior and after those procedures are explained.

The first step was to choose the design method and the number of factors. Since the objective of this work was to investigate the effect printing parameters on the tensile strength of the PEI parts and its main characteristic is its thermal properties, temperature related parameters were chosen, and a response surface design were seen as the best choice as they are able to accurately predict the response and consider quadratic effects.

Considering that BBD contains zones of lower prediction quality, the design was set on the Central Composite Design. The parameter choice was very direct as, in principle, the three factors that most relate to temperature are the Nozzle, Bed and Chamber temperatures. The printing speed was also considered since it influences overall temperature but, as it would increase the number of runs exponentially, only 3 factors were defined.

Afterwards, two other aspects had to be defined, the value of α, that represents the distance of the star points to the center of the cube regions and the number of experiments and replicates. For α, three options were considered: $\alpha =$ some value, that would result in a circumscribed design (CCC), where the star points stablish new extremes for the experiments; $\alpha = \pm 1$, resulting in a face centered design (CCF) where the star points are just another level of the factors and, a CCD design where the factors itself are divided by α, and the star points are placed at the limits of the experiment called inscribed design (CCI) [85].

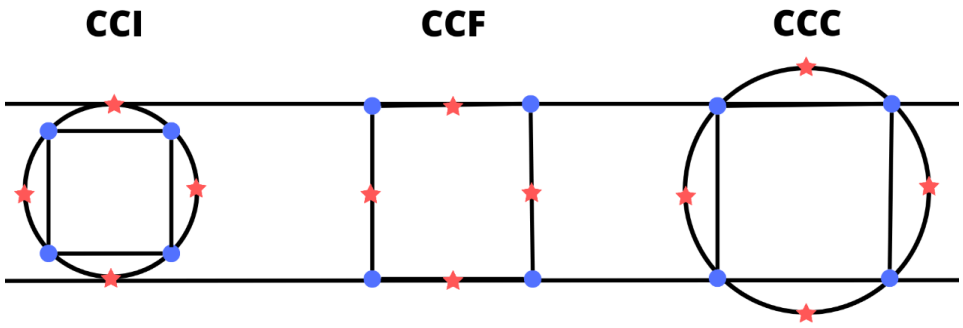


Figure 29 - Inscribed, face centered and circumscribed CCD methods.

Since the limits of the machine weren't a problem as it could surpass the limits of the material, a circumscribed design was chosen and the value of α was set to be $F^{1/4}$ where F is the number of points in the factorial portion of the experiment since it causes the experiment to become rotable, maintaining its prediction variance unchanged under any rotation of the coordinates [89].

As for the number of experiments it was decided to not follow the software (Minitab) recommendation of 20 runs per replicate (8 factorial points, 6 star points, and 6 center points) and instead use 19 runs (with only 5 center points) and 3 replicates. The center points and replicates are used to account for experimental uncertainties and improve model accuracy,

however, since three replicates would already be performed, removing one center point from each would not have a significant impact on the final result and would save time and resources. After everything was set, the different combinations of parameters were generated by Minitab statistical software as well as a random order for their printing and testing (Table 13).

Table 13 - Parameters levels combinations.

Combination No.	Sample No.	Bed Temp. (ºC)	Nozzle Temp. (ºC)	Chamber Temp. (ºC)
1	9, 28, 47	120	375	100
2	1, 20, 39	135	360	90
3	5, 24 ,43	135	360	110
4	3 ,22, 41	135	390	90
5	7, 26, 45	135	390	110
6	11, 30, 49	158	350	100
7	13, 32, 51	158	375	83
8	15-19, 34-38, 53-57	158	375	100
9	14, 33, 59	158	375	117
10	12, 31, 50	158	400	100
11	2, 21, 40	180	360	90
12	6, 44, 25	180	360	110
13	4, 23, 42	180	390	90
14	8, 27, 46	180	390	110
15	10, 29, 48	195	375	100

3.2.4 Printing of the samples

With the design of experiment planning done the printing process of the samples began. Besides the 3 temperatures that were varied during the experiments the other relevant print parameters used can be found on Table 14. The procedure was performed according to the random order given by Minitab statistical software and each sample produced following a defined order of work represented in Figure 30.

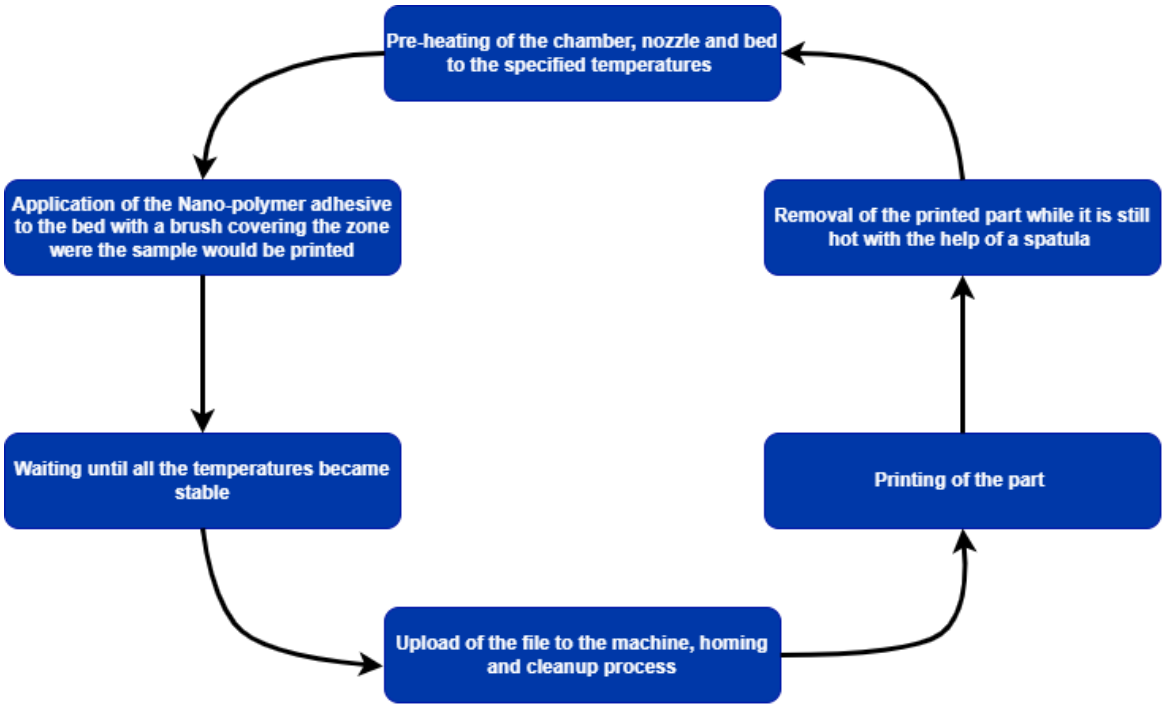


Figure 30 - Samples printing process cycle.

Table 14 - Printing parameters of the samples (PrusaSlicer).

Parameter	Value
Printing Speed	30 mm/s
Layer Thickness	0.2mm
Perimeters	2
Horizontal Shells	0 top and bottom
Infill	100% zigzag +45/-45
Orientation	Flat on the bed

The nano polymer adhesive by the American company VisionMiner (Figure 31) was used to assure that the first layer would stick to the glass printing bed during the printing process while also being easy to remove once the process was finished. The adhesive is especially designed for assisting with the print of high-temperature engineering materials reducing print fails due to warping and part slippage [98].



Figure 31 - NanoPolymer adhesive by VisionMiner.

The samples were removed while still hot firstly because it was a recommendation of the adhesive fabricant and secondly because high temperature printing materials are known for contracting after cooling down, thus, if the specimen reached a low temperature it would stick to the print bed with such force that its contraction could break the glass bed and a removal without damaging the bed or the sample would be virtually impossible.

This method required three days to complete in order to get all of the specimens because each printing cycle took about 20 minutes. Two procedures were carried out between each day to ensure that all samples were kept in constant conditions. The glass plate was rinsed with soap and water, and any leftover adhesive was scraped off. The filament was dried overnight in the lab furnace at 120ºC, which removed any moisture (Figure 32).



Figure 32 - Filament in the oven overnight.

Also, for future analysis, all the information regarding each sample was registered in order to verify if incontrollable variables such as day and hour of the print had any influence on the final result. Even though the vast majority of the prints were achieved without further problems, some, especially those with lower temperatures, had to be printed more than once, what resulted in the need for 64 printing cycles to achieve acceptable samples. The final specimens selected to proceed to the tensile strength test can be found below in Figure 33.



Figure 33 - Final specimens.

3.2.5 Tensile Strength Test

The tensile strength tests were carried out using a custom built machine available at INEGI´s facility with a 2t VETEK load cell. A custom setup had to be assembled on the machine since the it was designed for testing of bigger specimens and wasn´t able to correctly attach the self-tightening clamps. The solution used a threaded rod and a metal plate with a threaded hole on the load cell. This way the clamps were able to be secured on the top part of the machine and on the load cell (Figure 34). This solution was able to perform good quality experiments, even though the samples only became centered once some force was applied on them.

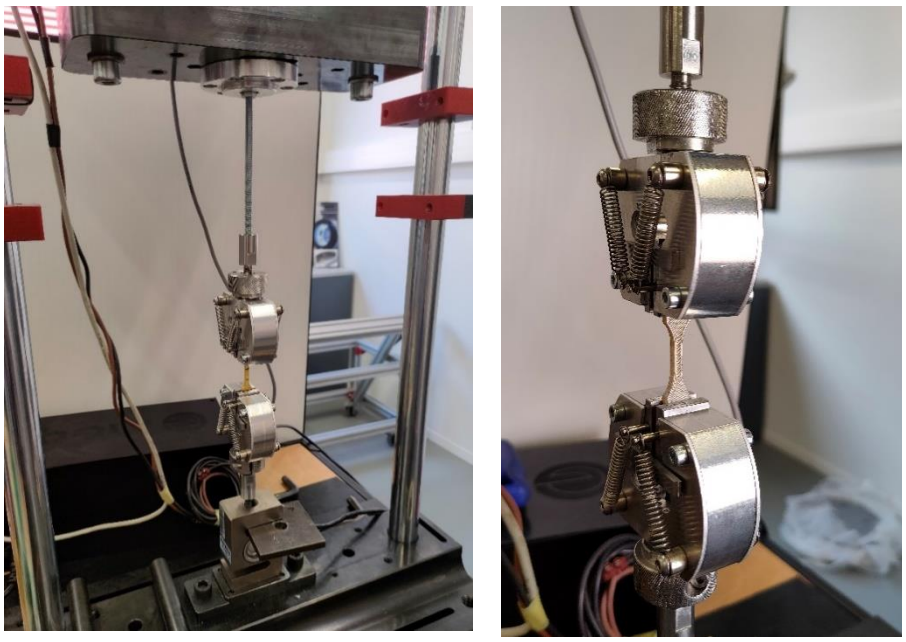


Figure 34 - Tensile tests setup.

According to ASTM D638 V the samples were positioned in self-tightening clamps with a 25mm distance between the clamps. Also, according to the standard, the tests were carried out with a constant speed of 1mm/min. The load cell was capable os measuring the load 25 times a second and the data was registered in an Excel table through INEGI´s custom software.

3.2.6 Digital Image Correlation

Beyond registering the loads during the tensile strength tests, the digital image correlation method was also used to evaluate the behavior of the specimens during the process. This digital analysis method allows an in-depth analysis of the displacement and strain of the specimen surface that can be correlated to its macrostructure.

To perform this method all the samples had to go under a painting process prior to the tensile testing. In this process, using an airbrush, first they were coated in white painting and after drying the airbrush was used again, this time to produce a speckle of small black dots using black ink (Figure 35 a). Then, during the tensile testing a camera (BASLER acA 1600-20um) was used to take high quality pictures of the sample every 500ms (Figure 35 b).

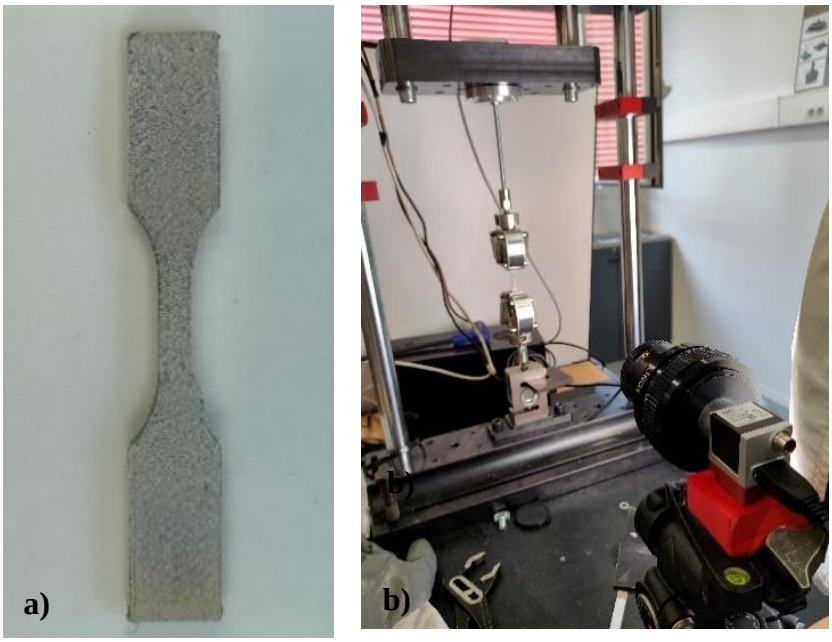


Figure 35 - DIC setup; a) speckled sample; b) camera setup.

After that the photos were uploaded to the VIC-2D software by Correlated Solutions Inc. In this software an interest zone was set only on the critical zone of the specimen and the imagens were calibrated so that the pixel could correspond to real measurement in mm. Finally, the analysis were performed and with the output information it was possible to obtain the total strain using a digital extensometer and images of the evolution of the strain during the test (Figure 36)

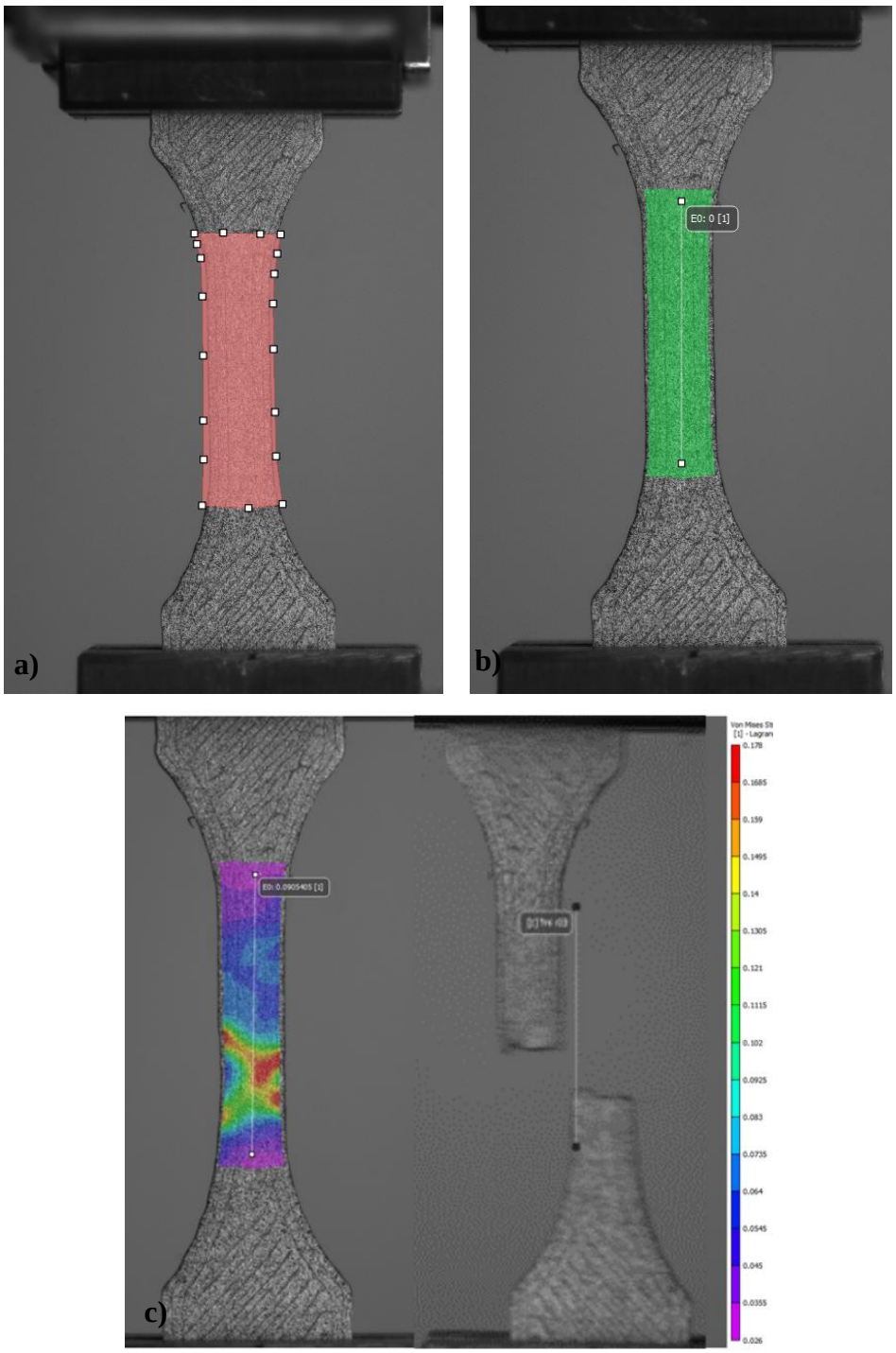


Figure 36 - DIC; a) definition of interest zone; b) positioning of a digital extensometer; c) maximum strain before failure.

An image os all the samples after the tests were performed can be found in Figure 37 below.

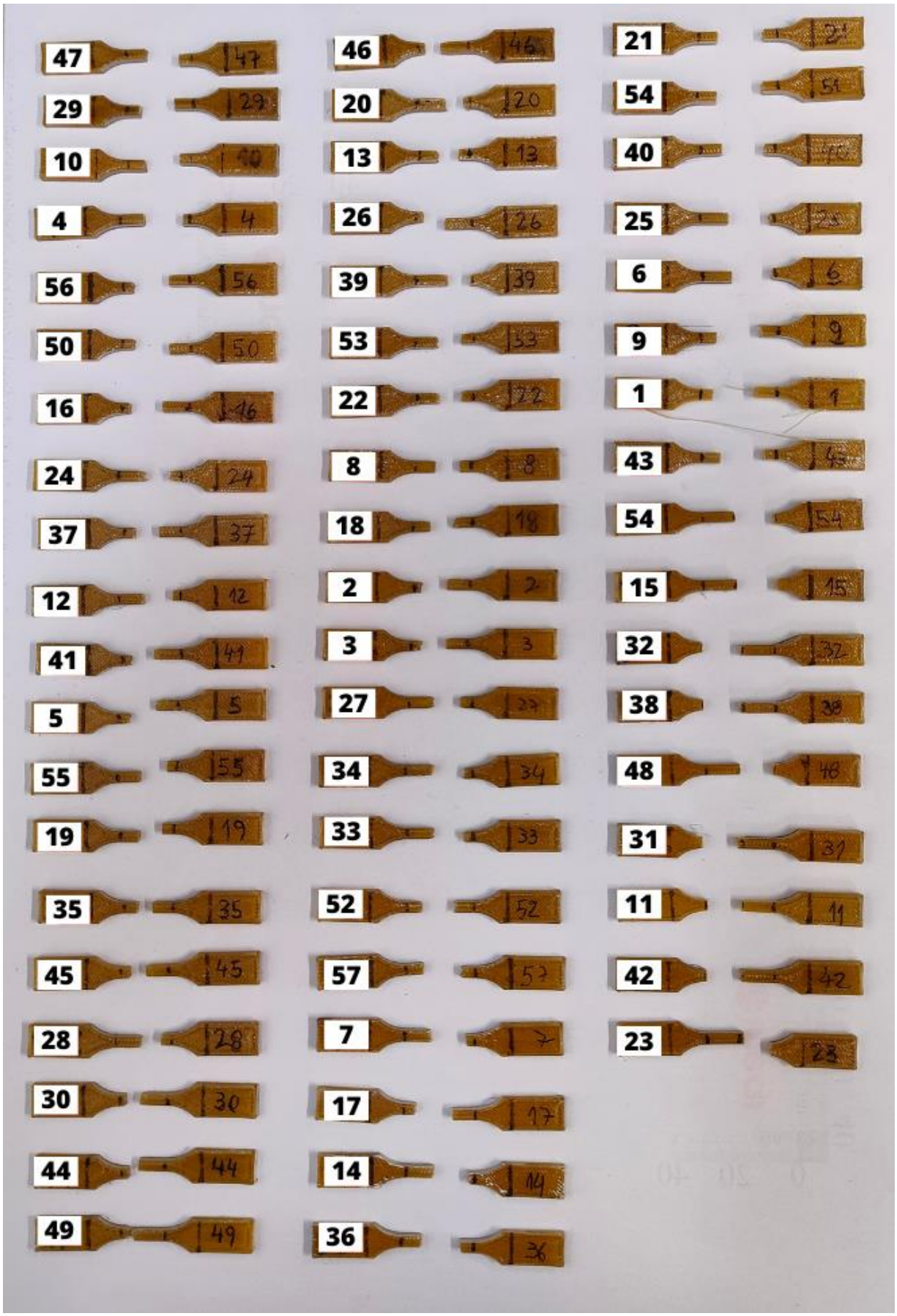


Figure 37 - Samples after the tensile strength test.

4 Results and Discussion

4.1 Maximum Tensile Strength Results

Following all the tensile strength tests some of the samples had to be removed from the analysis since the fracture occurred outside the critical section defined by the standard. On Figure 38, it can be seen that for 3 specimens (23, 31 and 15) the failure occurred completely outside the acceptable limits whilst on 6 it happened right on top of that limit. Nevertheless, it was decided to exclude those samples from future analysis since they may not exhibit trustworthy results.

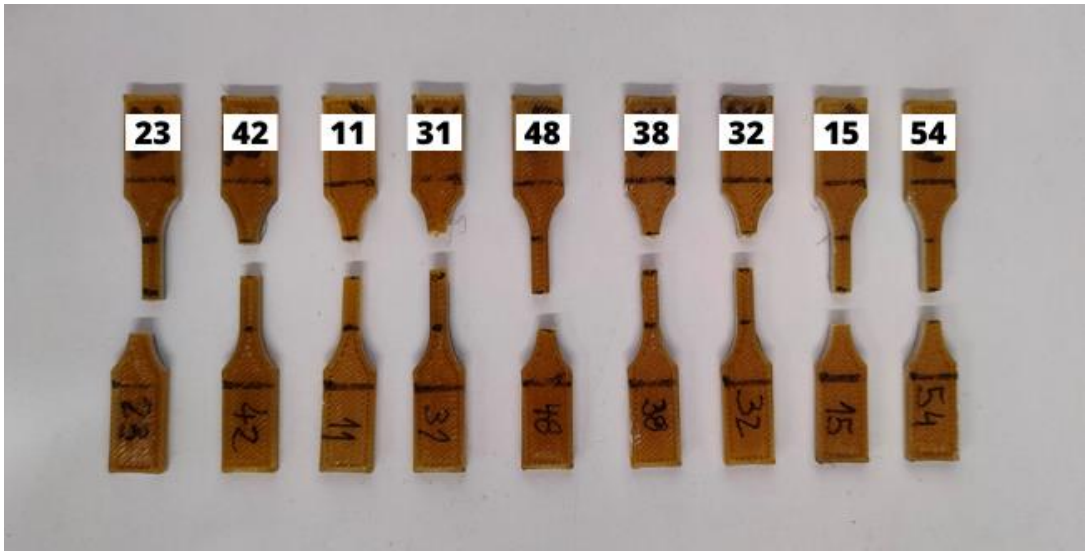


Figure 38 - Samples removed from the analysis.

After some research it was found that these failures were completely random, not being related to any choice of parameter or other variable like day or time of printing and testing. Although a misfortune to the overall accuracy of the DoE, those problems were expected to happen as there is currently no defined standard for mechanical testing of 3D printed parts and the use of standards for molded and extruded plastics lead to undesired breaks at areas of stress concentration such as width transition zones and interface zones between perimeters and infill.

Proceeding with the analysis of the tensile strength, all the registered loads had to be interpolated with the measurements from the digital extensometer of the DIC analysis, since the load cell registered loads 25 times a second and the pictures during DIC were taken a rate of 2 pictures a second, in order to obtain the Stress-Strain curves of each test. During the DIC process 2 samples (20 and 51) had problems regarding their image's detection on the software and their graphs were not plotted.

ANNEX A shows the stress-strain curves as well as the maximum tensile strength and strain achieved in each test. It can be seen that most of the tests of each combination of parameters

displayed very similar behavior and maximum values, with the exception of a couple of outliers. Moreover, although it is hard to see the individual effects of each factor, it is possible to observe that the overall increase of all three temperatures lead to an increase of the maximum tensile strength and a reduction of the total strain (Figure 39).

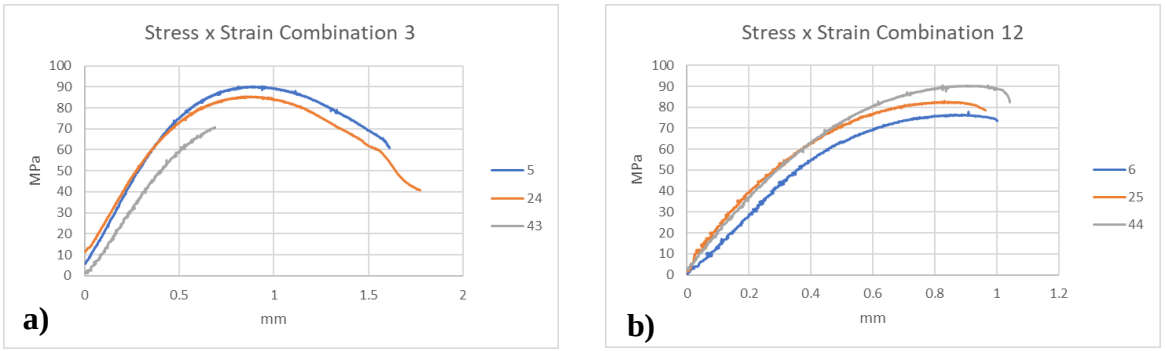


Figure 39 - Example of a) low temperatures behavior and b) high temperatures behavior.

Samples printed in high temperatures were able to achieve higher loads but proceeded to break right after reaching their peak. Parts printed with lower temperatures are not able to achieve loads as high as the previous ones but tend to stretch a lot before breaking. To further investigate the effects of the temperatures on the maximum strength a graph (Figure 40) of the average maximum tensile strength of the 15 combinations was plotted following the order presented in Table 13.

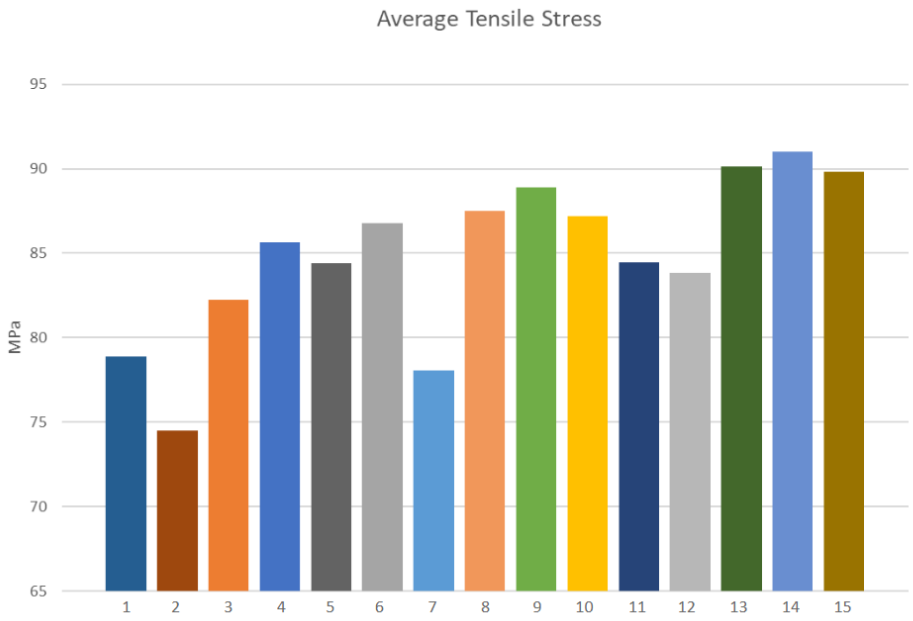


Figure 40 - Average tensile stress of each combination of temperatures.

Although not completely linear it is possible to recognize some degree of influence of the temperatures on the final values of tensile strength. The increase can be explained by a series of different hypotheses since the factor of most influence is still unclear.

4.2 Design of Experiments Results

The implementation of the DoE method made it much easier to recognize which of the factors had the most influence on the final response. It was also able to fit a model capable of predicting the response of the process using theoretical values that was later confirmed through testing. In this chapter the results of the DoE analysis made using Minitab Statistical Software are presented.

4.2.1 ANOVA

After performing the full quadratic analysis following the CCD method the following ANOVA table was obtained (Figure 41)

Analysis of Variance

Source	DF	Adj SS	Adj MS	F-Value	P-Value
Model	9	756,14	84,015	2,51	0,023
Linear	3	612,44	204,146	6,11	0,002
Bed	1	322,24	322,240	9,64	0,004
Nozzle	1	134,53	134,529	4,03	0,052
Chamber	1	124,50	124,505	3,73	0,061
Square	3	104,79	34,929	1,05	0,384
Bed*Bed	1	54,63	54,631	1,64	0,209
Nozzle*Nozzle	1	4,26	4,263	0,13	0,723
Chamber*Chamber	1	66,69	66,686	2,00	0,166
2-Way Interaction	3	24,46	8,154	0,24	0,865
Bed*Nozzle	1	0,26	0,263	0,01	0,930
Bed*Chamber	1	19,16	19,160	0,57	0,454
Nozzle*Chamber	1	8,14	8,139	0,24	0,624
Error	38	1269,61	33,411		
Lack-of-Fit	5	134,70	26,940	0,78	0,569
Pure Error	33	1134,91	34,391		
Total	47	2025,75			

Figure 41 - ANOVA table.

With the ANOVA table the identification of how the factors influence the final response becomes very straightforward. It can be seen that with a P-Value of 0.004 the bed temperature is responsible for the biggest variations in the maximum tensile strength. Following as the most significant factors are the nozzle temperature with a P-Value of 0.052 and the chamber temperature with a P-Value of 0.061. However, these values fall just short of being deemed significant. It is also possible to notice that both the quadratic effects and the interaction effects do not have much impact on the final mechanical properties.

4.2.2 Regression Model

The regression equation obtained, and its summary can be found in Figure 42. Its interpretation shows that all the interactions, quadratic or not, have a small influence on the final response when compared to the three main effects. Since it was obtained in uncoded units, the predicted response can be obtained by simply inserting the temperatures in Celsius on the equation.

The summary on the other hand shows not very promising results with a low R^2 and a high standard deviation (S) indicating that the model does not have great accuracy. Such low values happened due to the missing data points originated by the removed samples from erroneous failures which led to the use of only 46 samples in the final analysis.

Regression Equation in Uncoded Units

Tensile = -649 + 1,24 Bed + 1,76 Nozzle + 5,27 Chamber - 0,00254 Bed*Bed
- 0,00167 Nozzle*Nozzle - 0,0142 Chamber*Chamber + 0,00033 Bed*Nozzle
- 0,00428 Bed*Chamber - 0,00418 Nozzle*Chamber

Model Summary

S	R-sq	R-sq(adj)	R-sq(pred)
5,78022	37,33%	22,48%	0,00%

Figure 42 - Regression Model Equation and Model Summary.

4.2.3 Plots and Charts

Using the software's capabilities, it was also possible to obtain a series of graphs that facilitate the understanding of the behavior of the test results. By looking at the Normal probability plot of the residuals on Figure 43, it becomes evident that the residuals of the experiment are normally distributed with only 3 points being somewhat distant from the fitted line, the samples 1, 9 and 43 that were considered unusual observations by the software (Figure 44).

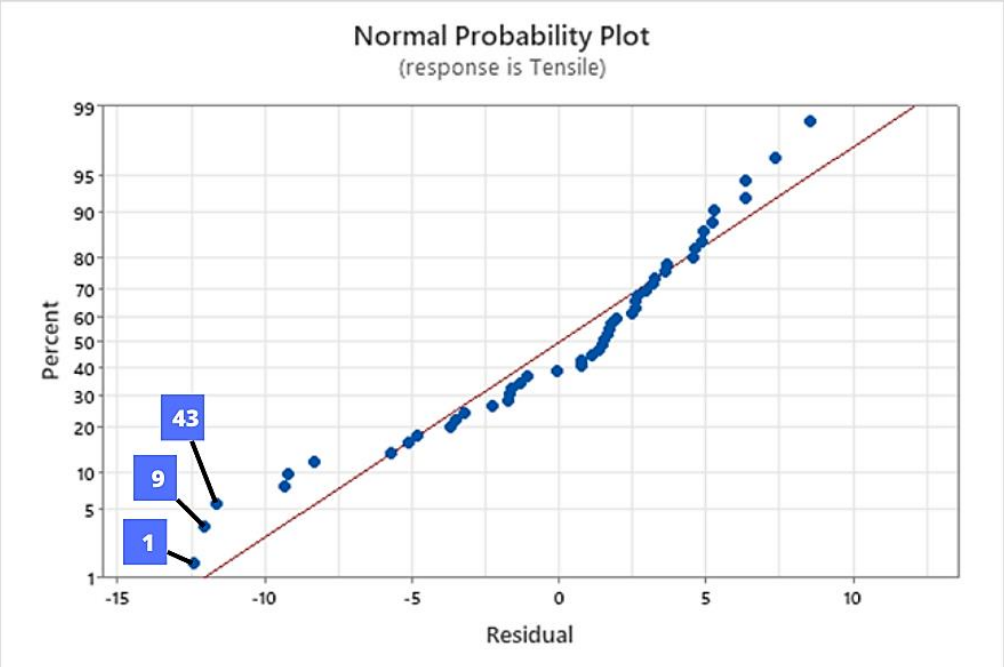


Figure 43 - Normal Probability Plot of the Residuals.

Fits and Diagnostics for Unusual Observations

Obs	Tensile	Fit	Resid	Std Resid	
1	63,50	75,94	-12,44	-2,47	R
9	67,07	78,73	-11,66	-2,27	R
43	70,84	82,94	-12,10	-2,42	R

R Large residual

Figure 44 - Fits and Diagnostics for Unusual Observations.

Next, the Normal and Half-Normal probability plots of standardized effects were also plotted (Figure 45 and Figure 46). Those graphs, as mentioned before, can be used to identify the most significant effects on the experiment. Since the confidence level of the analysis was set for 95%, which results in an α of 0.05, only one factor was far away enough from the line to be considered significant, the bed temperature.



Figure 45 - Normal Plot of the Standardized Effects.

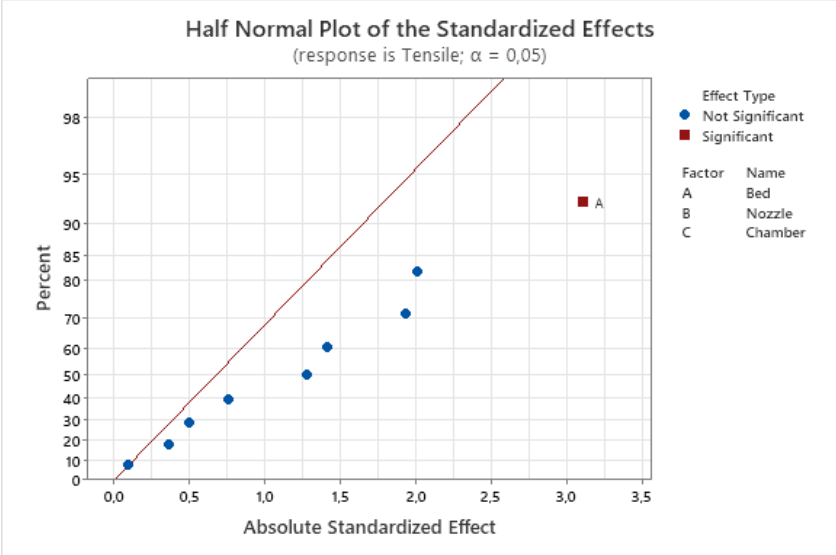


Figure 46 - Half Normal Plot of the Standardized Effects.

A pareto chart of the standardized effects was also plotted to easily rank the parameters and interactions effects on the final result. Again, only the bed temperature was able to surpass the threshold to be considered significant and the other two main factors came very close.

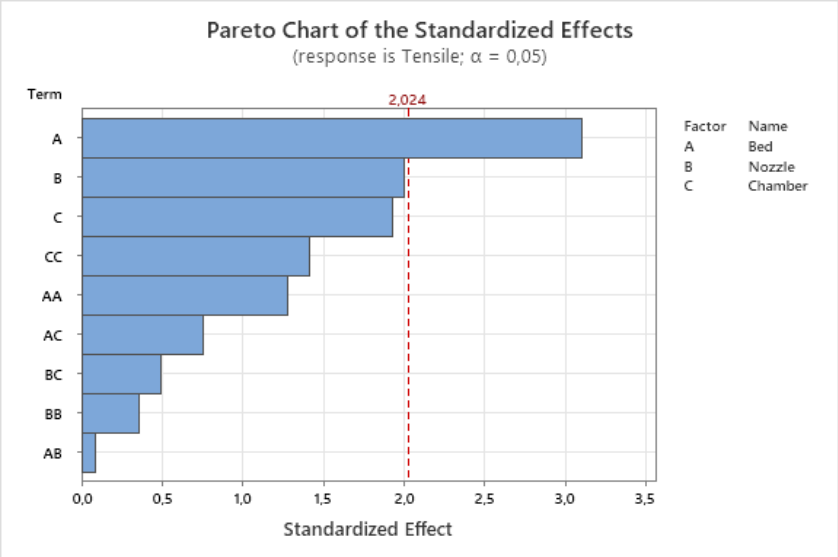


Figure 47 - Pareto Chart of the Standardized Effects.

4.2.4 Contour and Surface Plots

With the fitted equation for the response the software was also able to create surface and contour plots enabling an easy and direct visualization of the results as well as the prediction of theoretical combinations of parameters. The contour plots provide a more simplified view of the interaction results of two factors at a time. Due to the quadratic analysis those graphs show curvatures and present zones that reflect an interval of maximal tensile strengths.

It can be observed that the graphs (Figure 48,Figure 49 and Figure 50) suggest an optimal zone with elevated bed and nozzle temperatures and average chamber temperatures. Both the Chamber vs. Nozzle and the Bed vs. Nozzle graphs display a small and near the edge optimal zone, which suggests that further improvement can be obtained outside the studied range. As for the Bed vs. Chamber graph, two conclusions can be obtained, first that the range studied is able to cover the optimal zone as great part of the plotted area is occupied by this zone, second that this combination of factors does not have great significance as the optimal zone is big and altering the values of both factors does not lead to much change.

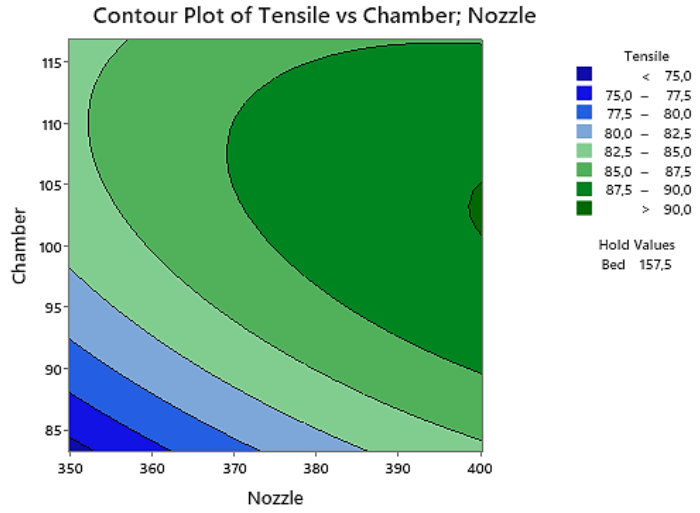


Figure 48 - Contour Plot of Tensile Strength for Chamber temp. vs. Nozzle temp.

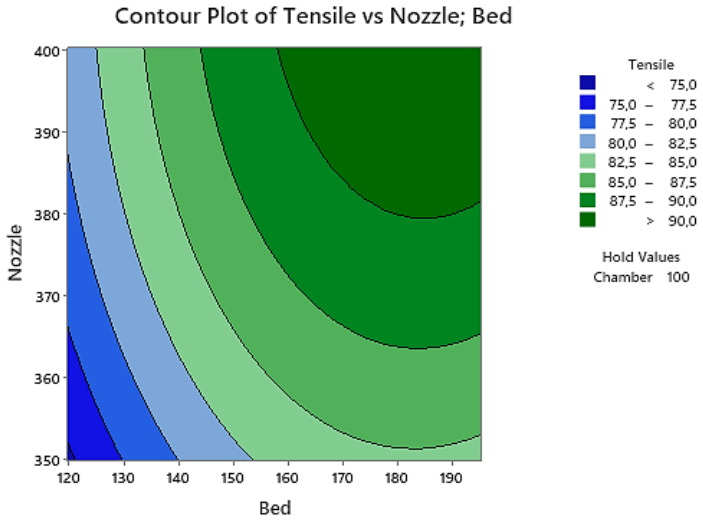


Figure 49 - Contour Plot of Tensile Strength for Nozzle temp. vs. Bed temp.

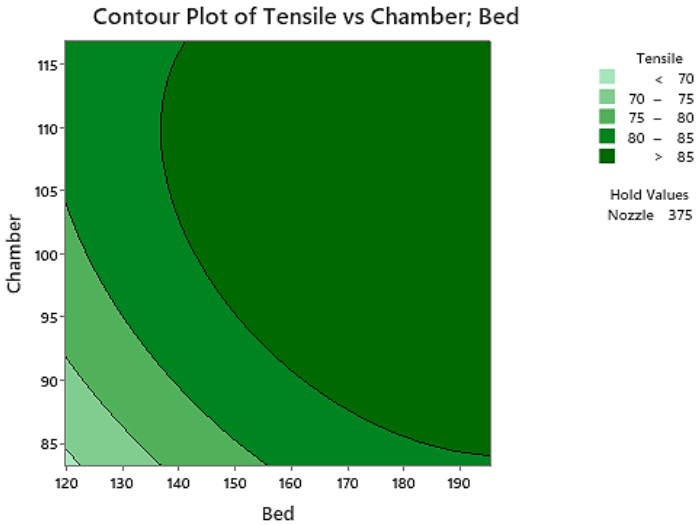


Figure 50 - Contour Plot of Tensile Strength for Chamber temp. vs. Bed temp.

The surface plots are able to provide a more detailed view of the interaction between two factors and their influence on the final response. Again, due to the quadratic analysis and the regression

model obtained, the plotted surface shows curvature and can predict response values more accurately. The 3D surface generated from the combination of the factors can be found on Figure 51, Figure 52 and Figure 53.

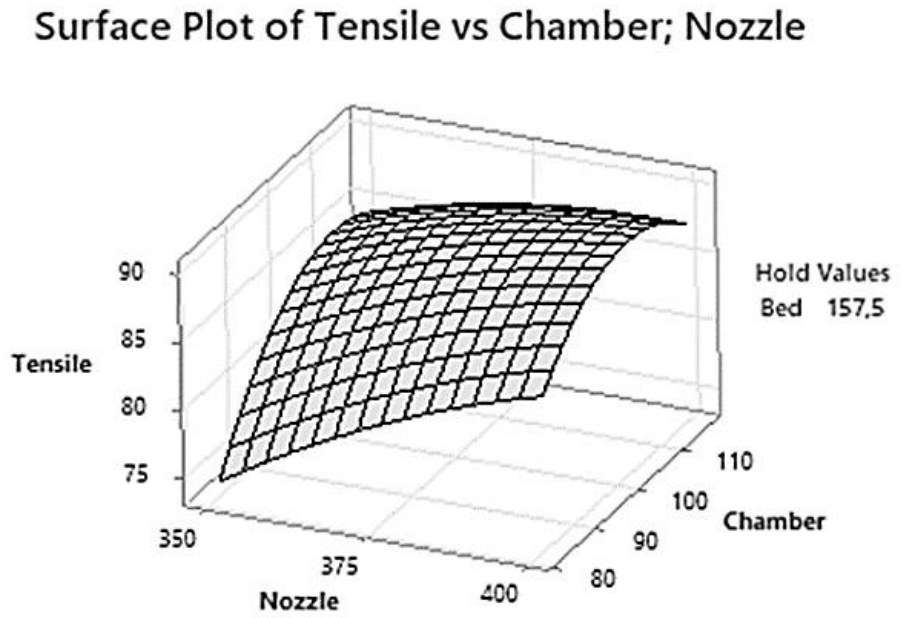


Figure 51 – Surface Plot of Tensile Strength for Chamber temp. vs. Nozzle temp.

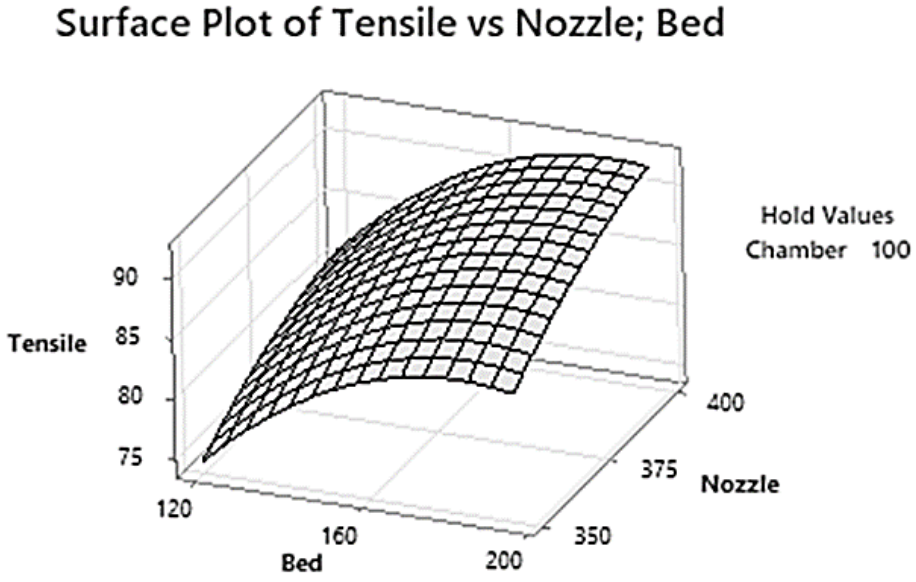


Figure 52 – Surface Plot of Tensile Strength for Nozzle temp. vs. Bed temp.

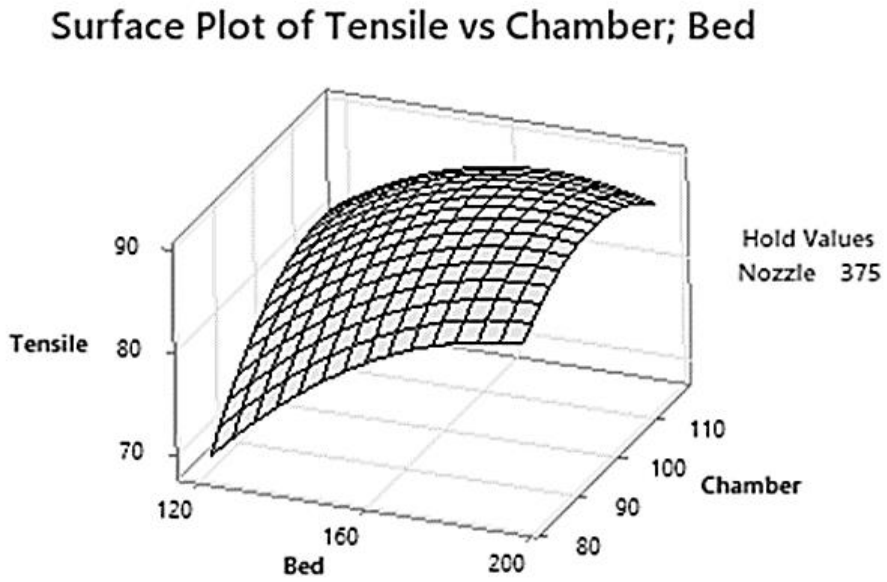


Figure 53 – Surface Plot of Tensile Strength for Chamber temp. vs. Bed temp.

Although the examination of those plots provides the same findings of the contour plots, they enable a clearer perception of the steepness between some parameter's combination. It becomes even clearer that when both factors are at low level the tensile strength is minimal, on the other hand, a combination of max level temperatures only reaches peak performance when looking at the Nozzle vs. Bed plot (Figure 52). On the other two, the max values for tensile strength are located on a plateau.

4.2.5 Factorial Plots

The factorial plots obtained allow the visualization of the relationship between the response and the variables. Two types of factorial plots were obtained using Minitab, first, the main effects plot in Figure 54, that approximates the effect of the main variables on the final tensile strength. Although not completely accurate, as the effect of a single variable on the response cannot be measured since it also depends on all the other variables, it is able to give some insight that allows for easy comparison of the effect sizes.

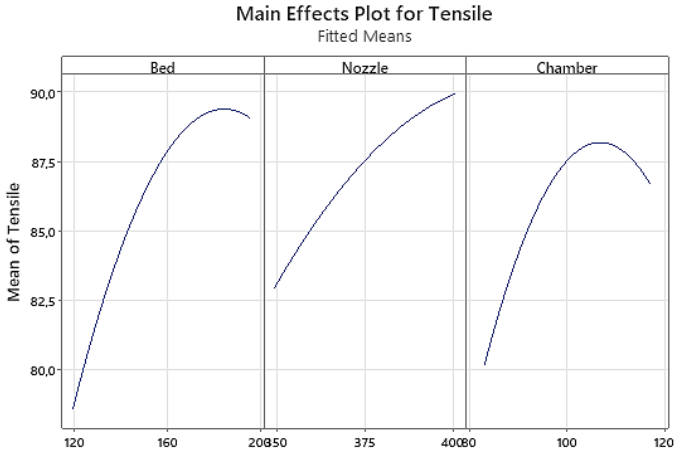


Figure 54 - Factorial Plots of the Main Effects for Tensile Strength.

Second, the interaction plot in Figure 55 can display how the value of a second variable affects the relationship between one variable and a fitted answer giving a more accurate prediction of the real process.

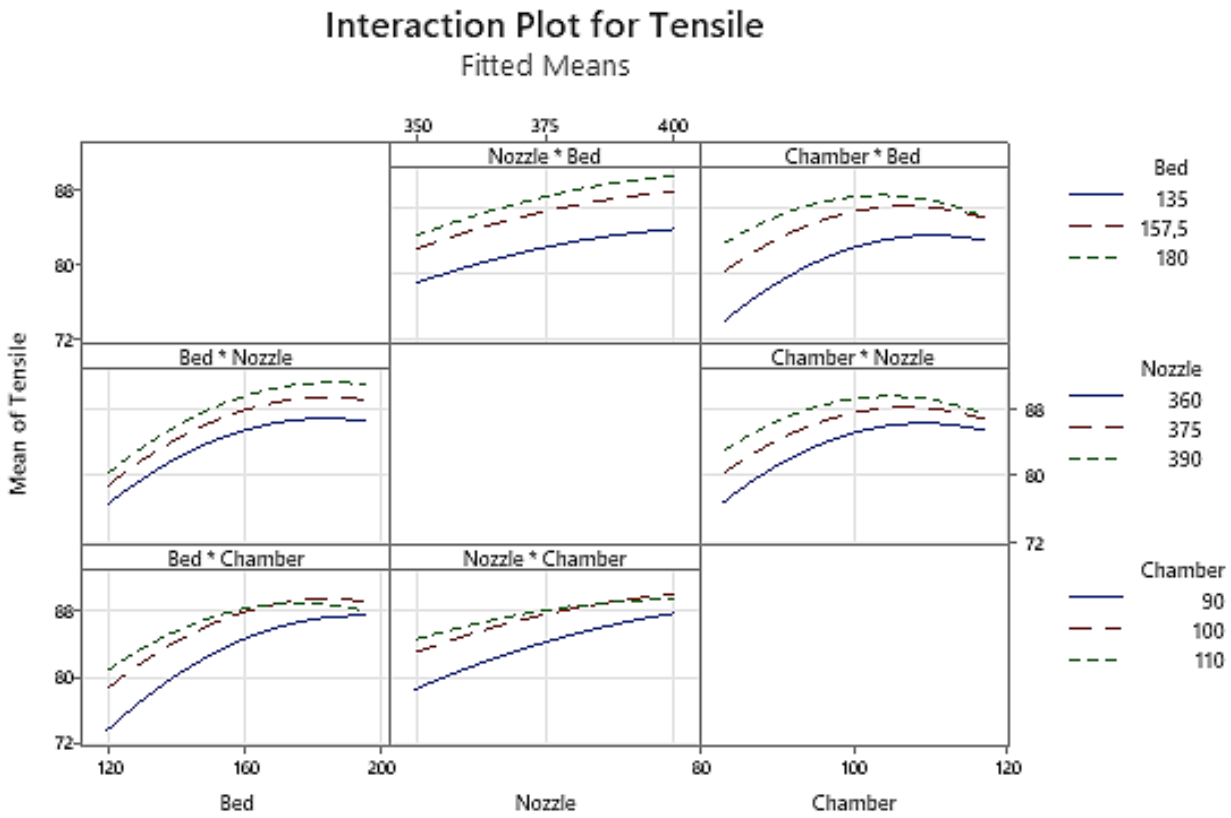


Figure 55 - Interaction Plots for the Different Factors Combinations.

Once again, as all these graphs are obtained based on the regression model, the results show that a high set of temperatures tends to produce samples with higher mechanical properties, what happens very evidently in the nozzle bed combination. Nevertheless, this graph allows the detection on the yet seen fact that when the temperatures start to reach the limit defined in this work their effect start to converge in certain combinations which creates the hypothesis that an even greater increase in those temperature will not lead to better results.

4.2.6 Optimizer

Based on the model equation, Minitab software is also able to predict the parameters levels for an optimized response. By setting the desired response to maximum the predicted values are as in Figure 56

Parameters

Response	Goal	Lower	Target	Upper	Weight	Importance
Tensile	Maximum	63,5	93,1		1	1

Variable	Setting
Bed	187,696
Nozzle	400,227
Chamber	98,4711

Response	Fit	SE Fit	95% CI	95% PI
Tensile	92,04	5,16	(81,59; 102,49)	(76,35; 107,73)

Figure 56 - Optimized parameter values for maximum tensile strength.

After the predictions five samples printed with the given temperatures were tested. The results can be seen in Figure 57 and Table 15.



Figure 57 - Tested samples with optimized parameters.

Table 15 - Max stress of the optimized samples and its average.

No	Max. Stress (MPa)
1	88.07
2	65.74
3	86.55
4	93.51
5	94.23
Average	90.59

Considering the maximum stress of sample 2 an outlier, as it failed out of the defined zone by the ASTM standard, it can be observed that all the samples were close to the predicted value of 92.04 MPa and fell into the confidence and predicted intervals.

4.3 Discussion

4.3.1 Nozzle Temperature

Analyzing the results, it is possible to conclude that the nozzle temperature was the second most influential factor out of the 3 main factors studied. Although not considered significant by the statistical analysis, through the results it becomes clear that an increase in the nozzle temperature results in an increase in the overall tensile strength.

As verified by previous researchers [47, 61], by increasing the extruder temperature the thermoplastic material becomes more viscous inducing a better neck formation between the deposited beads. The nozzle is also capable of re-heating the already deposited material with temperatures higher than its melting point facilitating even more the bond between layers while

also performing a heat treatment capable of further enhancing the sample's mechanical properties.

Although usually being recognized in previous studies [47, 61] as one of the most important factor when it comes to mechanical properties, this temperature ranked second and wasn´t even considered significant mainly due to the slow printing speed (30mm/s) of the process and also the chosen infill pattern. By taking too much time when depositing the new layer of material, the previous one had already cooled down, which made the necking process difficult as the new and previous beads of material had a bigger thermal gradient between them.

Nevertheless, considering the obtained graphs, it is possible to assume that there is still room for improvement of the mechanical properties of the parts with an increase of the nozzle temperature beyond the manufacturer's recommended values, although that could also lead to other issues. The factorial plots related to this temperature do not show a peak and the contour and surface plots only show a minimum area of the best performance which suggests that even better results can be obtained.

4.3.2 Chamber Temperature

Similar to the nozzle temperature, the chamber temperature was also considered not significant enough by Minitab and ranked third between the main parameters.

This temperature as previously studied by Forés-Garriga *et al.* [34] and Zaldivar *et al.* [35] is able to influence the tensile strength of the PEI parts. Its increase is reflected in an increase of the mechanical properties since it facilitates the bond between layers as it maintains the temperature of the surfaces high. With high environmental temperatures, the tensile strength of the samples can also be increased since it alleviates internal stresses and prevent warping caused by thermal contractions of the material that lead to stress concentration spots that could cause premature fails.

During the experiment, samples subjected to the highest chamber temperatures showed much less warpage than those printed in the low-levels range.

Nevertheless, two observations could be made after the analysis of the results. First that even though it almost reached the threshold to be considered a significant factor, out of the three main effects it was only ranked third. Second that increasing the temperature of the chamber only really benefits the maximum tensile strength until a value of about 100-110 degrees after which the there is no enhancement of the property or in some cases and adverse effect with the decrease of the maximum strength.

The first observation can be justified by the fact that due to the high thermal resistance of PEI, being able to support working temperatures of 170ºC, the temperature inside the enclosure is not enough to have a significant impact on the microstructure of the parts. Moreover, when compared to the temperatures used for the nozzle, more than 3 times higher and beyond the material melting point, and of the bed, that almost reaches the material T_g it becomes clear why those two parameters had a bigger influence on the sample's behavior.

Once again, the fact that PEI is a thermoplastic material with exceptional thermal resistance capabilities can serve as support for the second observation. Up to temperatures of 110ºC the chamber temperature is able to influence the part by maintaining the temperature differences between the newly deposited material and the already existing part low, as well as slowing down any warping but, beyond that point nothing different can be obtained. One hypothesis is that only chamber temperatures above the working temperature of PEI would be high enough to have an impact on the properties of the parts.

Even so, the importance of the ambient temperature in preventing warpages and stress concentration during the printing process cannot be neglected as it is fundamental to obtain parts with acceptable geometry accuracy and better mechanical properties.

4.3.3 Bed Temperature

From the previous graphs and analyses, the bed temperature could be easily identified as the factor that most influenced the response, being the only one considered significant by Minitab analysis.

Based on previous studies with different materials [47, 49, 60] it was expected that increasing the bed temperature would result in a slight enhancement of the mechanical properties of the samples. Even so, to be ranked as the parameter that most influence the final response proved that this factor is not only important for part adhesion and warpage prevention but also crucial to the optimization of the mechanical properties of high-performance materials.

One of the possible reasons for such an impact was the small thickness of the samples that allowed the temperature to affect the majority of the sample structure. Sun *et al.* [62] through microphotography analysis was able to verify that the neck growth between adjacent beads on the bottom layers of the sample were larger than on the top. In their experiment samples of 3.1mm were used so it's only natural to assume that the platform temperature had an even bigger effect on the samples of 2.8mm used in this work.

Peng *et al.* [47] through SEM images achieved a very similar result, in this case with PEEK. With higher temperature at the base, more energy is provided to the part what facilitates the diffusion and bonding of adjacent layers reducing the airgaps and originating a more "solid" part.

Moreover, by using bed temperatures that almost reached the material T_g (and possibly reached since the halogen bulbs could provide up to an additional 30ºC) the bonding procedure is improved even further since when above the T_g the material transitions from a rigid, glassy state to a more flexible, rubbery state improving the bond between adjacent layers.

Other parameter that influenced this result was the orientation of the printed samples on the bed since while being printed flat much more surface area was in contact with the heated surface and the part height was equal to its thickness causing almost all of its interior to be affected by the temperature. It is very likely that if the parts were printed in other orientations the effect of the bed temperature on the tensile strength wouldn't be this high.

4.3.4 Interactions

The effects of the interaction between parameters were very minor if compared to the main effects. One explanation for this low influence is the fact that the temperature related factors do not conflict with each other. Since in almost all the cases better properties were obtained with higher temperatures there wasn't really a difference on how that temperature was raised in relation to the parameter's levels chosen, if they were high.

Their non-influential behavior becomes even more evident when looking at the influence of parameters with higher temperatures as was the case with the nozzle-bed. All things considered, as long as a high temperature was achieved, the combination used to do was not relevant. Still, it was important to consider them to obtain a more accurate prediction model.

4.3.5 Model accuracy

Although the regression model yielded low R^2 values, it still managed to achieve acceptable values when confirming the predicted optimized outcomes. While the model demonstrates the

ability to predict results, it does so with a considerable range of potential values, thus lacking precision. The main contributing factor to this limitation is the dearth of data points, stemming from the failure of approximately 16% of the samples.

This lack of data has a direct impact on the model's precision. With fewer data points available for analysis, the model's ability to capture the true underlying patterns and relationships within the data becomes constrained.

Despite this imprecision, the model still retains validity, as it successfully captures the general trends and patterns observed in the dataset providing valuable insights and predictions that align with the overall behavior of the data.

The precision of the model is also affected by the inconsistency of the values obtained in the tests since the standard used is defined for injected plastic specimens and not printed ones, which puts in question the repeatability and validity of the analysis.

5 Conclusions and Future Works

5.1 Conclusions

The development and implementation of a design of experiments methodology to optimize the printing parameters of the high-performance PEI filament was proposed as part of this master's thesis. To achieve this objective, a series of steps were taken starting from the machine assembly and passing through process parametrization, development of the DoE and finally the analysis of the results. The main milestones and findings reached in this work were:

- A custom machine capable of printing high-performance thermoplastics was reassembled and upgraded to be able to reach higher chamber temperatures in less time.
- During pre-experimental testing it was found that it was almost impossible to print PEI samples with bed temperatures below 120ºC.
- Also, during pre-experimental testing, it was found out that samples printed following the ASTM D638 V geometry and with 2 perimeters showed consistent behavior during tensile strength testing.
- A DoE method, namely the Central Composite Design, was implemented using the software Minitab. Three different temperature factors, the bed, chamber, and nozzle temperatures, were selected and their influence on the final tensile strength of the samples was analyzed.
- Good quality PEI samples were printed using the custom printer and were prepared for digital image correlation analysis and tensile strength tests.
- An initial analysis of the obtained Stress vs. Strain graphs and max tensile strengths concluded that by increasing the overall printing temperature parts with higher tensile loads and less strain could be achieved.
- Using different statistical analysis methods, it was discovered that the bed temperature was the factor that, out of the three, influenced the tensile strength the most followed by the nozzle and chamber temperatures.
- It was also discovered that the interaction of parameters does not have major influence on the final response of the experiment.

- A regression model capable of predicting the response based on the inputs was obtained and later validated through testing, with the achieved values of tensile strength using the optimum parameters falling inside the predicted range.

- It was found that the optimal parameters for printing PEI in INEGI's custom built printer are a bed temperature of 187.6ºC a nozzle temperature of 400ºC and a chamber temperature of 98.5 ºC.

5.2 Future Works

Following the same line of work, some next steps could be taken to improve even more the current analysis, serving as follow-up studies to fully characterize the process behavior:

- Re-analyze the current DoE with a complete set of samples to obtain better results mainly in what concerns the R^2 of the regression model.

- Perform a microscopic analysis of the samples to further investigate the effect of the temperature parameters on the bonding of the internal layers.

- Develop a similar DoE but with the addition of the build orientation as a fourth factor in order to fully understand the effect of the bed temperature on the tensile strength of the samples.

- Broaden the frontiers of the DoE by investigating the effect of other printing parameters, apart from the temperature related, with the objective of fully characterizing the behavior of PEI filament printing.

- Research other mechanical properties of PEI printed parts such as flexural and bending strengths.

References

1. Molitch-Hou, M., *Overview of additive manufacturing process*, in *Additive manufacturing*. 2018, Elsevier. p. 1-38.
2. Wong, K.V. and A. Hernandez, *A review of additive manufacturing.* International scholarly research notices, 2012. **2012**.
3. ISO/ASTM52900-15, *Standard terminology for additive manufacturing—general principles—terminology*. American Society for Testing and Materials, West Conshohocken, 2015.
4. Ian Gibson, I.G., *Additive manufacturing technologies 3D printing, rapid prototyping, and direct digital manufacturing*. 2015, Springer.
5. Kumar, S.A. and R.V.S. Prasad, *Chapter 2 - Basic principles of additive manufacturing: different additive manufacturing technologies*, in *Additive Manufacturing*, M. Manjaiah, et al., Editors. 2021, Woodhead Publishing. p. 17-35.
6. Svetlizky, D., et al., *Directed energy deposition (DED) additive manufacturing: Physical characteristics, defects, challenges and applications.* Materials Today, 2021. **49**: p. 271-295.
7. Conceição, J.P.C., *Production of Sustainable Composite Powders for Direct Energy Deposition (DED).* 2022.
8. Sun, S., M. Brandt, and M. Easton, *2 - Powder bed fusion processes: An overview*, in *Laser Additive Manufacturing*, M. Brandt, Editor. 2017, Woodhead Publishing. p. 55-77.
9. Bhavar, V., et al., *A review on powder bed fusion technology of metal additive manufacturing.* Additive manufacturing handbook, 2017: p. 251-253.
10. Pagac, M., et al., *A Review of Vat Photopolymerization Technology: Materials, Applications, Challenges, and Future Trends of 3D Printing.* Polymers, 2021. **13**(4): p. 598.
11. Dilberoglu, U.M., et al., *The Role of Additive Manufacturing in the Era of Industry 4.0.* Procedia Manufacturing, 2017. **11**: p. 545-554.
12. Zhang, Z., et al., *Binder jetting 3D printing process optimization for rapid casting of green parts with high tensile strength.* China Foundry, 2021. **18**: p. 335 - 343.
13. Shakor, P., et al., *Review of binder jetting 3D printing in the construction industry.* Progress in Additive Manufacturing, 2022. **7**: p. 643 - 669.
14. Gülcan, O., K. Günaydın, and A. Tamer, *The state of the art of material jetting—a critical review.* Polymers, 2021. **13**(16): p. 2829.

15. Turner, B.N. and S.A. Gold, *A review of melt extrusion additive manufacturing processes: II. Materials, dimensional accuracy, and surface roughness.* Rapid Prototyping Journal, 2015.

16. *RepRap*. [cited 2023 03/05]; Available from: https://reprap.org/wiki/RepRap.

17. Jones, R., et al., *RepRap–the replicating rapid prototyper.* Robotica, 2011. **29**(1): p. 177-191.

18. Shaqour, B., et al., *Gaining a better understanding of the extrusion process in fused filament fabrication 3D printing: A review.* The International Journal of Advanced Manufacturing Technology, 2021. **114**: p. 1279-1291.

19. Jerez-Mesa, R., et al., *A comparative study of the thermal behavior of three different 3D printer liquefiers.* Mechatronics, 2018. **56**: p. 297-305.

20. *The Types of FDM 3D Printers: Cartesian, CoreXY, & More*. [cited 2023 28/05/2023]; Available from: https://all3dp.com/2/cartesian-3d-printer-delta-scara-belt-corexy-polar/.

21. *Original Prusa i3 MK3S+ 3D printer*. [cited 2023 07/03/2023]; Available from: https://www.prusa3d.com/product/original-prusa-i3-mk3s-3d-printer-3/.

22. *Ender-5 S1 3D Printer- Direct Extrusion | High-temp Printing | Up To 250mm/s Printing Speed*. [cited 2023 07/03/2023]; Available from: https://www.creality3dofficial.eu/products/ender-5-s1-3d-printer.

23. *SCULPTO PRO2 3D PRINTER*. [cited 2023 07/03/2023]; Available from: https://sculpto-shop.com/products/sculpto-pro2-3d-printer.

24. *TRILAB DeltiQ 2 Plus*. [cited 2023 07/03/2023]; Available from: https://www.prusa3d.com/product/trilab-deltiq-2-plus-6/.

25. Chadha, A., et al., *Effect of fused deposition modelling process parameters on mechanical properties of 3D printed parts.* World Journal of Engineering, 2019. **16**(4): p. 550-559.

26. Ahn, S.-H., et al., *Anisotropic material properties of fused deposition modeling ABS.* Rapid Prototyping Journal, 2002. **8**.

27. Croccolo, D., M. De Agostinis, and G. Olmi, *Experimental characterization and analytical modelling of the mechanical behaviour of fused deposition processed parts made of ABS-M30.* Computational Materials Science, 2013. **79**: p. 506-518.

28. Gebisa, A.W. and H.G. Lemu, *Investigating effects of fused-deposition modeling (FDM) processing parameters on flexural properties of ULTEM 9085 using designed experiment.* Materials, 2018. **11**(4): p. 500.

29. Onwubolu, G.C. and F. Rayegani, *Characterization and optimization of mechanical properties of ABS parts manufactured by the fused deposition modelling process.* International Journal of Manufacturing Engineering, 2014. **2014**: p. 1-13.

30. Chacón, J.M., et al., *Additive manufacturing of PLA structures using fused deposition modelling: Effect of process parameters on mechanical properties and their optimal selection.* Materials & Design, 2017. **124**: p. 143-157.

31. Sood, A.K., R.K. Ohdar, and S.S. Mahapatra, *Experimental investigation and empirical modelling of FDM process for compressive strength improvement.* Journal of Advanced Research, 2012. **3**(1): p. 81-90.

32. Hernandez, R., et al. *Analyzing the tensile, compressive, and flexural properties of 3D printed ABS P430 plastic based on printing orientation using fused deposition*

modeling. in *2016 International Solid Freeform Fabrication Symposium*. 2016. University of Texas at Austin.

33. Górski, F., et al., *Strength of ABS parts produced by Fused Deposition Modelling technology–a critical orientation problem.* Advances in Science and Technology Research Journal, 2015. **9**(26): p. 12--19.
34. Forés-Garriga, A., et al., *Role of infill parameters on the mechanical performance and weight reduction of PEI Ultem processed by FFF*. Materials & Design, 2020. **193**: p. 108810.
35. Zaldivar, R., et al., *Influence of processing and orientation print effects on the mechanical and thermal behavior of 3D-Printed ULTEM® 9085 Material.* Additive Manufacturing, 2017. **13**: p. 71-80.
36. Byberg, K.I., A.W. Gebisa, and H.G. Lemu, *Mechanical properties of ULTEM 9085 material processed by fused deposition modeling.* Polymer Testing, 2018. **72**: p. 335-347.
37. *3D Print Speed vs Quality; Best Settings!* [cited 2023 28/04/2023]; Available from: https://3dsolved.com/3d-printing-speed-vs-quality/.
38. *INNOVATEFIL PEEK NATURAL S 400G - SMART MATERIALS 3D.* [cited 2023 01/06/2023]; Available from: https://evolt.pt/produto/innovatefil-peek-natural-s-400g-smart-materials-3d/.
39. *THERMAX PEEK*. [cited 2023 01/06/2023]; Available from: https://www.3dxtech.com/product/thermax-peek/.
40. *PEEK Filament*. [cited 2023 01/06/2023]; Available from: https://www.3d4makers.com/products/peek-filament?_pos=1&_sid=736b79c55&_ss=r.
41. *Essentium PEEK*. [cited 2023 01/06/2023]; Available from: https://filament2print.com/pt/avancados/1642-essentium-peek.html#/257-color-natural/217-diametro-175_mm/223-formato-bobina_750_g.
42. *PEI ULTEM 1010*. [cited 2023 28/05/2023]; Available from: https://filament2print.com/pt/avancados/892-pei-ultem-1010.html.
43. *PEI 500G PEIJET 1010 ULTEM NATUR - FILAMENT PM*. [cited 2023 28/05/2023]; Available from: https://evolt.pt/produto/pei-500g-peijet-1010-ultem-natur-filament-pm/.
44. *THERMAX PEI MADE USING ULTEM 1010*. [cited 2023 28/05/2023]; Available from: https://www.3dxtech.com/product/thermax-pei-using-ultem-1010/.
45. *PEI Ultem 1010 Filament*. [cited 2023 28/05/2023]; Available from: https://www.3d4makers.com/products/pei-filament.
46. *The Best Polycarbonate (PC) Filaments of 2023*. [cited 2023 01/06/2023]; Available from: https://all3dp.com/2/polycarbonate-pc-filament-basics-best-brands/.
47. Peng, W., et al., *Effects of FDM-3D printing parameters on mechanical properties and microstructure of CF/PEEK and GF/PEEK.* Chinese Journal of Aeronautics, 2021. **34**(9): p. 236-246.
48. Li, H., et al., *The effect of process parameters in fused deposition modelling on bonding degree and mechanical properties.* Rapid Prototyping Journal, 2018.
49. Qureshi, A., et al. *Design for Scalability and Strength Optimisation for components created through FDM process*. in *DS 80-6 Proceedings of the 20th International*

Conference on Engineering Design (ICED 15) Vol 6: Design Methods and Tools-Part 2 Milan, Italy, 27-30.07. 15. 2015.

50. Santana, L., *Avaliação das capacidades da impressão 3D de baixo custo na fabricação de snap-fits: uma relação de reconhecimento usuário-sistema de impressão.* 2019.
51. Carneiro, O.S., A.F. Silva, and R. Gomes, *Fused deposition modeling with polypropylene.* Materials & Design, 2015. **83**: p. 768-776.
52. Weinmann, J., et al. *Application of design of experiments (DOE) on the processing of rapid prototyped samples*. in *2003 International Solid Freeform Fabrication Symposium*. 2003.
53. Rankouhi, B., et al., *Failure analysis and mechanical characterization of 3D printed ABS with respect to layer thickness and orientation.* Journal of Failure Analysis and Prevention, 2016. **16**: p. 467-481.
54. Sood, A.K., R.K. Ohdar, and S.S. Mahapatra, *Parametric appraisal of mechanical property of fused deposition modelling processed parts.* Materials & Design, 2010. **31**(1): p. 287-295.
55. Pandelidi, C., et al., *Parametric study on tensile and flexural properties of ULTEM 1010 specimens fabricated via FDM.* Rapid Prototyping Journal, 2021. **27**(2): p. 429-451.
56. Wu, W., et al., *Influence of layer thickness and raster angle on the mechanical properties of 3D-printed PEEK and a comparative mechanical study between PEEK and ABS.* Materials, 2015. **8**(9): p. 5834-5846.
57. Baich, L., G. Manogharan, and H. Marie, *Study of infill print design on production cost-time of 3D printed ABS parts.* International Journal of Rapid Manufacturing, 2015. **5**(3-4): p. 308-319.
58. Mahmood, S., et al., *Tensile strength of partially filled FFF printed parts: experimental results.* Rapid prototyping journal, 2017. **23**(1): p. 122-128.
59. Spoerk, M., et al., *Effect of the printing bed temperature on the adhesion of parts produced by fused filament fabrication.* Plastics, Rubber and Composites, 2018. **47**(1): p. 17-24.
60. Xiaoyong, S., et al. *Experimental analysis of high temperature PEEK materials on 3D printing test*. in *2017 9th International conference on measuring technology and mechatronics automation (ICMTMA)*. 2017. IEEE.
61. Jiang, S., et al., *Mechanical properties analysis of polyetherimide parts fabricated by fused deposition modeling.* High Performance Polymers, 2019. **31**(1): p. 97-106.
62. Sun, Q., et al., *Effect of processing conditions on the bonding quality of FDM polymer filaments.* Rapid prototyping journal, 2008.
63. Tymrak, B., M. Kreiger, and J.M. Pearce, *Mechanical properties of components fabricated with open-source 3-D printers under realistic environmental conditions.* Materials & Design, 2014. **58**: p. 242-246.
64. Liu, X., et al., *Mechanical property parametric appraisal of fused deposition modeling parts based on the gray Taguchi method.* The International Journal of Advanced Manufacturing Technology, 2017. **89**: p. 2387-2397.
65. Ziemian, C., M. Sharma, and S. Ziemian, *Anisotropic Mechanical Properties of ABS Parts Fabricated by Fused Deposition Modelling*. 2012.
66. Es-Said, O.S., et al., *Effect of layer orientation on mechanical properties of rapid prototyped samples.* Materials and Manufacturing Processes, 2000. **15**(1): p. 107-122.

67. Durgun, I. and R. Ertan, *Experimental investigation of FDM process for improvement of mechanical properties and production cost.* Rapid Prototyping Journal, 2014.

68. Ziemian, S., M. Okwara, and C.W. Ziemian, *Tensile and fatigue behavior of layered acrylonitrile butadiene styrene.* Rapid Prototyping Journal, 2015.

69. Schöppner, V. and K.P. KTP. *Mechanical properties of fused deposition modeling parts manufactured with Ultem* 9085*. in *Proceedings of the 69th Annual Technical Conference of the Society of Plastics Engineers (ANTEC'11), Boston, MA, USA*. 2011.

70. Shojib Hossain, M., et al. *Improving tensile mechanical properties of FDM-manufactured specimens via modifying build parameters*. in *2013 International Solid Freeform Fabrication Symposium*. 2013. University of Texas at Austin.

71. Alvarez C, K.L., R.F. Lagos C, and M. Aizpun, *Investigating the influence of infill percentage on the mechanical properties of fused deposition modelled ABS parts.* Ingeniería e Investigación, 2016. **36**(3): p. 110-116.

72. Joseph Arockiam, A., et al., *A review on PLA with different fillers used as a filament in 3D printing.* Materials Today: Proceedings, 2022. **50**: p. 2057-2064.

73. *Material Guide - PLA*. Prusa Knowledge Base [cited 2023 05/05/2023]; Available from: https://help.prusa3d.com/article/pla_2062.

74. *Material Guide - ABS*. Prusa Knowledge Base [cited 2023 05/05/2023]; Available from: https://help.prusa3d.com/article/abs_2058.

75. *Prusa Material Table*. [cited 2023 01/06/2023]; Available from: https://help.prusa3d.com/materials.

76. *Polymers for material extrusion additive manufacturing: Part-1*. Additive Manufacturing Inc [cited 2023 05/05/2023]; Available from: https://aminception.com/Blog/Details/10.

77. *Material Guide - Polycarbonate (PC)*. Prusa Knowlwdge Base [cited 2023 05/05/2023]; Available from: https://help.prusa3d.com/article/polycarbonate-pc_165812.

78. *Material Guide - Flexible materials* Prusa Knowledge Base [cited 2023 05/02/2023]; Available from: https://help.prusa3d.com/article/flexible-materials_2057.

79. El Magri, A., S. Vanaei, and S. Vaudreuil, *An overview on the influence of process parameters through the characteristic of 3D-printed PEEK and PEI parts.* High Performance Polymers, 2021. **33**.

80. Antony, J., *Introduction to Industrial Experimentation*. 2003. p. 1-5.

81. Jankovic, A., G. Chaudhary, and F. Goia, *Designing the design of experiments (DOE)–An investigation on the influence of different factorial designs on the characterization of complex systems.* Energy and Buildings, 2021. **250**: p. 111298.

82. Ranga, S., et al., *A review on Design of Experiments (DOE).* Int. J. Pharm. Chem. Sci, 2014. **3**(1): p. 216-24.

83. Weissman, S.A. and N.G. Anderson, *Design of experiments (DoE) and process optimization. A review of recent publications.* Organic Process Research & Development, 2015. **19**(11): p. 1605-1633.

84. Vanaja, K. and R. Shobha Rani, *Design of experiments: concept and applications of Plackett Burman design.* Clinical research and regulatory affairs, 2007. **24**(1): p. 1-23.

85. *NIST/SEMATECH e-Handbook of Statistical Methods*. Available from: http://www.itl.nist.gov/div898/handbook/.

86. Basto, J.A.d.S.B., *Apontamentos da Unidade Curricular - Process Engineering and Continuous Improvement*. 2022.

87. Mason, R.L., R.F. Gunst, and J.L. Hess, *Statistical design and analysis of experiments: with applications to engineering and science*. 2003: John Wiley & Sons.

88. Krishnaiah, K. and P. Shahabudeen, *Applied design of experiments and Taguchi methods*. 2012: PHI Learning Pvt. Ltd.

89. Khuri, A.I. and S. Mukhopadhyay, *Response surface methodology*. Wiley Interdisciplinary Reviews: Computational Statistics, 2010. **2**(2): p. 128-149.

90. Box, G.E. and D.W. Behnken, *Some new three level designs for the study of quantitative variables.* Technometrics, 1960. **2**(4): p. 455-475.

91. Draper, N.R. and F. Pukelsheim, *An overview of design of experiments.* Statistical Papers, 1996. **37**: p. 1-32.

92. Anderson, M.J. and P.J. Whitcomb, *DOE simplified: practical tools for effective experimentation*. 2017: CRC press.

93. Antony, J., *Design of experiments for engineers and scientists*. 2014: Elsevier.

94. Domingues, T., et al., *Development of a custom setup for additive manufacturing of high-performance thermoplastics.* Procedia Structural Integrity, 2022. **37**: p. 847-856.

95. Gardner, J.M., et al., *High temperature thermoplastic additive manufacturing using low-cost, open-source hardware*. 2016.

96. D638, A., *ASTM D638, Standard Test Method for Tensile Properties of Plastics*. 2014, American Society for Testing and Materials, EUA.

97. 527-2, I., *ISO 527-2, Plastics-determination of tensile properties, part 2: test conditions for moulding and extrusion plastics*. 2012, International Standard Organization Std Geneva, Switzerland.

98. *NANO POLYMER ADHESIVE*. [cited 2023 28/05/2023]; Available from: https://visionminer.com/products/nano-polymer-adhesive.

ANNEX A - Stress-Strain graphs and maximum values

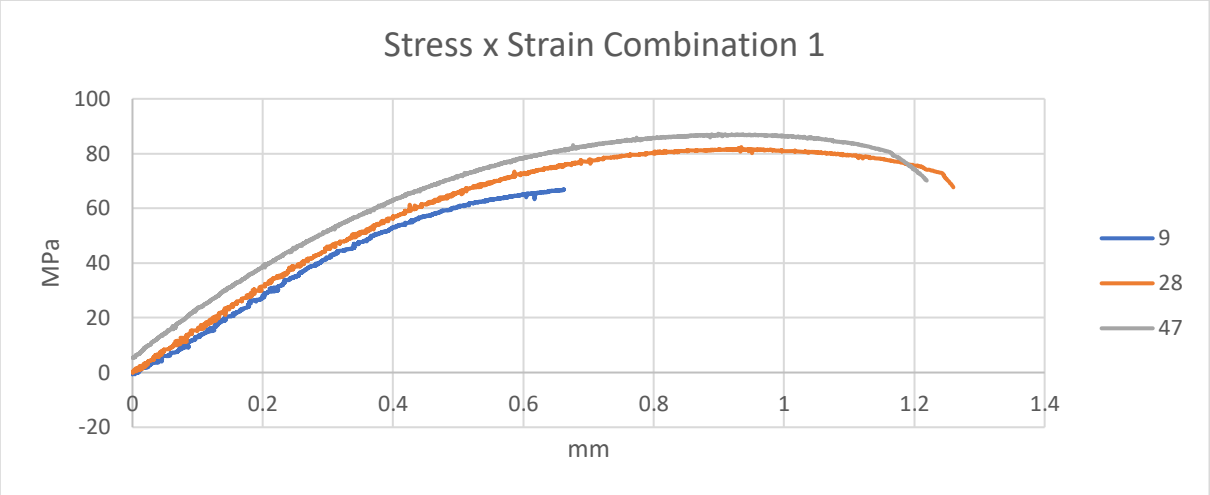


Figure 58 - Stress-Strain curve of samples with parameters combination 1

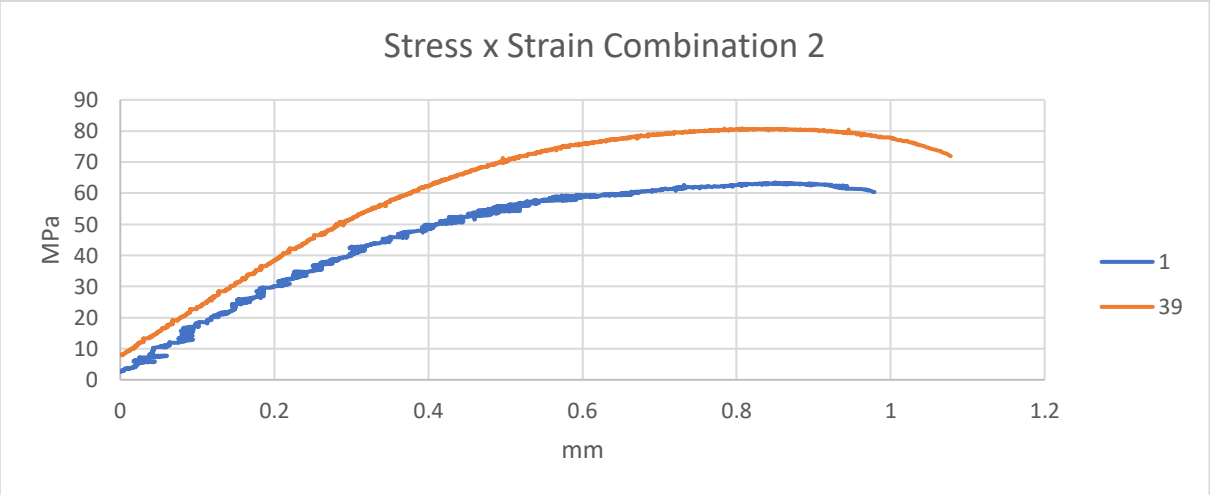


Figure 59 - Stress-Strain curve of samples with parameters combination 2

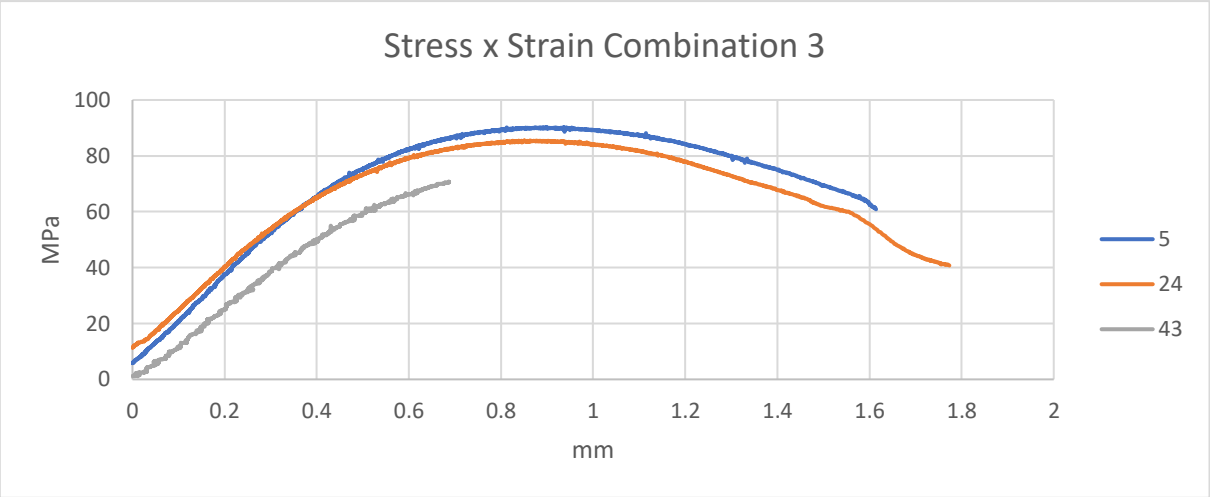


Figure 60 - Stress-Strain curve of samples with parameters combination 3

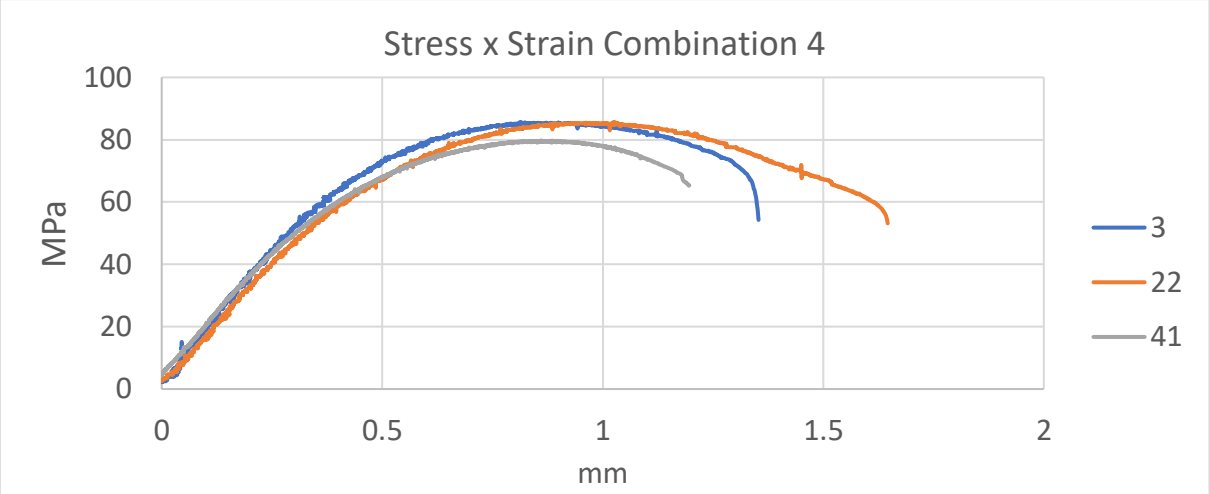


Figure 61 - Stress-Strain curve of samples with parameters combination 4

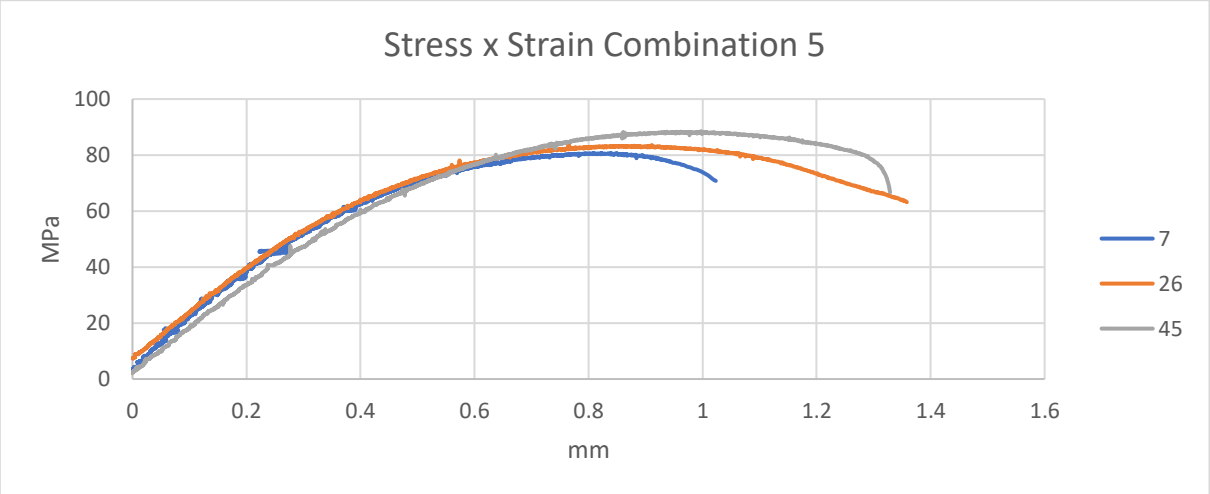


Figure 62 - Stress-Strain curve of samples with parameters combination 5

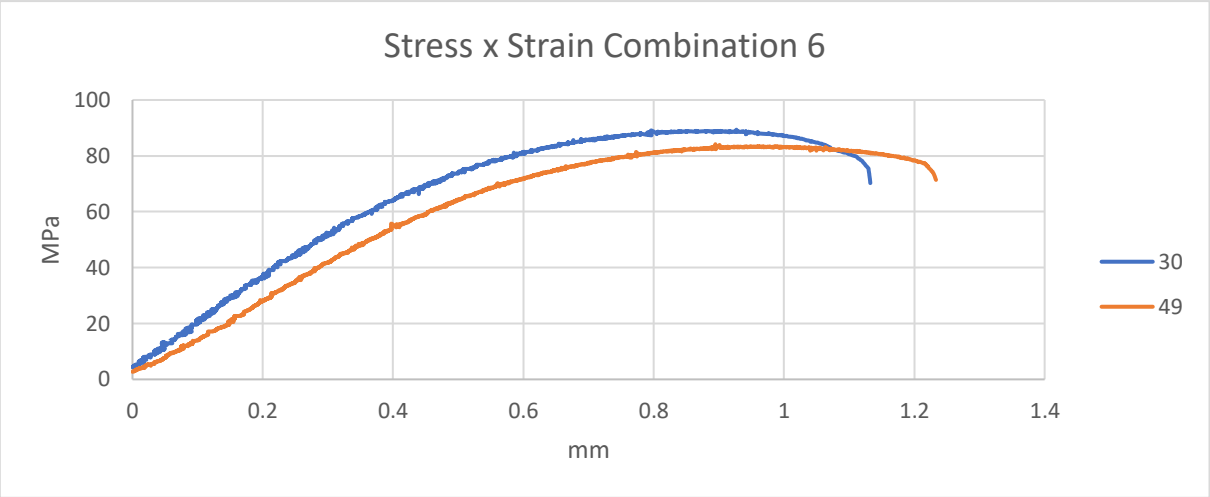


Figure 63 - Stress-Strain curve of samples with parameters combination 6

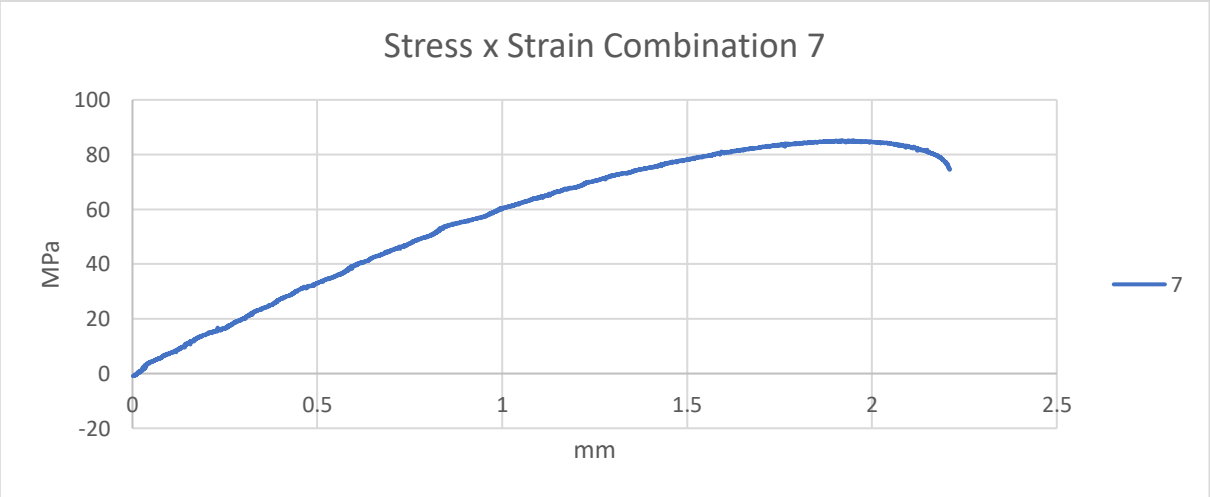


Figure 64 - Stress-Strain curve of samples with parameters combination 7

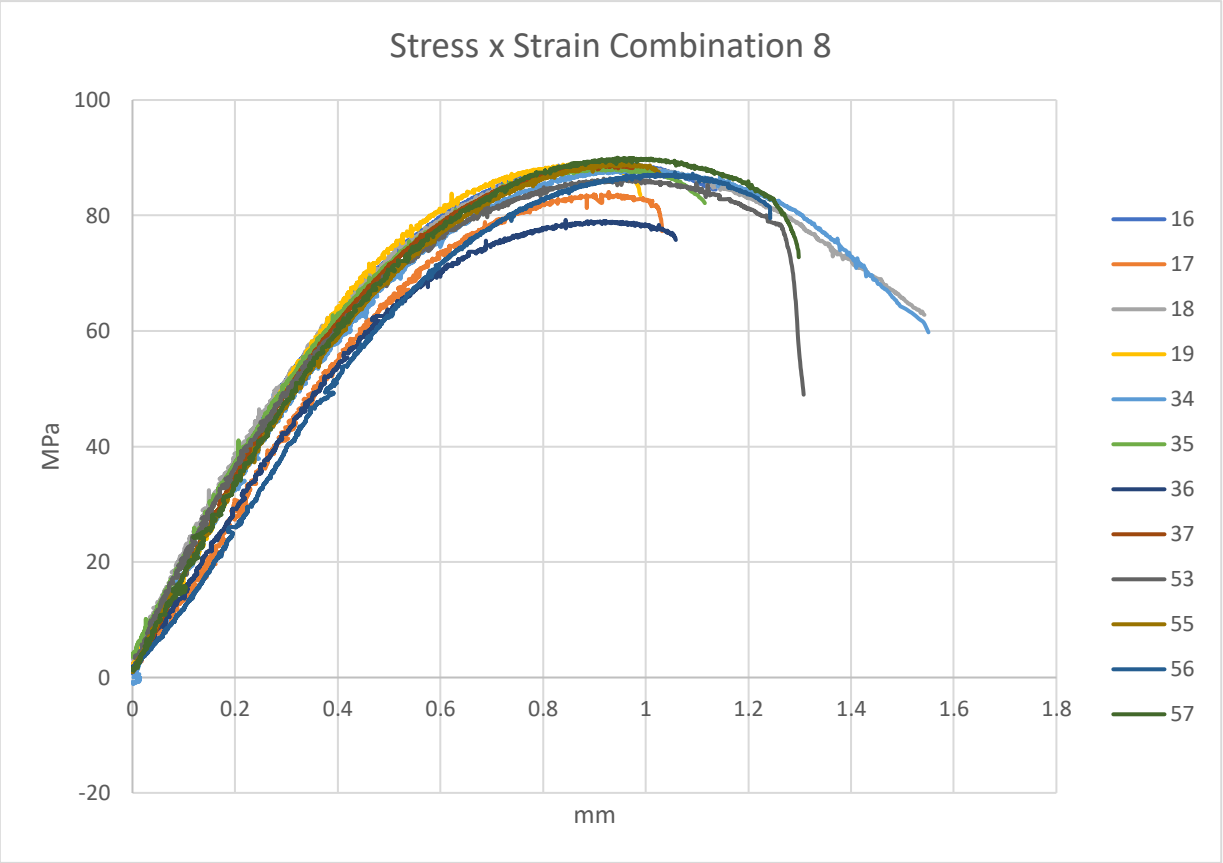


Figure 65 - Stress-Strain curve of samples with parameters combination 8

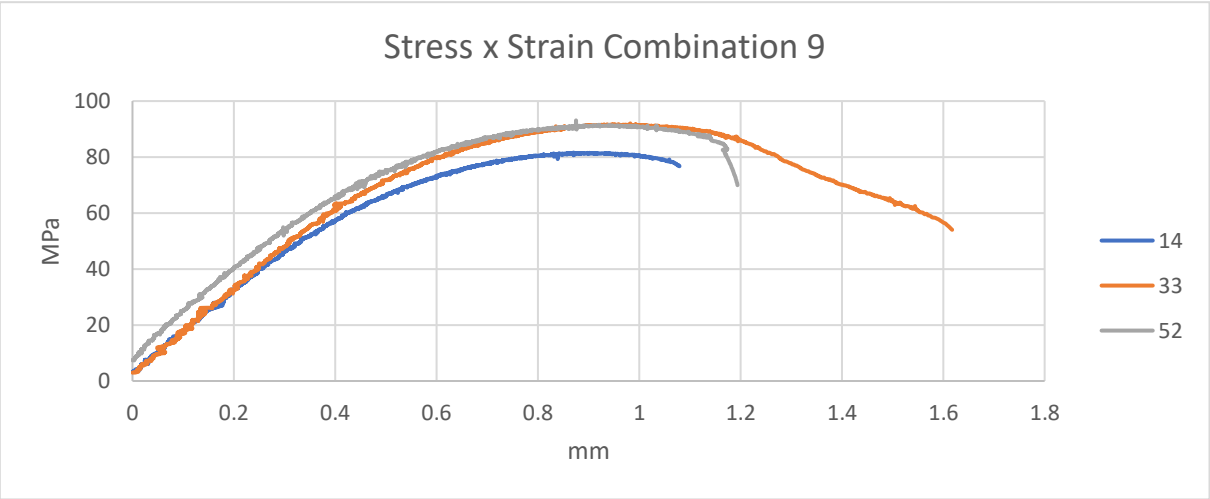


Figure 66 - Stress-Strain curve of samples with parameters combination 9

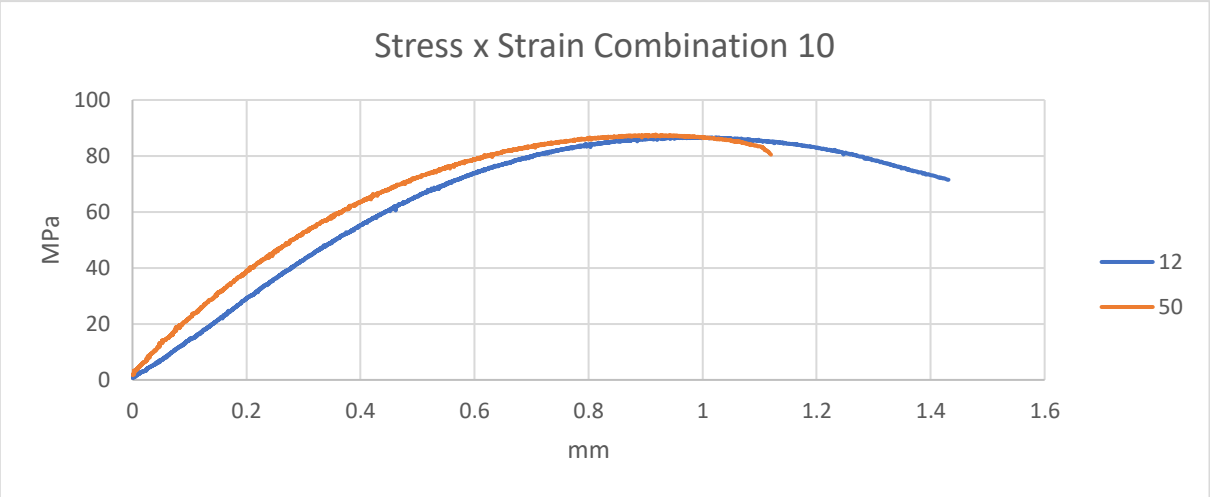


Figure 67 - Stress-Strain curve of samples with parameters combination 10

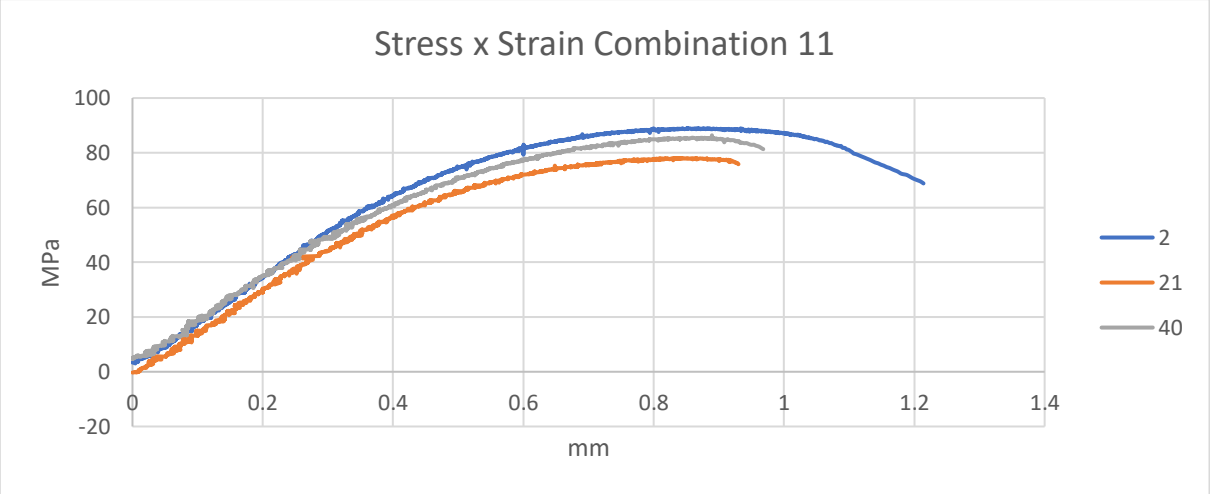


Figure 68 - Stress-Strain curve of samples with parameters combination 11

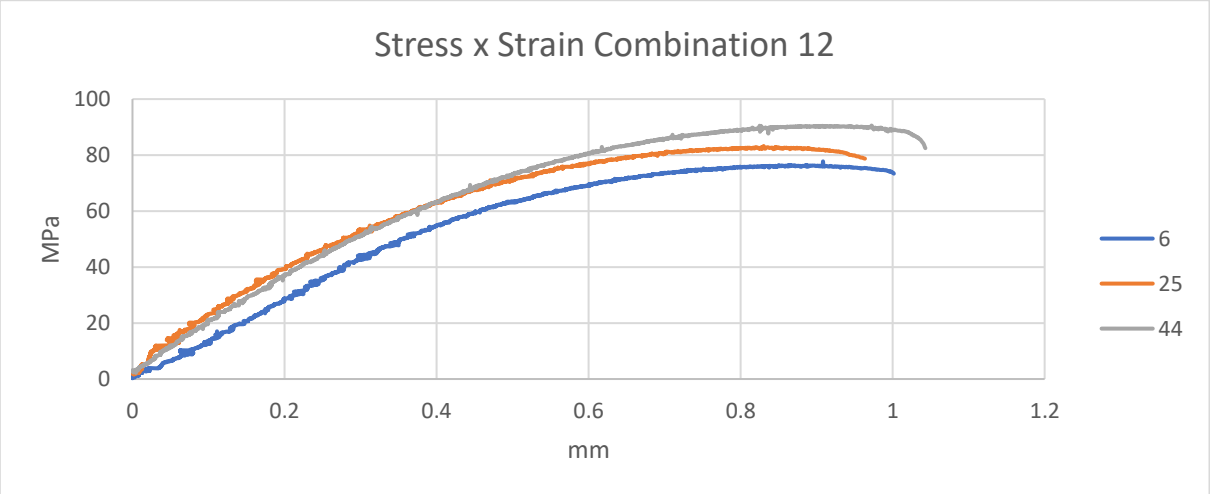


Figure 69 - Stress-Strain curve of samples with parameters combination 12

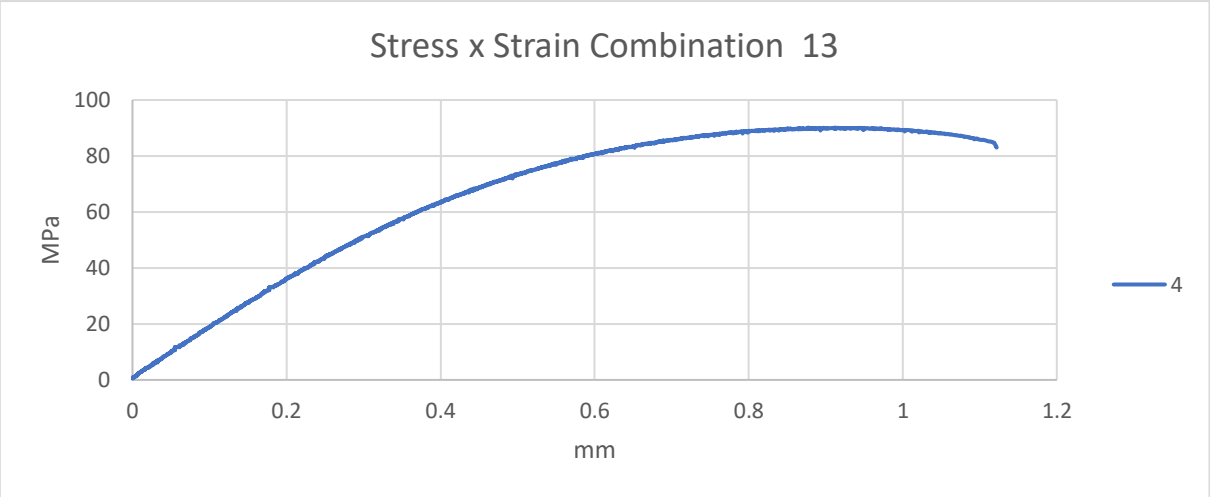


Figure 70 - Stress-Strain curve of samples with parameters combination 13

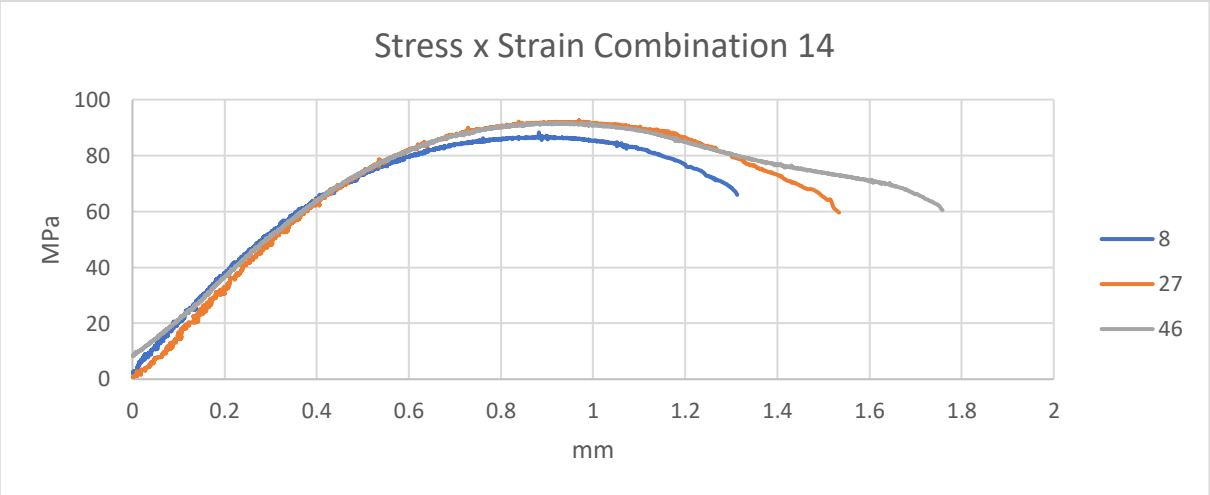


Figure 71 - Stress-Strain curve of samples with parameters combination 14

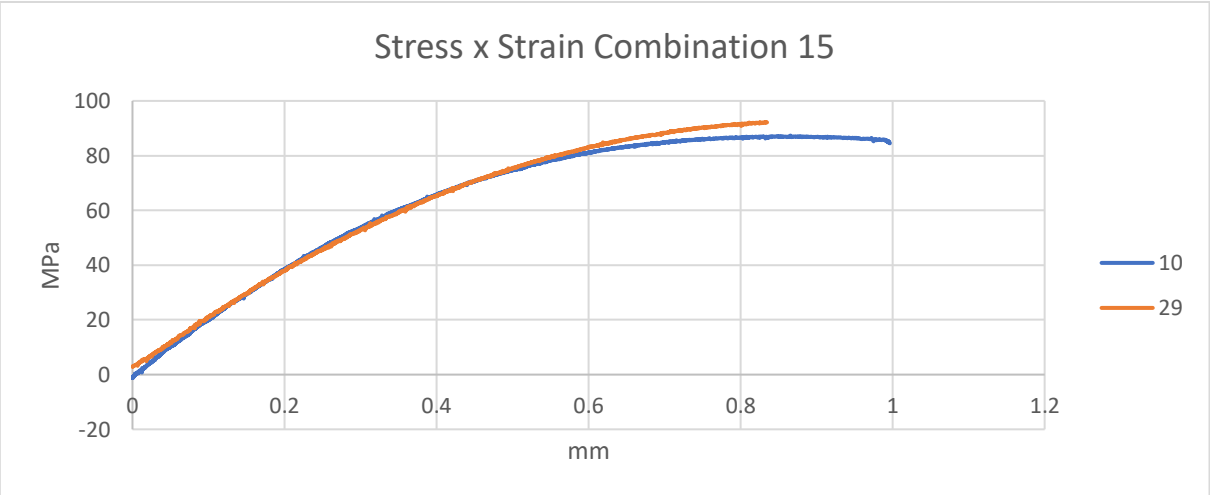


Figure 72 - Stress-Strain curve of samples with parameters combination 15

Table 16 - Maximum Stress and Strain

Combination	Sample	Stress (MPa)	Strain (mm)
1	9	67.07	0.662
	28	82.38	1.26
	47	87.27	1.219
2	1	63.50	0.981
	20	79.18	-
	39	80.83	1.08
3	5	90.27	1.614
	24	85.55	1.774
	43	70.84	0.686
4	3	85.65	1.354
	22	85.7	1.647
	41	79.78	1.197
5	7	80.73	1.027
	26	83.98	1.359
	45	88.54	1.329
6	11	-	-
	30	89.37	1.132
	49	84.17	1.234
7	13	85.17	1.179
	32	-	-
	51	70.95	-
8	15	-	-
	16	89.31	1.137
	17	84.03	1.032
	18	89.24	1.544
	19	88.88	0.99
	34	88.99	1.555
	35	88.28	1.117
	36	79.24	1.058
	37	89.05	0.975
	38	-	-

Continuation of Table 16

Combination	Sample	Stress (MPa)	Strain (mm)
8	53	86.47	1.308
	54	-	-
	55	89.2	1.03
	56	87.5	1.242
	57	90.02	1.298
9	14	81.6	1.08
	33	92.03	1.619
	52	93.1	1.194
10	12	86.71	1.433
	31	-	-
	50	87.68	1.12
113	2	88.99	1.216
	21	78.07	0.931
	40	86.38	0.969
12	6	77.75	1
	44	90.55	1.043
	25	83.24	0.964
13	4	90.14	1.122
	23	-	-
	42	-	-
14	8	88.34	1.314
	27	92.68	1.537
	46	91.97	1.767
15	10	87.34	0.996
	29	92.3	0.835
	48	-	-

.